DOSIMETERS USING PLASTIC SCINTILLATORS AND FIBRE OPTICS.

A thesis submitted in partial fulfilment of the
requirements for the degree
of
Doctorate of Philosophy in Medical Physics
at the
University of Canterbury

By
Mohammad Ali Alhabdan

University of Canterbury
2005

Abstract

A plastic scintillation detector exhibiting minimum interference using two different optical fibre light guides have been designed, constructed and evaluated for dosimetry (potentially *in-vivo*) of the high energy beams used in radiotherapy practice. One detector system contains the radiation resistant SiO_2 optical fibre, while the other contains PMMA fibre, which has less resistance to radiation. Each fibre is connected to an independent photodiode. Also, each fibre is connected to a cylindrical water equivalent scintillator measuring 3mm in diameter and 10mm in length. The scintillator is coated with a thin, optically reflective coating. The light arising from the scintillator is transmitted by the fibre optic light guide and is detected at the photodiode. Each fibre has its own focusing and optical filtering techniques based on the fibre acceptance angle, so the photodiode for SiO_2 and PMMA are the same. The photodiodes are connected to an electronics box with a digital integrator and counting system. The interference radiation could be minimised using inherent optical filtration and digital integration consistent with pulses from the linear accelerator, thereby avoiding the use of a second optical fibre to compensate for background signals.

The SiO_2 and PMMA fibre light guides have different properties especially with respect to flexibility. The dose distribution in water of each fibre light guide coupled scintillator is measured and shows good agreement with ionisation chamber results. Spatial resolution and water equivalence are the most important properties of minuature scintillator detectors. It is shown that these systems are not energy dependent, they do not disturb the main radiation beam, are independent of beam angle and have very good linearity with dose. The current study may stimulate the use of SiO_2 and PMMA fibre coupled plastic scintillation detectors in medical dosimetry applications. The results of the PMMA scintillation detector are good and it is a promising detector for *in vivo* measurements due to its flexibility and low cost.

Contents

Abstract. ii

List of tables. vii

List of figures. viii

Chapter 1

Introduction. 1

1.1 Thesis objective 1

1.2 Radiotherapy. 6

Chapter 2

Uncertainties in Radiation Delivery. 8

2.1 Introduction. 8

2.2 Patient contour. 9

2.3 Geometric uncertainty. 10

2.4 Positioning uncertainty. 11

2.5 Systematic and random positioning errors. 13

2.6 Organ motion. 14

2.7 Minimizing damage to normal tissue. 15

2.8 Accuracy of the absolute does determination 17

2.9 Unavoidable uncertainties. 18

Chapter 3

Detector system. 20

3.1 Scintillation Dosimetry. 20

3.1.1 Introduction. 20

3.1.2 Light output and electron energy. 21

3.1.3 Scintillator materials. 22

3.2 Optical coupling. 23

3.3 Optical fiber light tubes. 25

3.3.1 Radiation effects on optical fiber. 31

3.3.1.1 Ionising radiation effects on optical fiber. 31

3.3.1.2 Stem light within optical fiber. 32

3.4 Optical lens. 33

3.5 Optical filter. 35

3.6 Light detection. 37

3.6.1 X-Omat V film. 38

3.6.2 Silicon photodiode. 38

3.7 Digital integrator system. 39

Chapter 4

Pre-design Studies. 43

4.1 Simplicity of the detection system. 43

4.2 Radiation detection part of the system. 44

4.3 Light guide system. 44

4.4 Light detection system. 45

4.5 Detector response based on plastic scintillator light and stem effect light. 45

4.6 Photographic detection experiments. 51

4.7 Detector system efficiency. 55

4.7.1 Intrinsic efficiency. 55

4.7.2 Light coupling efficiency. 55

4.7.3 Scintillator size. 56

4.8 Signal to noise (S/N) definition. 61

Chapter 5

Characteristics of SiO_2 & PMMA scintillation detectors for x-ray beam. 67

5.1 Introduction. 67
5.2 Reproducibility and stability of detector signals. 68
5.3 Dose rate proportionality. 69
5.4 Depth dose distribution in water. 74
5.5 Photon beam profiles. 79
5.6 Intensity linearity of the miniaturized detector. 80
5.7 Dependence on irradiation fibre length. 85
5.8 Dependence on irradiation field size. 88
5.9 Beam directional dependence. 88

Chapter 6

Ultimate design characteristics of detectors. 94

6.1 Introduction. 94
6.2 Linearity of the detectors signals at the integrator. 94
6.3 Detector sensitivity to field factor. 101
6.4 Reproducibility and stability of integrator signal. 104
6.5 Dose rate proportionality. 107
6.6 Intensity with distance. 112
6.7 Effect of incident beam angle on detectors response. 112
6.7.1 Effect of incident beam angle on fibre optics response. 115
6.7.2 Effect of incident beam angle on SiO_2 scintillation detector response. 115
6.7.3 Effect of beam incident angle on PMMA scintillation detector response. 119
6.8 Efficiency of optical filtration on fibres response. 126

6.8.1 Efficiency of optical filtration on SiO_2 fibre response. 127
6.8.2 Efficiency of optical filtration on PMMA fibre response. 130
6.8.3 Assessment of amount of unfiltered interference radiation. 134
6.9 Threshold of SiO_2 and PMMA scintillation detectors. 136

Conclusions. 140
Acknowledgements. 143
References. 145
Appendix A: Background information. 149
Appendix B: Electronic circuits. 157

List of Tables.

3.1	Principle characteristics of tissue equivalent plastic scintillator crystal (EJ-200) used in this study.....	24
3.2	Standard specifications of the optical fibre cables used.	30
3.3	Common specifications for fluorescence filter appropriate for this study. The filter was manufactured by Corion filters [32].	36
3.4	Standard specifications of photodiode used.	40
4.1	Densitometer reading for irradiation at two different beam angles, with and without plastic scintillator.	54
4.2	"d" parameter as a function of energy for plastic scintillators of 1.0mm and 2.0mm in diameter, both 10.0mm in length, for which L = 4V/S = 0.095 mm and 0.181 mm respectively.	59

List of Figures.

3.1 An optical fibre is a cylindrical dielectric waveguide. 26

3.2 Longitudinal cross-section of a single mode fibre. The critical angle (θ_c) for total reflection and acceptance cone half angle (θ_a) are also shown. 27

3.3 Geometry, refractive – index profile, and typical light rays in: (a) a multimode step-index fibre, (b) a single mode step-index fibre, and (c) a multimode graded-index fibre. 29

3.4 Schematic diagram shows the guiding plastic scintillator light: (a) transmitted light from fibre optic cable; (b) plano-convex lenses; (c) narrow bandwidth optical filter; (d) photodiode. 34

3.5 BPW21 photodiode spectral sensitivity from R.S Components.. 41

4.1 Response of plastic scintillator detector (signal) compared to calculated response using inverse square law when exposed to a 6 MV x-ray beam at 1.5cm depth in the water tank. 47

4.2 Percent depth dose in water phantom tank using plastic scintillator (P.S) and compared to the depth dose obtained using ionisation chamber (I.C) for 6 MV x-ray beam, 40X40cm^2 as field size, 250MU, and 100cm as source to surface distance. 48

4.3 6 MV x-ray beam linear accelerator x-ray beam profile in water tank phantom using prototype plastic scintillator (P.S) and compared to ionisation chamber (I.C). 49

4.4 Prototype plastic scintillator (P.S) as a main signal and plastic fibre guide (background) detector response from three different 6 MV x-ray beam angles. 90°, -45° (toward plastic scintillator) and 45° (toward photodiode), as the length of fibre optic cable under the beam increased. 50

4.5 Prototype plastic scintillator (signal) and plastic fibre guide (background) detector response from different irradiation beam size using 6 MV x-ray beam, 250MU, at 100cm SSD with 15&100mm depths in water tank. 52

4.6 Parameter "d" as a function of photon energy for two cylindrical plastic scintillators of 1.0mm and 2.0mm in diameter, both 10.0mm in length. 60

4.7 Optical response of plastic scintillators (p.s) of lengths 5.0mm, 10.0mm, and 15.0mm and of diameters 1.0mm, 2.0mm, and 3.0mm on irradiation by 16MU beam. 62

4.8 Optical response of plastic scintillators (p.s) of lengths 5.0mm, 10.0mm, and 15.0mm and of diameters 1.0mm, 2.0mm, and 3.0mm on irradiation by 8MU beam. 63

4.9 Optical response of plastic scintillators (p.s) of lengths 5.0mm, 10.0mm, and 15.0mm and of diameters 1.0mm, 2.0mm, and 3.0mm on irradiation by 4MU beam. 64

5.1 Response of miniaturized plastic scintillation detector using SiO_2 fibre in a 6 MV x-ray beam, with $10\times10cm^2$ as field size, 250MU, and 100cm source to phantom distance 70

5.2 Response of miniaturized plastic scintillation detector using PMMA fibre in a 6 MV x-ray beam, with $10\times10cm^2$ as field size, 250MU, and 100cm source to phantom distance 71

5.3 Detector response vs. dose rate of miniaturized prototype scintillation detector 10mm in length and 3mm in diameter at 6 MV photon energies using SiO_2 fibre optic light guide cable. ... 72

5.4 Detector response vs. dose rate of miniaturized prototype scintillation detector 10mm in length and 3mm in diameter at 6 MV photon energies using PMMA fibre optic light guide cable. 73

5.5 Percentage depth dose in water obtained using the miniaturized prototype plastic scintillation detector (p.s), using SiO_2 fibre optic cable. The results are compared to the depth dose obtained using 0.125 cm^3 PTW Semiflex chambers (I.C) for a 6 MV photon beam. 75

5.6 Percentage depth dose in water obtained using the miniaturized prototype plastic scintillation detector (p.s), using PMMA fibre optic cable. The results are compared to the depth dose obtained using 0.125 cm^3 PTW Semiflex chambers (I.C) for a 6 MV photon beam..... 76

5.7 Transverse dose profile of a 6 MV photon beam for 10x10 cm^2 field size at 15mm depth in water tank phantom using miniaturized plastic scintillation detector (p.s) which spliced into SiO_2 fibre optic material and compared with 0.125 cm^3 PTW Semiflex ionisation chambers (I.C). 81

5.8 Radial dose profile of a 6 MV photon beam for 10x10 cm^2 field size at 15mm depth in water tank phantom using miniaturized plastic scintillation detector (p.s) which spliced into SiO_2 fibre optic material and compared with 0.125 cm^3 PTW Semiflex ionisation chamber chambers (I.C). 82

5.9 Transverse dose profile of a 6 MV photon beam for 10x10 cm^2 field size at 15mm depth in water tank phantom using miniaturized plastic scintillation detector (p.s) which spliced into PMMA fibre optic material and compared with 0.125 cm^3PTW Semiflex ionisation chambers (I.C)..... 83

5.10 Radial dose profile of a 6 MV photon beam for 10x10 cm^2 field size at 15mm depth in water tank phantom using miniaturized plastic scintillation detector (p.s) which spliced into PMMA fibre optic material and compared with 0.125 cm^3 PTW Semiflex ionisation chambers (I.C). 84

5.11 Detectors response using SiO_2 and PMMA fibre optic light guides for 6MV photon beam at different source to surface distances, using 100MU, SSD=100, d_{max}=15mm on solid water phantom and dose rate of 250M/min. 86

5.12 Percentage increase on detector response due to irradiation of fibre optic cables, compared with plastic scintillators response only. Irradiation made using 6MV photon beam, 100MU, SSD=100cm, d_{max}=15mm at Perspex phantom and dose rate of 250M/min. 87

5.13 Effect of beam size on miniaturized plastic scintillation detector response using SiO_2 and PMMA fibre optic light guide for 6MV photon beam with 100MU, SSD=100cm, d_{max}=15mm at Perspex phantom and dose rate of 250M/min. 89

5.14 Experimental set-up of SiO_2 and PMMA fibre optic light guide in the photon beam to study the effect of beam angle on detector response. The beam size was fixed to be $10\times10cm^2$ during all experiments. 90

5.15 The radiation induced light intensity for SiO_2 and PMMA fibre optic light guide at different photon beam angles irradiated toward photodiode as in set-up shown in figure 7.14. 91

5.16 The radiation induced light intensity for SiO_2 and PMMA fibre optic light guide at different photon beam angle irradiated toward plastic scintillator as in set-up in figure 5.14. 93

6.1 Response using a pulse integrator of the SiO_2 cable scintillation detector 3mm in diameter and 10mm long exposed to 6MV x-ray photon beam, at field size of $10x10cm^2$. 95

6.2 Response using a pulse integrator of the SiO_2 cable scintillation detector 3mm in diameter and 10mm long exposed to 6MV x-ray photon beam, at field size of $20x20cm^2$. 96

6.3 Response using a pulse integrator of the PMMA cable scintillation detector 3mm in diameter and 10mm long exposed to 6MV x-ray photon beam, at field size of $10x10cm^2$. 97

6.4 Response using a pulse integrator of the PMMA cable scintillation detector 3mm in diameter and 10mm long exposed to 6MV x-ray photon beam, at field size of $20x20cm^2$. 98

6.5 Response of SiO_2 fibre irradiated by 6MV x-ray beam, field size of $10x10cm^2$ respectively, and compared to the values calculated by multiplying the first measured reading by the same factor by which the doses were increased. 99

6.6 Response of SiO_2 fibre irradiated by 6MV x-ray beam, field size of $20x20cm^2$ respectively, and compared to the values calculated by multiplying the first measured reading by the same factor by which the doses were increased. 100

6.7 Response of PMMA fibre irradiated by 6MV x-ray beam, field size of $10x10cm^2$ respectively, and compared to the values calculated by multiplying the first measured reading by the same factor by which the doses were increased. 102

6.8 Response of PMMA fibre irradiated by 6MV x-ray beam, field size of $20x20cm^2$ respectively, and compared to the values calculated by multiplying the first measured reading by the same factor by which the doses were increased. 103

6.9 Response of SiO_2 scintillation detector irradiated by 6MV x-ray beam size of $10x10cm^2$ and $20x20cm^2$. 105

6.10 Response of PMMA scintillation detector irradiated by 6MV x-ray beam size of $10x10cm^2$ and $20x20cm^2$. 106

6.11 Response of plastic scintillation detector using SiO_2 fibre in a 6 MV x-ray beam, 10x10cm^2 as field size, 250MU/min dose rate, d_{max}=15mm, and 100cm source to surface distance in water phantom, vs. number of readings for a total dose of 20cGy. 108

6.12 Response of plastic scintillation detector using PMMA fibre in a 6 MV x-ray beam, 10x10cm^2 as field size, 250MU/min dose rate, d_{max}=15mm, and 100cm source to surface distance in water phantom, vs. number of readings for a total dose of 20cGy. 109

6.13 Dose rate independence of SiO_2 scintillation detector, at 6 MV photon energy, 10x10cm^2 field size, SSD of 100cm and d_{max} 15mm in water phantom for a total dose of 20cGy. 110

6.14 Dose rate independence of PMMA scintillation detector, at 6 MV photon energy, 10x10cm^2 field size, SSD 100cm and d_{max} 15mm in water phantom for a total dose of 20cGy. 111

6.15 Measured response of SiO_2 scintillation detector at different SSD and calculated response due to inverse square law (ISL) for a total dose 20cGy, d_{max}=15mm, dose rate of 250M/min at water phantom. 113

6.16 Measured response of PMMA scintillation detector at different SSD and calculated response due to inverse square law (ISL) for a total dose 20cGy, d_{max}=15mm, dose rate of 250M/min at water phantom. 114

6.17 Effect of incident beam angle on SiO_2 and PMMA fibre optic response for 20x20cm^2 half field, using Varian 2400C 6MV linear accelerator. 116

6.18 Effect of incident beam angle on SiO_2 fibre optic response for $20x20cm^2$ half field, using Varian 2400C 6MV linear accelerator. 117

6.19 Effect of incident beam angle on PMMA fibre optic response for $20x20cm^2$ half field, using Varian 2400C 6MV linear accelerator. 118

6.20 Effect of incident beam angle on SiO_2 scintillation detector response for $10x10cm^2$ half field, using Varian 2400C 6MV linear accelerator. 120

6.21 Effect of incident beam angle on SiO_2 scintillation detector response for $20x20cm^2$ half field, using Varian 2400C 6MV linear accelerator. 121

6.22 Effect of incident beam angle on PMMA scintillation detector response for $10x10cm^2$ half field, using Varian 2400C 6MV linear accelerator. 122

6.23 Effect of incident beam angle on PMMA scintillation detector response for $20x20cm^2$ half field, using Varian 2400C 6MV linear accelerator. 123

6.24 Effect of incident beam angle on SiO_2 and PMMA scintillation detector response for $10x10cm^2$ half field, using Varian 2400C 6MV linear accelerator. 124

6.25 Effect of incident beam angle on SiO_2 and PMMA scintillation detector response for $20x20cm^2$ half field, using Varian 2400C 6MV linear accelerator. 125

6.26 Radiation detected from irradiating the SiO_2 fibre without the scintillator with a 10 x 10 cm^2 field size..... 128

6.27 Radiation detected from irradiating the SiO_2 fibre without the scintillator with a 20 x 20 cm^2 field size..... 129

6.28 Radiation detected from irradiating the PMMA fibre without the scintillator with a 10 x 10 cm^2 field size..... 132

6.29 Radiation detected from irradiating the PMMA fibre without the scintillator with a 20 x 20 cm^2 field size..... 133

6.30 Effect of optical filter on SiO_2 and PMMA fibre optic light guide response for 10x10cm^2 field size. 135

6.31 Absorption curve (lead absorber) of 6MV x-ray beam. The beam was attenuated by a factor of $^1/_{32}$ for 10x10cm^2 field size, dose of 2Gy, SSD=100cm, d_{max}=15mm and 250MU/min as dose rate..... 138

6.32 Absorption curve (lead absorber) of 6MV x-ray beam as described in figure 8.32 but in sem-log plot to demonstrate the exponential nature of the curves. 139

CHAPTER 1

INTRODUCTION

1.1 Thesis objectives

Tissue equivalent plastic scintillators are an interesting development in high-energy photon dosimetry. They have the potential to reduce the number of corrections needed to obtain accurate absorbed dose measurements in tissue and they can provide fast, real-time measurements [1]. Although tissue equivalent plastic scintillators have been shown to have many desirable dosimetric properties, there is no successful commercial detector system of this type available for routine clinical use in radiation oncology [2]. The main factor preventing this technology is the minimization of noise capture [2].

A typical tissue equivalent plastic scintillator probe consists of a small volume of organic scintillator material coupled to a photodiode by an optical fibre light guide. The optical fibre light guide can be made from silicon dioxide (SiO_2) or polymethyl-methacrylate (PMMA) and is long enough to position the photodiode safely away from the radiation field. This relatively simple dosimeter is not without problems. The light received at the photodiode has been shown to be a combination of the main signal emitted by plastic scintillator and interference light from Cerenkov and fluorescence radiation created in the optical fibre. Only the light signal from the scintillator material is related to the radiation dose of the tissue. The Cerenkov and optical fibre fluorescence is related to amount and position of the optical fibre exposed to the radiation. Therefore, the signal measured by the photodiode must be corrected for the contribution from Cerenkov and fluorescence radiation to allow truthful measurement of the absorbed dose deposited in the scintillator material [1].

Clift *et al.* [3] suggested that two optical fibres should be used in parallel. One fibre is spliced with plastic scintillator to measure the main scintillation

signal and interference signals while the other fibre without the plastic scintillator will only measure the interference signals. In this way, the two signals can be subtracted to yield the scintillation signal only. The use of a second optical fibre as a background detector limits the use of this promising dosimeter and has prevented the commercialization of the dosimeter [2]. The second optical fibre not only makes the dosimeter much larger, but also makes the fibre much more rigid. Therefore, it is desirable to investigate new methods that eliminate the signal contribution from Cerenkov and fluorescence radiation to the detector output and that do not require a second background detector.

The aim of this work is to minimize the Cerenkov and fluorescence contributions to a miniaturized plastic scintillator dosimeter. The present study achieved this reduction by developing a scintillator detector system that is capable of maintaining the plastic scintillator signal and filters out the interference signals. The techniques that are used to eliminate unwanted signal includes a combination of optical and time filtration of the light signals. Light signals that are not consistent with the emission spectrum of the plastic scintillator and time profile of the linear accelerator pulse are rejected.

The present research is conducted to assess the feasibility of measuring *in-vivo* doses of high-energy photon beams with a miniature scintillator dosimeter. To this end, this study will evaluate the general properties of these detectors. The accuracy and precision of the proposed dosimeter will be determined by comparing it to other common dosimeters. The advantages and disadvantages of the PMMA optical fibre light guide will be compared to SiO_2 fibre optic light guide.

1.2 Radiotherapy

To understand why a miniature scintillator dosimeter would be advantageous to use in radiotherapy, we first must review the goals and

limitations of radiotherapy. In particular, we consider problems faced when trying to target the high energy radiation to the tumour.

High energy x-rays, gamma rays or electron radiation therapy are used extensively to treat cancer [4]. Radiation is effective in treating the abnormal growth of tissues because it damages cancer cells [4]. However, surrounding normal tissues may also be effected and damaged, which is one reason for the occurrence of side effects. The objective of radiation therapy is to destroy cancer cells with as little damage as possible to the adjacent normal tissues.

The most common application of radiotherapy is usually used to treat cancer. This treatment can be termed curative radiotherapy. To be curative, the treatment must eradicate all cancer cells and prevent them from regrowing and multiplying. This type of curative treatment is achieved by delivering high radiation doses to the region of cancer. Radiation therapy may also be used to relieve cancer symptoms or reduce the growth rate. This type of treatment is termed palliative radiotherapy. Palliative radiotherapy may be applied to relieve pain in cases such as bone invasion, headaches due to brain metastasis, paralysis due to spinal cord compression, or to stop bleeding due to involvement of the skin, bladder, or bowels. In this type of treatment, radiation therapy requires fewer treatments or lower dose treatments than curative radiation therapy because not all of the cancer cells have to be killed to relieve the symptoms.

The two most basic types of radiation treatment are external beam radiation therapy and radioactive implants (brachytherapy). In external beam radiation therapy, a linear accelerator is used to direct the radiation to the cancer through the skin surface. Currently, most of the patients who are treated with radiation therapy are treated with external beam irradiation. In radioactive implants, radioactive materials are placed inside the body within or next to the tumour using intra-cavity, intravenous, intra-arterial or inhalation methods. These types of treatments are mostly used to treat well-defined and localized tumours with minimum radiation doses to the surrounding healthy tissues. Also in some

particular cases, patients may receive a combination of external beam radiation therapy followed by a radioactive implant.

Radiotherapy is technically difficult to deliver appropriate doses to the tumour without significant risk of damaging normal critical structures. In recent years, an x-ray radiograph, a fluoroscopy image, a computerized axial tomography scan, or other medical image of the cancer region helps the radiation oncologist to determine how one should direct the treatment beams in order to give a maximum radiation dose to the tumour, while sparing as much of the surrounding normal tissues as possible [5].

In order to reduce the amount of radiation delivered to normal tissue while trying to make certain that the tumour receives the full dose, beams are customarily shaped so that they treat tissues a few centimetres beyond the margins of the tumour. It is necessary that the patient be treated while lying in a comfortable position and that his or her position be the same each day to avoid possible slight daily variations to the area targeted by the radiation [5].

In an attempt to save normal tissue from as much irradiation as possible, high energy electromagnetic (photon) beams are used to treat tumours deep in thick body parts [5]. Low energy photon beams and high energy electron beams are used to treat tumours lying near the skin and tumours lying over radiation sensitive structures such as the spinal cord [5]. In an attempt to reduce the damage to normal structures surrounding a cancer, fractionation of radiation treatment may help to achieve a desired level of biological damage to the gross tumour volume and spare the surrounding healthy volume [6]. To improve the objectives in radiotherapy, the radiation beam must be well collimated by the use of collimators, blocks, and wedges. However, some healthy tissues will inevitably be irradiated because the tumour is almost always surrounded by normal tissue [7].

An important question with respect to radiation therapy is what degree of accuracy in dose delivery can be achieved in clinical practice [8]. In clinical

practice, the desired level of accuracy may not be possible to achieve. An overall check of the whole dosimetry procedure is therefore useful and can be carried out by performing dose measurements during treatment. An *in vivo* dose measurement can be performed as entrance dose, exit dose or intracavity dose determination [8]. Entrance dose measurements can sometimes lead to a modification of treatment techniques. Entrance dose measurements combined with exit dose measurements can be used to demonstrate possible deviations between planned and actual radiation absorption. The entrance and exit dose measurements can result in recommendations for improved dose calculations, although such corrections still rely upon several assumptions about the specific anatomy of the patient and how much each different tissue absorbs and scatters the radiation.

Clinical studies [8] have shown the usefulness of *in vivo* dose measurements for the verification of an accurate dose delivered to patients. The ultimate check of the actual dose delivered to an individual patient can only be performed at the patient level, by means of *in vivo* dosimetry. Therefore, it is recommended by the International Commission on Radiation units (ICRU) [9]. Yet, *in vivo* dosimetry is rarely performed because we lack the appropriate miniature dosimeters to make such measurements.

In-vivo radiation dose measurements are an important treatment quality assurance process. In this process the accuracy of the dose delivered is verified, information is provided on beam location, and it checks that radiation is not delivered to nearby healthy tissue. The requirements for a clinical useful dosimeter include: very small size, being tissue equivalent, having a fast response, having a linear response with dose and relatively inexpensive. The small size is needed to assess local doses, and to avoid exposure of sensitive tissue peripheral to the radiation beam. If small enough, it may be possible to insert one or more dosimeters inside the human body. As a tissue equivalent dosimeter, the response per unit dose would be independent of radiation energy and calibration repetitions will not be necessary when the energy of the incident radiation has changed. As a fast response dosimeter, the dose can be evaluated immediately and the exposure

time can be modified accordingly. An inexpensive dosimeter may be disposable and several dosimeters can be used simultaneously.

Currently, *in-vivo* patient monitoring is commonly performed using LiF thermoluminescent dosimeters (TLD's), diode detectors, metal oxide semiconductor field effect transistors (MOS-FET) and optically stimulated luminescence (OSL). However, these current systems do not satisfy the all desired requirements [10,11].

TLD's are excellent integrating dosimeters. They are available in a wide variety of forms and sizes and their thickness makes them useful for surface dosimetry. They are insensitive to changes in photon and electron radiation, energy, dose rate, and radiation direction. They have a long useful lifetime. Despite all of these advantages, there are several drawbacks to the use of this system for *in-vivo* measurements. The primary drawback is that the read out system is not coupled to the detector, meaning that real time feedback is not possible. This necessitates the need for post irradiation evaluation with a relatively long processing time.

Silicon diodes can replace small ionisation chambers as *in-vivo* dosimeters. Silicon diodes are the most popular dosimeters for routine clinical measurements. The diodes produce an electrical current when irradiated. The current is collected and integrated to obtain a reading corresponding to absorbed dose. The main disadvantages of diodes are their size, which limits their use as internal dose monitors, the response is temperature dependent and they have a finite operational lifetime due to accumulated dose.

MOS-FET dosimeters are new to clinical radiation dosimetry. Their size relative to diodes significantly improves spatial accuracy relative to diodes. The sensitivity of MOS-FET is similar to that of diodes and they can be used for surface dose measurements as they lack inherent build up. The main drawbacks of MOS-FET as dosimeters are the short operational lifetime and the requirement for

frequent recalibration. Also, the angular dependence of their dose response can vary up to 17%. Moreover, the response of MOS-FET is non linear at high doses [10].

An OSL radiation dosimeter system for the remote monitoring of radiation sources has been documented. The system includes a radiation sensitive optically stimulated dosimeter that utilizes a new, doped glass material that stores energy from ionising radiation and releases the stored energy in the form of optically stimulated luminescent light when stimulated by light at a second wavelength. This system is characterized by low noise interference, but suffers from significant fading and not being a tissue equivalent. Moreover, this system requires injecting light energy to heat and anneal the crystal, which complicates its use in routine clinical radiotherapy dosimetry [10].

The research in this thesis proposes a dosimeter consisting of a tissue equivalent plastic scintillator mounted on an optical fibre. When the scintillator is exposed to radiation, visible light (~ 400-500 nm) is produced, and transmitted through light guide. At the distal end of the light guide, the photodiode converts light into an electrical signal; the current produced is proportional to the dose rate. The total signal produced will be proportional to the total dose received.

The dosimeter can be very small and is tissue equivalent. The scintillator and optical fibre are relatively inexpensive and may be made as disposable devices. The scintillator and photodiode have very fast responses of about 1 ns. This system, if it responds as anticipated, fulfils the requirements for an *in vivo* dosimeter.

CHAPTER 2

Uncertainties in Radiation Delivery: the Need for *in vivo* Dosimeters

2.1 Introduction

An important question with respect to radiation therapy is what degree of accuracy can be achieved for dose delivery in clinical practice. Unfortunately, the desired level of accuracy cannot always be achieved. An overall check of the whole dosimetry procedure is therefore useful and can be carried out by performing dose measurements in real time during treatment. Measuring the entrance dose, the exit dose, or the intracavity dose using miniature plastic scintillator dosimeters can perform such *in-vivo* dose measurements. Only the intracavity measurement of the dose gives the explicit dose without underlying assumptions.

In radiation therapy, two important aspects must be considered to improve the accuracy and precision of dose delivery. First, one must consider the actual dose delivered to the tumour and surrounding normal tissue. Second, one must consider geometry of treatment delivery [12]. These two aspects are essential to ensure better outcomes in terms of greater tumour control and reduced complication rate to the adjacent normal tissue. ICRU recommended that the radiation dose delivered to the defined target volume should be within ±5% [12]. Real time *in-vivo* dose measurements may help to achieve the desired level of accuracy in real practice.

To deliver a certain radiation dose to the gross tumour volume with highest accuracy, several procedures must take place. These procedures involve the calibration of the linear accelerator, the localization of the gross tumour volume and all relevant biological structures using advance imaging modalities, the

treatment planning, the dose calculation and the delivery geometry. Each of these procedures has different contributions and related uncertainties to the actual radiation dose delivered to the tumour and surrounding healthy tissue. The relative dosimetry is defined as a dose ratio between two different points [10]. Therefore, it is important to calibrate all radiation beams to minimise any contribution from absolute dosimetry to the overall uncertainty in the delivered dose.

Uncertainties are an unavoidable part of the radiotherapy process. Uncertainty in the dose deposited in the tumour can also arise from many other factors. To name a few, the uncertainty can also be influenced by organ motion, patient positioning errors, fluctuations in machine output, delineation of regions of interest, the modality of imaging used, treatment planning algorithm assumptions and calibration techniques. There is uncertainty in the dose required to eradicate a tumour due to inter-patient variations in patient-specific variables such as sensitivity to radiation; and there is uncertainty in the dose-volume restraints that limit doses to normal tissue. Real investigation of the actual dose delivered to target and normal tissue, the effect of dose uncertainty on radiobiological indices, and techniques to display the dose uncertainty in a treatment planning system are essential factors in the radiotherapy process.

Here we will discuss some of the uncertainties that affect the dose of radiation delivered to a tumour site. We will also discuss the need for accuracy when irradiating a patient. As we elucidate below, the sources of the uncertainties come from many sources, including the equipment, the patient, and a lack of knowledge of the specific tumour. As you read through this section, keep in mind how a miniature *in vivo* dosimeter might be helpful in reducing the uncertainties and lead to known accuracy in the delivered dose.

2.2 Patient contour

Radiation treatment planning value depends on the accuracy of the position and shape of the patient on a course-to-course basis during the entire treatment

[7]. The linear accelerator table on which the patient will be treated should match in every respect the table on the simulator where the patient contour will be specified. The overweight patient has a contour that changes from day-to-day, while the patient with less padding might find the hard table so uncomfortable that it is difficult to lie still for the duration of the treatment. Therefore, immobilization devices such as patient moulds or shells become important, especially for treatment of the head and neck tumours [7]. For treatment in the trunk, a greater dependence is placed upon the ability of the therapist to position the patient in the same way each time during course of treatments, with special attention given to the position of the lower and upper extremities.

A patient shell that fits and immobilizes the patient enables the planning and treatment to be carried out with acceptable accuracy. A good shell enables accurate determination of the location of the tumour from surface markers attached to the shell, achievement of accurate position of the patient each day during the course of treatment, provides an accurate and constant patient contour, and provides accurate beam entry and exit points. Generally, the patient should be treated in one position if possible because both internal anatomy and external contours can change dramatically if the patient is treated in both the supine and prone positions for anterior and posterior fields, respectively [7].

In vivo dosimeters would help to understand these changes of tumour position in the patients due to orientation, obesity, imaging errors and many other factors. There is clearly a clinical need for such a dosimeter.

2.3 Geometric uncertainty

To achieve maximum objectives of dose escalation and increase tumour control; the geometric precision of radiotherapy treatments must be increased

[13]. Practically, many approaches may help to reduce geometric uncertainties of radiotherapy, these include use of immobilization devices and set-up aids during the treatment procedures. These might also reduce random and systematic components of set-up errors and unavoidable organ motion. Jaffray D.A. *et al.* [13] divided these approaches into two categories: off-line and on-line. The risk associated with each approach must also be considered and justified.

To evaluate geometric uncertainty in radiation therapy procedures, ICRU Report 62 suggests drawing margins around organs at risk. However, the latest developments on dose computation, linear accelerator and imaging techniques will increase the geometry precision on radiation dose delivery.

2.4 Positioning uncertainty

Patient positioning is one of the major uncertainties in radiation therapy due to several anatomical and psychological factors that need consideration. Dose delivery to the tumour relates to the ability to set up the patient accurately and reproducibly from day to day. Therefore, it is important that at the beginning of the planning process, a comfortable and reproducible patient position is developed. The specific patient positioning strategy will depend strongly on the volume to be irradiated. High dose and small volume techniques might require millimetre precision, whereas some large volume techniques might allow for a larger margin of error [12]. Reproducibility of patient positioning is very important on radiation treatment procedure, and to ensure that several techniques are used in real practice to minimize uncertainty in patient positioning during radiation treatment. These techniques are generally divided into four categories; no immobilization that involves patient positioning aids such as pillows and a headrest. For such a set-up it is possible that the patient position might change during the actual beam-on time. Hence a review of patient set-up immediately after treatment will give some indication of stability. Simple immobilization is another category; it involves some restriction of movement and requires voluntary

help from the patient. Complex immobilization involves individualized immobilization devices that restrict patient motion and ensure reproducible patient positioning.

Monitoring techniques include techniques for monitoring patient positioning and reproducibility of set-up, and may or may not be used in conjunction with immobilization devices. However, the results of monitoring techniques provide information on improvements required in the immobilization techniques that are used. Television monitoring provides a means of detecting obvious changes in patient position. Real time electronic portal imaging provides a means of observing patient positioning, although the resultant image gives only a beam's eye perspective of the irradiated volume [12]. These techniques allow the radiation therapy technologist to make positioning adjustments either before giving a full daily dose from all fields or by stopping the irradiation during treatment.

The quality of the radiation therapy delivered in the treatment of breast cancer, as an example, is subject to setup errors and organ motion uncertainties. Mavroidis P. *et al.* [14] reported on 60 breast cancer patients (24 resected with negative node involvement, 13 resected with positive node involvement and 23 ablated), who were treated with three different irradiation techniques. He stated that uncertainties in dose delivery distributions in the lung were affected and taking positioning uncertainty and breathing effects into account is essential. In this way the real dose distributions delivered to the patients can be more accurately determined. Breathing is assumed to have a linear behaviour, because of the regular chest wall movement during expiration and inspiration, and this may reduce the degree of uncertainty.

In some cases, traditional radiotherapy calls for imaging studies several days before treatment to determine the precise location of tumours and normal surrounding tissues. Use of these images to develop a treatment plan may include some uncertainty because tumours are likely to change shape or move in the pre-

treatment period. For this reason, a margin of error is introduced and a zone around the tumour that is larger than the tumour itself is normally treated. This uncertainty about the exact position of the tumour has always meant using lower than desired radiation doses to avoid applying excessive doses to the surrounding normal tissue. To avoid these uncertainties, pre-treatment images should be obtained just before treatment, with the patient in the exact position he or she will be treated in. This means not only less chance for errors in tumour targeting and in patient positioning, but also the ability to increase the dose to the tumour by virtue of more certainty in the location of the tumour.

Rosenthal S.A. *et al.* [15] determined the magnitude of patient positioning errors associated with six field conformal therapies for carcinoma of the prostate. The mean and median simulation-to-treatment variability was 0.4 cm for those patients treated with immobilization, versus 0.6 cm for those treated without immobilization. Also, there was a significant reduction in the number of patients with treatment-to-treatment variability $\geq$ 0.5 cm for patients treated with immobilization. Most oncologists conclude that the use of immobilization devices significantly reduces errors in-patient positioning, potentially permitting the use of smaller treatment volumes, and it should be a component of conformal radiation therapy programs for prostate carcinoma.

2.5 Systematic and random positioning errors

Prostate, lung, and breast cancer are some of the most commonly diagnosed cancers in the world. One of the common treatment modalities for these cancers is external beam radiation therapy (EBRT). Photons or electrons that are generated by linear accelerator are used to target the cancer cells during external beam radiation therapy procedures. This procedure includes two major processes, treatment planning and treatment delivery, and each of these major processes may be subdivided into a number of tasks according to the generation and type of linear accelerator and planning system. The small errors that occur from each task in these procedures may combine to form large errors. During treatment

preparation errors may arise and create a detectable impact on the entire treatment. This type of errors is called systematic errors. While the errors that occur during treatment delivery are termed random errors [49].

Poor positioning of a patient during simulation procedure; organ motion; errors that arises due to low image contrast; fluctuation in the linear accelerator output; errors arise due to planning software problems and mechanical faults of linear accelerator are the common systematic errors in real practice [49]. Inaccurate patient positioning, continuous organ motion and variability of the linear accelerator output are the most random errors in practice [49]. To detect systematic and random positioning errors, portal images may be acquired to assess the actual position of radiation fields used in treatment delivery.

Clinically, the irradiation of prostate cancer as an example that is primarily associated with the use of fixation devices [17]. The normal range of the margin around the prostate is 0.6 cm to 1.5 cm [17]. This wide range is justified due to the rectum and bladder volume. For this reason the patient under prostate irradiation is usually asked to empty the bladder prior to each treatment fraction. T. Haken *et al*, illustrated that the prostate could move up to 2.0 cm between treatment fractions [18]. This demonstrates the significant uncertainties in the actual radiation dose received by the tumour.

2.6 Organ motion

The total positional changes of the organ from inspiration and expiration determine the total organ movement. Random and cyclical movement are the common types of organ motion within human body [49]. Breathing will create cyclical moving of the abdominal organs, while the organs in the pelvic cage will move randomly between the treatment fractions. Practically, a bony landmarks is described at the simulation procedure to help in measuring inter fraction deviation during the treatment. Recently, the study of systematic errors between planning

CT images and the mean organ positioning during fractionated treatment has led to significant interest in systematic organ motion error [1]. The respiratory forces are responsible for the major random inter patient systematic organ motion error during a delivered dose. Therefore, many authors report that they are measuring the total organ movement for abdominal organs.

On an attempt to determine the magnitude of organ motion, the volume that contains all movements of the clinical target volume must be specified and compared with bony anatomical landmarks. Two main possible variations may take place in clinical practice. First, inter fraction variations that may occur when a patient voids before some fractions or when the patient sit or lie in an inconsistent position on the treatment table. Second, intra fraction variation that may occur due to un avoidable reasons such as breathing, digestive processes or heart movement [49].

Due to un avoidable movement of the organs surrounding the treatment target, the internal planning target volume (IPTV) which describes a volume to contain all movements of the clinical target volume (CTV) must be enlarged to cover all the tumour and surrounding normal tissues which justifies the real need of the *in-vivo* radiation dose measurements in real practice toward reducing the internal planning target volume.

2.7 Minimizing damage to normal tissue

In the absence of *in vivo* measurements to absolutely determine the dose of radiation delivered to a tumour, there are several strategies that radiation oncologists routinely utilize to keep the risk of damage to normal tissue as low as possible. These strategies include; use of high energy x-rays to avoid any energy deposition on the skin and to penetrate deep within the body. Obviously the surface receives some radiation, but unless the skin is specifically targeted for treatment, radiation "skin burns" are now very uncommon. Also, tumour volume

under treatment must be well defined as possible to receive the full impact of treatment while the normal tissue surrounding should, ideally, receive only obligatory amount of radiation. Practically, it is too difficult to deliver a certain radiation dose to a particular volume within irregular area without a significant irradiation of the volume surrounding to the gross target volume. For this reason, unavoidable radiation dose delivered to the normal tissue adjacent to the gross target volume should be evaluated. Ideally, one would like to measure the amount of radiation incident upon the normal adjacent tissue using some form of dosimeter that does not interfere with the treatment.

In practice, it is not easy to determine the exact location that needs to be irradiated. Therefore, the radiation oncologist should take all the advantages of all available modalities to define the actual volume that has to be irradiated. X-ray, CT, MRI are the suitable techniques for most of the radiation oncologist to localize the tumour volume with high precision. Moreover, these modalities have great value for the assessment of radiation hazards to the normal tissues surrounding the gross target volume.

Based on the risk benefit rule, the normal tissue surrounding the tumour must be spared. Therefore, the radiation oncologist should have enough knowledge of internal anatomy and metastasis profiles to ensure the irradiation of all cancerous cells and in the same time spare as many of the normal tissue cells as possible.

Radiation therapy typically requires 30-40 treatments, and the dose delivery must be precisely given to the same target volume within 0.5 – 1.0 cm daily variation [4]. The risk of under dosing the tumour and/or overdosing the surrounding normal tissues especially critical structures like the spinal cord and kidneys, must be well defined and fully justified during radiation therapy treatment. Also, the use of multiple treatment fields is a good technique toward reducing the risk to normal tissue because the total irradiated volume will be sharply specified and minimized.

Moreover, a basic principle of modern radiation oncology is that of fractionation which plays an important role in reducing the risk to normal tissue. Since the radiation beam cannot distinguish between tumour and normal tissue, radiation oncologists must take advantage of any inherent differences between the two types of tissue. Fortunately most types of cancer cells are irreversibly damaged and killed by radiation at much lower doses than are normal cells. In other words, cancer cells tend to be more sensitive and normal tissues more resistant to radiation. Therefore, a dose of radiation is chosen for each individual treatment or fraction that is high enough to cause some damage to the cancer, but sufficiently low that most, if not all, of the normal tissue will be spared permanent damage. By delivering multiple such *fractions* in rapid succession, it is possible to administer a total dose of radiation that is adequate to kill off the tumour, yet only minimally damaging the surrounding normal tissue.

2.8 Accuracy of the absolute dose determination

An ionisation chamber is the first choice to evaluate the accuracy in the absolute dose measurement [12]. The ionisation chamber and its accessories such as cables and connectors must be well designed and regularly maintained to ensure normal functioning according to the specifications. Small polarity effect, low ion recombination, and a low leakage are the most important characteristics affecting the accuracy of the absolute dose determination [12]. Therefore, it is important to maintain a suitable high voltage supply in order to determine these effects. The electrometer should be regularly calibrated to ensure long-term stability. Also, the electrometer must comply with all the required features of the ionisation chamber and should have enough digits to reduce rounding errors. In order to determine the conversion and correction factors required for the absorbed dose calculation, it is essential that the materials and dimensions of the wall, central electrode and build up cap are well known and clearly specified [12]. The uncertainty in the calibration factor obtained from the standard dosimetry

laboratory is yet another important contribution to the overall accuracy of dose measurement. Moreover, the correction and conversion factors required in the computation of the absorbed dose from the ionisation chamber reading confers additional uncertainty.

2.9 Unavoidable uncertainties

This chapter has demonstrated the importance of considering the unavoidable uncertainty during the planning and delivery of a radiotherapy treatment. Across all sites, detailed knowledge regarding the values and characteristics of errors should be considered. Combined with techniques to control the magnitude of errors, careful efforts are needed to account for them as well. The best opportunity to account for uncertainty is in the planning process, using methods that reflect the statistical nature of many of the errors. The prostate has been illustrated to move up to 2 cm inter fraction due to rectal, and to a lesser extent, bowel distension [18]. Following the suggestions of the ICRU reports [9], combined with statistical dose based techniques, suitable CTV>PTV margins can be calculated. But, a large unpredicted movement is always possible, as is a patient-specific trend. Repositioning the patient is not trivial because the prostate is not visible in portal images. Other imaging techniques, such as kilo voltage or CT have been suggested in the literature. However these techniques have not been shown to be efficient or integrated into commercial treatment planning software. Clearly, the assessment of potential organ movement and patient position is the best option.

As described above, random and/or cyclical movement of the gross tumour volume and adjacent tissue is unavoidable. As a consequence real time *in vivo* measurements during treatment courses have the greatest priority for radiation oncology applications. These ensure real time evaluation of the delivered radiation dose, and give some information about any uncertainties within the planned treatment system. As yet, deviation in radiation delivery is crucial and

cannot be ignored especially deviations due to inter-patient or intra-patient movement. Most of the recent literature states that further studies and computational programs are necessary to improve the uncertainty values for radiation treatment techniques. Also, most of the new techniques to improve the precision of planning systems are extremely expensive and are not used in most treatment institutions. Therefore, there is a real need for a simplified tissue equivalent detector, which does not interrupt or attenuate the radiation beam and is easily applied to the patient with full flexibility. Such a system may reduce the unavoidable irradiation of the normal healthy tissue surrounding the gross tumour volume. Moreover, this system may reduce the size of the planned target volume and treated target volume.

CHAPTER 3

The Detector System

3.1 Scintillation Dosimetry

In this chapter is a description of the dosimeter that was constructed and review the components used in the construction. We discuss options that are available and why we chose particular components. We discuss the physical processes, the alternatives and advantages and disadvantages of the alternatives.

3.1.1 Introduction

Most translucent materials that luminesce in a suitable wavelength range when exposed to ionising radiation can act as a detector. Such detectors are broadly categorised as scintillators. Scintillators that are of particular interest in radiation therapy are those that show high translucence to the emitted light, with correspondingly high ionising radiation sensitivity and a fast response. For the particular application considered in this study, the chosen scintillation material was expected to convert the kinetic energy of charged particles into detectable light with high scintillation efficiency and with linear conversion. Thus, the visible light produced should be proportional to deposited energy of the ionising radiation over as large a range as possible. The translucent material density and atomic composition should resemble human tissue as closely as possible.

Luminescence is a general term defining the emission of electromagnetic radiation, typically visible or near-visible light, in excess of thermal radiation after some form of excitation. There are a number of processes that can lead to the emission of visible light. In the case of fast responding organic scintillators, fluorescence is the more exact terminology. Fluorescence is the near prompt emission of light in the visible range from a material following its excitation by some means [19]. It is typical to distinguish fluorescence from phosphorescence and delayed fluorescence, which differ from each other mainly in respect to the

duration of the emission process after the excitation is removed. Phosphorescence is the emission of light of longer wavelength than that of fluorescence, and with decay times greater than 10 microseconds [20]. Fluorescence decay times of most organic scintillator are of the order of nanoseconds, whereas delayed fluorescence results in the same emission spectrum as fluorescence, but with a much longer emission time following excitation and with a much lower yield or quantum efficiency.

It is also useful to differentiate between luminescence and thermo-luminescence. These differ from each other in the duration of the emission process after the excitation is removed. Thermoluminescence, a contraction for thermally stimulated luminescence, occurs when the mean excited state lifetime at room temperature is very long. The material in the excited state requires heating to release the trapped charge-carriers and the emission of light. Thermo-luminescence generally involves an organic scintillator, the fluorescence of which results from molecular de-excitation processes.

3.1.2 Light output and electron energy

The scintillator responds directly to ionisation generated by charged particles, such as electrons. Uncharged particles such as photons or neutrons are detected after they produce charged recoil nuclei within the scintillator. In both cases, the energy delivered to the scintillating material is by the primary or secondary charged particles through the many small coulomb-force interactions that occur along the track of each charged particle.

A relatively small fraction of the kinetic energy lost by a charged particle in a scintillator is converted into fluorescent light energy. The rest of the energy is dissipated non-radiatively, mainly in the form of lattice vibrations or heat. The scintillation efficiency (fraction of the particle energy converted to fluorescent light energy) differs for each type of scintillator and depends on the type of

charged particle producing the ionisation [20]. For an organic scintillator, electrons generate more light than do heavy particles of equal energy.

For dosimetry purposes, the scintillation efficiency is independent of the energy of the charged particles [20]. Thus, the light produced should have a linear dependence on the initial energy of the charged particles interacting within the scintillator. For organic scintillators such as anthracene, stilbene, and many other commercially available liquid and plastic scintillators, the response to electrons is linear for particle energies above about 125 KeV [19]. The response of plastic and liquid scintillators to heavier particles is linear only above much higher energies. Smith *et al.* [21] studied several commonly used organic scintillators over a relatively wide range of particle energy and found that the response to electrons is linear with particle energies above approximately 100 KeV.

3.1.3 Scintillator materials

The fluorescence process in organics arises from transitions in the energy level structure of a single molecule, and therefore can be observed from a given molecular species independent of its physical state [19]. So anthracene is observed to fluoresce as either a solid polycrystalline material, as a vapour, or as part of a multicomponent solution. There are several types of organic scintillators: firstly, a pure organic crystal, such as anthracene, which is the oldest organic material used for scintillation purposes and has the highest scintillation efficiency (greatest light output per unit energy—emission wavelength near 425 nm) Another type of pure organic crystal is stilbene, which has lower scintillation efficiency.

The second type of organic scintillator is liquid organic solutions that are produced by dissolving an organic scintillator in an appropriate solvent. Sometimes another constituent is added as a wavelength shifter to tailor the emission spectrum for particular purposes [19]. The small shifts in the wavelength usually decreases the efficiency of the scintillator. The third type of organic

scintillator is plastic scintillator. If the organic scintillator is dissolved in a solvent that can then be polymerized, the equivalent of a solid solution can be produced.

Since plastic scintillators are the easiest to be shaped and fabricated, plastic scintillators represent an extremely useful form of organic scintillator. The fourth type of organic scintillator is the thin film scintillator. In this type very thin films of plastic scintillator play a unique role in the field of radiation detectors [19]. These films act as transmission detectors that respond to only the fraction of energy lost by the particle as it passes through the detector.

Plastic scintillators are non-fluid solutions [19], consisting of fluorescent organic compounds dissolved in a solidified polymer matrix. The best polymers are polyvinyl toluene and polystyrene (polyvinyl-benzene) [19]. Small amounts of aromatic compounds are usually added to the polymers to increase the scintillator efficiency and transparency. The plastic scintillator chosen for this study is "EJ-200", which is manufactured by Eljen Technology [22]. This plastic scintillator is equivalent to BC470, which is manufactured by Bicron Corporation [23]. The relevant characteristics of this plastic are its high light output efficiency and its advantageous spectral response. Table 3.1 lists the principal characteristics of the plastic scintillator used in this study.

3.2. Optical Coupling

Miniaturized plastic scintillators are optically coupled to the SiO_2 and PMMA optical fibres with clear optical adhesive. Norland Products Inc. [24] manufactures such a optical coupling adhesive and was the product that we selected for this study. Outstanding characteristics of the adhesive are its low fluorescence and excellent transmission in the visible range. The optical adhesive is cured by ultraviolet light using a 100 Watt mercury spot lamp at 6 inches for 20 minutes.

Table 3.1: Principal characteristics of the tissue equivalent plastic scintillator crystal (EJ-200) used in this study.

Scintillator:	EJ-200
Light output % anthracene:	64%
Decay time, ns:	2.1
Rise time, ns:	0.9
Wavelength of maximum emission, nm:	425
No of H atoms per cm^3 $x10^{22}$:	5.23
No of C atoms per cm^3 $x10^{22}$:	4.74
Density, g/cc:	1.032
Polymer base:	Polyvinyl toluene
Refractive index:	1.58
Light output vs. temperature:	No change from +20 ^{0}C to -60 ^{0}C

3.3 Optical fibre light tubes

An optical fibre is a cylindrical dielectric waveguide made of low loss materials such as silica glass and plastics. It has a central core in which the light is launched and guided. The core is surrounded by a lower refractive index cladding layer as shown in figure 3.1. Light rays incident on the core-cladding boundary at an angle greater than the critical angle undergo total internal reflection and are transmitted through the core without refraction [25]. While the rays incident with greater inclination to the fibre axis lose part of their power into the cladding at each reflection and are not transmitted [25].

There are two main types of fibre optics; one is multimode (MM) fibre, and the other is single mode (SM) fibre. Each has characteristic applications and advantages and disadvantages. Light photons that enter a fibre are characterized by incident angle. When they meet with the fibre axis they may be refracted or reflected at the core cladding interface. To achieve total internal reflection, the cladding refractive index must be smaller than the refractive index of the core and the photon light should enter the fibre with an angle greater than the critical angle (θ_c) as in figure 3.2. This critical angle is given by the following equation:

$$\sin \theta_c = n_2 / n_1 \qquad (3.1)$$

where:

n_1 = refractive index of the fibre core.

n_2 = refractive index of the cladding material.

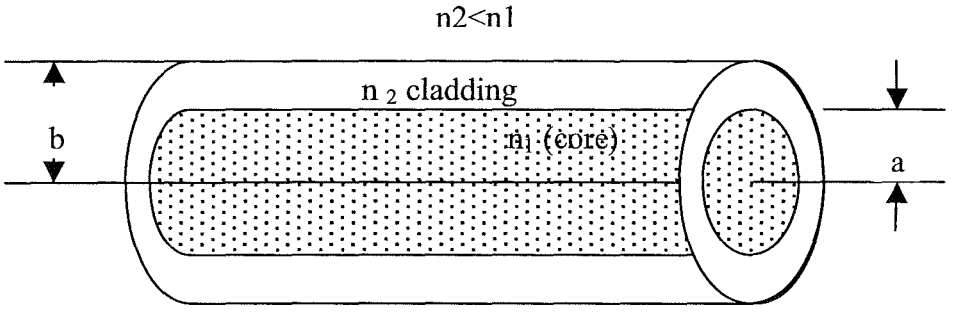

Figure 3.1: An optical fibre is a cylindrical dielectric waveguide.

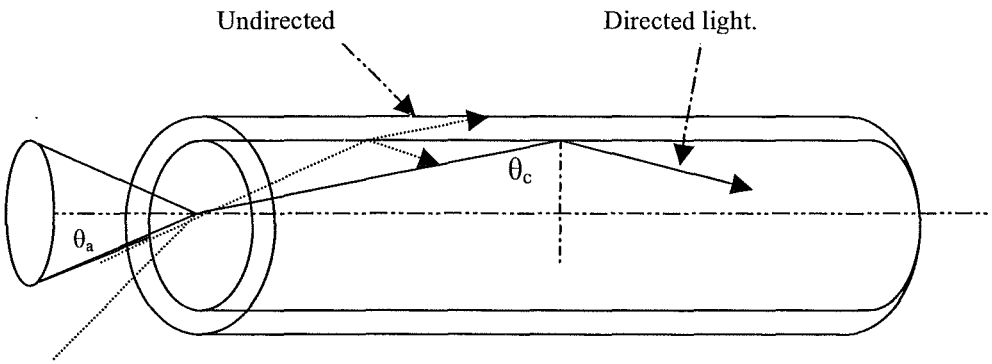

Figure 3.2: The longitudinal cross-section of an optical fibre. The critical angle (θ_c) for total reflection and acceptance cone half angle (θ_a) are also shown.

Optical fibres can be widely classified according to refractive index profile and dimensions. First, multimode step-index fibres (as shown in figure 3.3a) have a 50-1000 micron diameter core with a constant refractive index. They have good light collection efficiency and their large core makes them easy to use [25]. Second, single mode fibres (as shown in figure 3.3b) have step-index profiles and very small cores. These fibres have a poor light collection efficiency, but they maintain light pulses of very short (picosecond) durations. Third, multimode graded-index fibres, as shown in figure 3.3c have 50-100 micron diameter cores with a refractive index that decreases radially outward [25]. They support only one guided mode at their operating wavelength. Multimode step-index fibres (as shown in figure 3.3a) are the best fibre type for our present study, while single mode and multimode graded-index fibres (as shown in figure 3.3c) are preferred for telecommunications [20].

Plastic optical fibres of 1 mm diameter were chosen for this study because of their radiation resistance and their large numerical aperture, which maximise light collection at the interface between scintillator and fibre. The fibre core is surrounded by a thin PMMA doped cladding and a black polyethylene outer jacket. They are manufactured by Edmund Optics Corporation [26]. Specifications of the optic fibre used are shown in table 3.2.

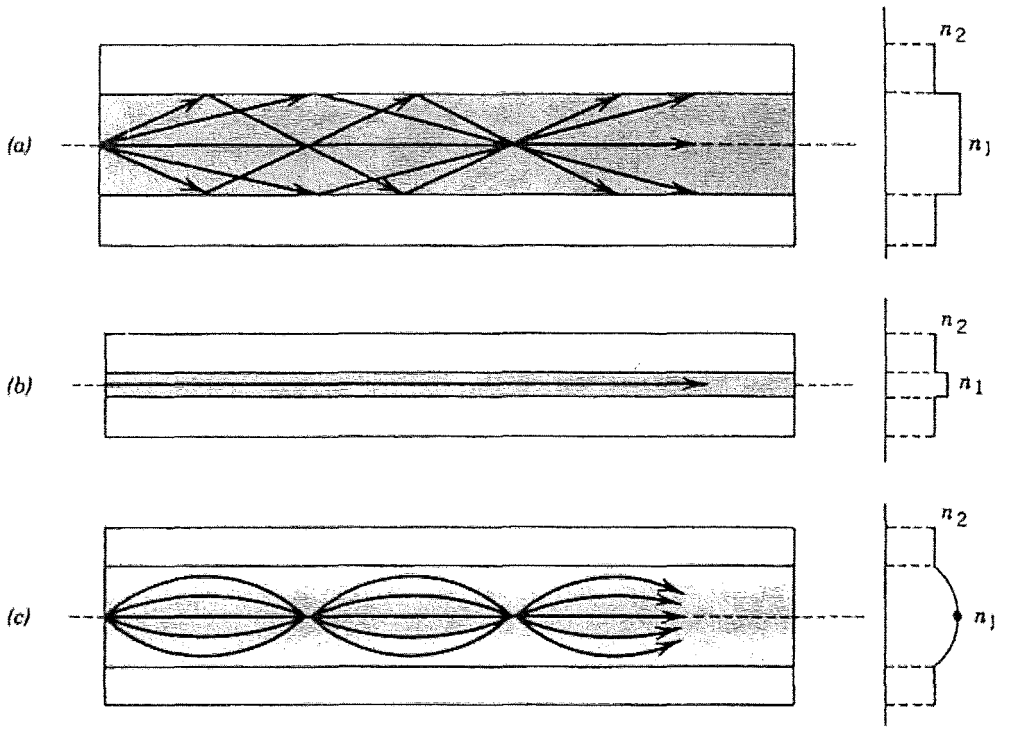

Figure 3.3: Geometry, refractive – index profile, and typical light rays in: (a) a multimode step-index fibre, (b) a single mode step-index fibre, and (c) a multimode graded-index fibre.

Table 3.2: Standard specifications of the optical fibre cables used.

Specifications	SiO_2 fibre optic cable	PMMA fibre optic cable
Model No.	OPT fibre UV/VIS 1000μm.	OPT fibre jacket 1000μm×1.
Attenuation. (dB/km)	10 @ 650nm	190 to 360 @ 650nm.
Minimum radius of Bend.	275mm	44mm.
Operation temperature (°C).	-40° C to +100° C.	-55° C to +70° C.
Spectral transmission range.	180nm-1200nm	400nm-2100nm
Acceptance Angle.	25.4 °.	61°.
Refractive Index.	Core: n_1= 1.458. Cladding: n_2= 1.441.	Core: n_1= 1.492. Cladding: n_2= 1.402.
Numerical Aperture.	0.22±0.2.	0.51±0.03.
Jacket.	Nylon Jacket.	Black Polyethylene.

3.3.1 Radiation effects on optical fibres

The short-lived radiation response of optical fibres (fluorescence) forms a background signal when mixed with the light output from a scintillator attached to an optical fibre. Therefore, the light detect by the photodiode is composed of the response of the scintillator probe itself plus the response of the portion of the optical fibre that was exposed to the primary radiation beam [27]. This chapter will discuss this effect and other detrimental effects of ionising radiation on optical fibres.

3.3.1.1 Ionising radiation effects on optical fibres

It is well-known that an optical signal is attenuated when transmitted through an optical fibre in an ionising radiation environment [25]. Attenuation occurs in optical fibres as a result of ionising radiation generating colour centres in the material [25]. These centres are areas in the material that appear opaque to some wavelengths of light and transparent to others. The radiation damage that occurs in the fibre is associated with the formation of colour centres. Some of these centres are permanent in the fibre core lattice and cause a constant attenuation in the transmission parameters of the fibre, while the others regularly recover with time after irradiation. The formation of radiation induced colour centres, giving rise to both increased attenuation and luminescent light generation. Colour centres describe the most serious form of degradation of the waveguide [28].

The amount of structural damage induced by radiation depends strongly on the material, the diameter of the fibre core, and the nature and energy of the radiation field [27]. In choosing a fibre for use in ionising radiation environments, it is important to consider the operating conditions. These parameters include the total radiation dose, the maximum dose rate, wavelength of operation, temperature and bandwidth requirements [28]. In the fibre optic industry, glass and doped

plastic fibres are commonly manufactured to be somewhat resistive to radiation damage to be suitable for long-term, indoor and outdoor applications. In the present study, solid large single core, Teflon cladding and durable, flexible SiO_2 and PMMA optical fibres were selected. Preliminary testing of the SiO_2 and PMMA fibres showed minimal radiation damage. Primary studies also showed a flat spectral response when a length of the fibre optic cable was irradiated.

3.3.1.2 Stem light within optical fibre

Most of the light produced in the silica or plastic optical fibre itself when irradiated by high energy photon or electron beams arises from the luminescence (primarily fluorescence) of the fibre core and from Cerenkov effects [29]. The fluorescent light emission is isotropic, while the Cerenkov effect is characterized by anisotropic emission. The amount of light produced by fluorescence and the Cerenkov effect can be evaluated to know the relative importance of these phenomena [29]. Although the efficiency of the optical fibre fluorescence or the Cerenkov effect is small compared to the efficiency of the scintillators, the scintillator is approximately 1000 times smaller than the length of optical fibre that could be exposed to the ionising radiation. Thus, what might be considered small effects could dominate the signal at the photodiode due to the small size of the scintillator.

In this study, we tried to eliminate stem effects including Cerenkov radiation and fluorescence within the fibre core. These effects act as background signals that add to the scintillator signals. Previous studies have showed different techniques to eliminate background signals due to stem effects. Some investigators use a reference fibre optic cable, which limits use in real applications. The reference optical fibre is a second fibre running parallel to the primary fibre. Only the primary fibre has a scintillator attached. The secondary fibre is without a scintillator.

The Cerenkov effect is expected to be small, when the fibre axis is at a 0° angle to the direction of the irradiation beams [30]. In such circumstances, optical fibre fluorescence would account for most of the background light emission. The mechanism responsible for light emission by the fibres at low dose rates and energy levels is primarily due to fluorescence, while at high dose rates of radiation the greatest effect accounting for light emission is due to the Cerenkov effect [30]. Moreover, the light emission from luminescence increases proportionally with increasing dose rate, and as the dose rate is increased the Cerenkov effect starts contributing to the total light emission [30].

3.4 Optical lens

A plano-convex lens is the most common type of lens element having a positive focus length. In this study it is useful to collect, collimate and focus the small amount of plastic scintillator light transmitted through the distal end of the fibre optic cable. The low f-number plano-convex lenses collect and transmit the light from one location to another with high transmission efficiency [25] as shown in figure 3.4. In an attempt to transmit the miniaturized plastic scintillator light through the optical filter with minimum light loss and high transmission efficiency, two BK7 plano-convex lenses are used. The first lens collects the diverged light from the distal end of the fibre optic and collimates it in parallel through the optical filter. The second lens collects the transmitted parallel light from the optical filter and focuses it toward the active area of the photodiode. In addition, as the incident angle of fibre light increases, the transmission curve of the optical filter will shift to lower wavelength. Therefore, optical lenses ensure parallel light transmission through the optical filter and thus avoid any shift on the plastic scintillator light to a lower wavelength.

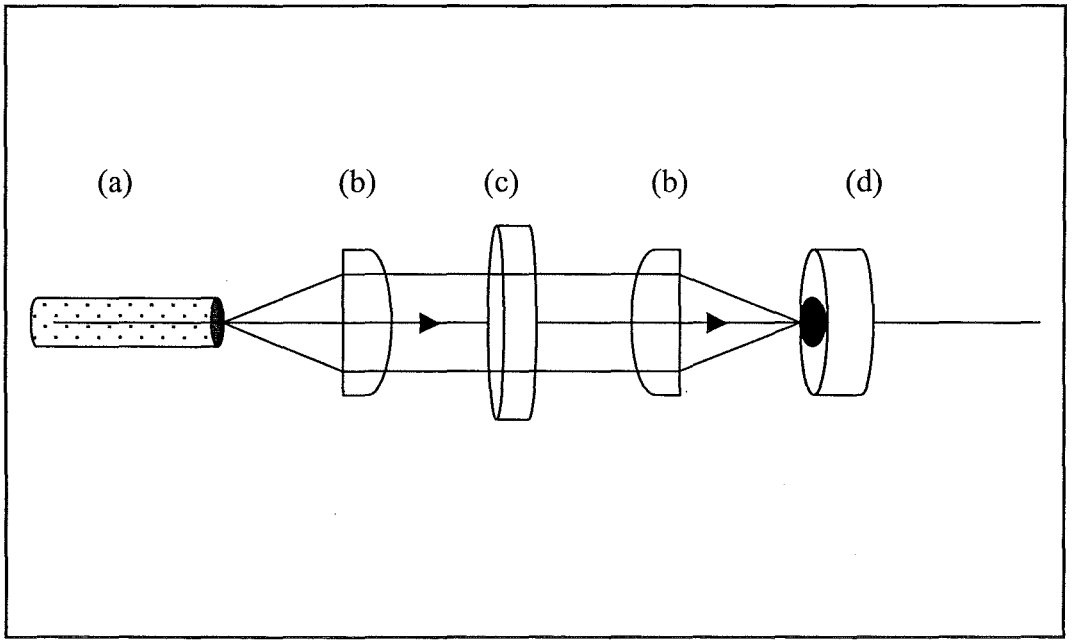

Figure 3.4: Schematic diagram shows the guiding plastic scintillator light: (a) transmitted light from fibre optic cable; (b) plano-convex lens; (c) narrow bandwidth optical filter; (d) photodiode.

Each f/1 lens has a diameter of 7 mm with a 7 mm focal length. Arranging the optical fibre to be 7 mm from the focal plane of the first will therefore ensure collection and collimation of the light from the optical fibre. The parallel light is transmitted through an optical filter, discussed below, and is then focused with a matching f/1 lens. The resulting image is the same size that the optical fibre core (magnification = 1). The collection angle of the lens is nearly 45 degrees.

To our advantage, the wavelength range (800 nm $\leq \lambda \leq$ 350 nm) of the optical lenses selected filters out part of the interference light especially from Cerenkov radiation, which is concentrated mainly in the UV region of the spectrum.

3.5 Optical filter

The narrow bandwidth optical interference filter transmits light with high efficiency a particular wavelength band while rejecting by absorption or reflection the out-of-band light energy. This represents the simplest and most cost effective way to transmit a well-defined band of light [31]. Compared with a monochromator system (slits and a diffraction grating), the cost of fluorescence interference filters is significantly lower [31]. Optical filters are manufactured with a wide range of standards to suit different applications and equipment.

This study selected a high performance optical filter suiting the operating environment of the miniaturized plastic scintillator detector. The design is based on transmitting most of the plastic scintillator light while rejecting the interference light due to fluorescence of the fibre optic cable and Cerenkov radiation. The important parameters associated with the specifications of the narrow bandwidth optical filter include bandwidth, centre wavelength and the maximum transmittance within the band pass. Table 3.3 shows the characteristics of the optical filter used in this study.

Table 3.3: Common specifications for fluorescence filter appropriate for this study. The filter was manufactured by Corion filters [31].

Central wavelength (nm)	Band width FWHM (nm)	T_{pk} Peak Transmittance (%)	Integrated Blocking	Spectral range	Minimum active area (mm)
425 +5, -0	35 ± 3.5	> 50 %	100,000:1	x-ray-925nm	7.6

The optical filters selected have a central wavelength equal to 425 nm (which corresponds to the maximum output of the scintillator used) and bandwidth equal to 35nm (which also approximates the bandwidth of the scintillator output). The filter is sandwiched between two plano-convex lenses to ensure parallel transmission through the filter. Therefore, most of the detector interference background that is not related to the plastic scintillator light and that exists out of the bandwidth is rejected.

Interference light that might distort the readings from the detector system is largely from fluorescence of the fibre optic material and Cerenkov radiation created within the fibre. These interferences are mostly concentrated in the UV region of the spectrum [32]. Conversely, most of the plastic scintillator light is concentrated in the visible region. In this way the optical filter and lenses transmit primarily the light coming from the plastic scintillator and blocks most light arising from other processes.

3.6 Light Detection

There are several ways to detect light photons launched through a light guide medium. In this study sensitive X-Omat film (Kodak, Auckland) was used for detection in the primary experiments and a photodiode was used as the final prototype light detection system. The film permitted long time integration when the light levels where very low. This helped during the initial phases of the research. On the other hand, the photodiodes permitted us to temporally resolve the light signal and measure only the signals that matched the pulses from the linear accelerator.

3.6.1 X-Omat V film

X-Omat V film/4508 is a relatively low-speed film designed for verifying orientation and for approximating patient dosage in radiation therapy procedures. It features the ready-pak that eliminates the need for loading cardboard cassettes. In this study the use of X-Omat V film primarily helped to assess the amount of light photons produced by the plastic scintillators. This assessment facilitates easy selection of the most appropriate photo detection device. Benefits of using X-Omat film include enabling a study of the densities of the plastic scintillator and Plexiglas materials, allowing assessment of the effectiveness of the reflecting paint used in this study and giving a recordable documentation of light leakage through the plastic scintillator surfaces.

3.6.2 Silicon photodiode

A photo detector is a device that measures photon flux by converting the energy of the absorbed photons into a measurable form. Two main classes of photo detectors are in common use: thermal detectors and photoelectric detectors. The photodiode is a p-n junction of which the reverse current increases as it absorbs photons. Whenever a photon is absorbed an electron-hole pair is generated [25].

Photodiodes have been constructed from many semiconductor materials; doped silicon is commonly used in such detectors. The main characteristics of photodiode light detectors are excellent linearity with respect to incident light, low noise, wide spectral response, mechanically rugged, compact and lightweight and long life span [25]. In addition, the photodiode does not need the high voltage bias required for photomultiplier tubes. Therefore, a photodiode was preferred as the photosensitive detector for this study.

This study utilizes a photodiode light detector, with acceptable spectral sensitivity, suiting the operating environment of the miniaturized plastic scintillator detector. Table 3.4 shows the specifications of the photodiode used in this study. The spectral sensitivity of a photodiode is governed principally by the wavelength dependence [25]. BPW21 photodiodes are more sensitive to light emitted by plastic scintillators (≥425nm), and have less sensitivity to interference light created by fluorescence of the fibre optic cable or Cerenkov radiation that lies mainly in the UV region. This property is conducive to reducing the amount of interference light on the entire detection system under investigation as shown in figure 3.5.

3.7 Digital integrator system

The output signal of a photodiode, under normal operation, is a very accurate measure of the total light intensity output that is transmitted through the fibre optic cable. The output current of a photodiode is proportional to the rate at which the radiation energy is absorbed in the scintillator. Light output of the plastic scintillator is proportional to the absorbed energy.

The fibre optic cable transmits the total light intensity created by the plastic scintillator plus the interference light due to Cerenkov radiation and fluorescence of the fibre material. The narrow bandwidth optical filter transmits the light created by the plastic scintillator and rejects most of the Cerenkov and fibre fluorescence light. The total amount of interference light transmitted through the optical filter is expected to be small compared with the amount of plastic scintillator light. Furthermore, this study proposes a technique to eliminate even the small amount of interference light from the final prototype detection system.

Table 3.4: Standard specifications of photodiode used.

Model No.	BPW21 Photodiode.
Spectral Response.	400 nm – 700 nm.
Peak wavelength sensitivity	560 nm
Active area.	7.5 mm^2
Rise time.	1 μs
Fall time.	Same as Rise time
Dark Current.	2 nA

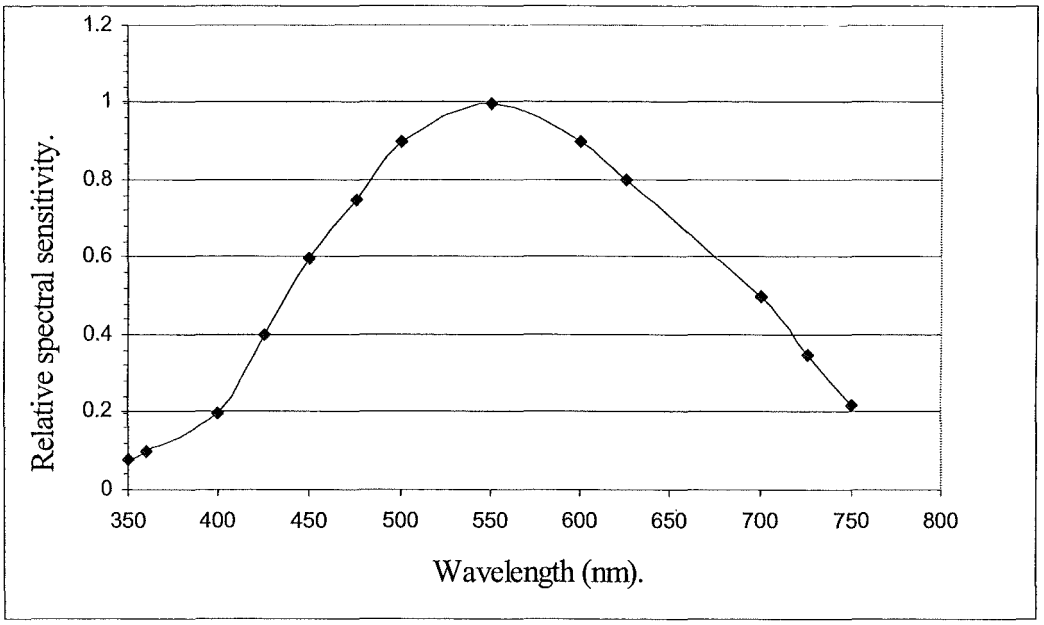

Figure 3.5: BPW21 photodiode spectral sensitivity from R.S Components. The line is drawn to guide the eye.

This study proposes dual dosimeter electronics consisting of two identical channels. The first channel is designed to suit SiO_2 fibre properties, while the second channel is designed to suit PMMA fibre properties. Each channel is divided into two essential parts, a diode amplifier, and an integrator and digital display. The amplifier consists of a transimpedance amplifier (2μA/volt), followed by two gain stages with a total gain of 100. The amplifier was designed and built for this purpose. The details of the circuit are in Appendix B.

The integrator is a modified version of the double correlated sampling type. It uses a microprocessor, an analogue to digital converter (ADC) and an operational amplifier to integrate the plastic scintillator signal plus the interference signal and then to integrate the interference noise only. Simultaneously, the integrator will subtract the interference signal (noise) from the plastic scintillator signal. Each new result is added to the previous total until the treatment is complete. In an attempt to eliminate light pulses not consistent with linear accelerator pulses, the integrator is interfaced directly with a modulator triggering outlet of the linear accelerator.

This technique has the potential to reduce the contribution from interference light that acts as noise in the final detection system. It is a promising technique that eliminates the interference light signal from the output of the plastic scintillator detector and it does not require a second background detector.

Appendix B, shows the timing diagram of dual integrator system and electronic circuits of the dosimeter integrator and photodiode amplifier.

CHAPTER 4

Pre-design studies

4.1 Simplicity of the detection system

In radiotherapy, it is strongly recommended to use a detection system to evaluate and assess the real radiation dose to be delivered to the region under treatment and to surrounding normal tissue. A detection system suitable for medical applications has to be simple to use. It would be advantageous for the detection system to have a tissue equivalent detector, like a plastic scintillator. The scintillator will convert the kinetic energy of charged particles into detectable light with a high efficiency. Also, this conversion must be linearly related to the intensity of the radiation and the light yield should be proportional to deposited energy over as wide a spectral range as possible. Moreover, if the scintillator index of refraction is near the index of the optical fibre this will permit efficient coupling of the scintillation light to a fibre optic light guide.

To make the detector system practical for clinical use, the fibre optic light guide should be resistive damage from high energy radiation and have reduced stem effects such as luminescence or fluorescence of the fibre optic light guide itself and light production due to Cerenkov radiation. These stem effects occur when part of the fibre is exposed to the radiotherapy beam. The most important property of the detection system is that interference with the planned radiotherapy beam should be negligible so that the detection system does not act as major scatterer of the radiation beam.

From a medical point of view, the system should be flexible enough to be placed over the skin of the patient or to be inserted within the cavities or arteries using suitable medical catheters. The detection system should not disturb either

the patient or the beam because the success of irradiation is based on these two important factors.

4.2 Radiation detection part of the system

In this study, plastic scintillators were selected to measure the radiation dose delivered to the patient during radiotherapy procedures with scintillation efficiency independent of energy of the charged particles. EJ-200 [22] organic scintillators, have a linear response to electrons for particle energies above 125 KeV [33]. This feature of energy independence of the scintillation efficiency guides the selection of the scintillation material to be used as the detecting medium of this miniature radiotherapy detector.

4.3 Light guide system

The radiotherapy room environment is a restricted area for radiation workers during the irradiation procedure due to the high levels of radiation. This high level of radiation may affect the electronics and semiconductor material inside the room. Moreover, high energy radiation has the ability to disturb the normal functioning of such sensitive devices. For such reasons and to avoid any direct response from stray radiation, the response of the plastic scintillator must be transmitted through a light guide to the outside the radiotherapy room. This can be achieved using optical light guide materials such as Plexiglas rods, hollow optical capillary tubes or optical fibre systems.

The radiation detector has to be miniaturized and its volume has to be small enough to act as a point detector. Reduction in the amount of light produced by the plastic scintillator is expected due to its small volume. It is important to avoid any further reduction in the light produced because the plastic scintillator represents the actual equivalent radiation dose deposited in that volume. Thus,

high radiation resistance, low attenuation medium, flexibility, scatterless medium were the desired properties of the light guide to carry the light signal from the treatment area to the control area outside the treatment room.

Pure fused silica fibre (SiO_2) or PMMA plastic fibre are recommended products due to their physical and mechanical properties. The SiO_2 fibre has a wider spectral range than the PMMA fibre and has less attenuation per meter than the PMMA fibre. On the other hand, the SiO_2 fibre has a small acceptance angle compared to plastic fibre, and that will limit the diameter of the plastic scintillator attached to it. Also, the SiO_2 fibre flexibility is considerably less than the PMMA fibre.

4.4 Light detection system

There are several methods to detect the light photons launched through the light guide. Each of these methods have different levels of sensitivity and create different levels of noise. The photo detector is a device that measures photon flux by converting the energy of the absorbed photons into a measurable form. Photodiodes have been constructed from many semiconductor materials such as doped silicon. The large area BPW21 photodiode will be use as the proposed detector. The fast response, window size that may matches the size of the fibre optic, linearity, and low noise are sufficient features to warrant selection as the photo detection device in this study.

4.5 Detector response based on plastic scintillator light and stem effect light

Scintillators respond directly to ionisation generated by charged particles. Preliminary investigations included checking the linearity of plastic scintillator (3mm in diameter × 10mm in length) coupled through the PMMA fibre cable

when irradiated by 6MV x-ray beam in a water tank as a phantom. The intensity was measured as a function of distance. Figure 4.1 shows response at different distances as compared with that calculated using the inverse square law. Excellent agreement is observed.

Another experiment shows the dose depth curve for plastic scintillator (signal) and plastic fibre guide (background). These results were obtained using a water phantom tank with a fully computerized system to control the depth of the detector. The results were compared to the depth dose obtained using a 0.125 cm^3 calibrated ionisation chamber. There is good agreement with the maximum signal near 10 mm depth as shown in figure 4.2. The slight difference is attributed to the differences of detector volumes. The scintillator has only 0.0707 cm^3 volume compared to the 0.124 cm^3 of the ionisation chamber.

Moreover, the preliminary experiments show a good match with ionisation chamber results for beam profiles in the penumbral region as shown in figure 4.3. Overall the preliminary results show no significant differences between the ionisation chamber response and the scintillation detector response for a $40\times40cm^2$ field size. Both the ionisation chamber and the scintillation detector were oriented perpendicularly with respect to the radiation beam so that their longitudinal axes were perpendicular to the beam central axis and to the scanning direction.

Additional, preliminary experiments investigated detector response as the irradiated fibre length increased. These results show the effect of beam angle and allow a rough estimate of the contribution from fluorescence and Cerenkov radiation. Three angles were selected for these experiments; 0° (perpendicular to the optical fibre), -45° (toward plastic scintillator) and 45° (toward photodiode). Figure 4.4 shows the change in detector response as the incident angle moved from -45° to +45°. The dependency of detector signal on beam angle indicates that stem effects are not eliminated from the detector system. Hence it is not possible for the system to act as a directional independent detector.

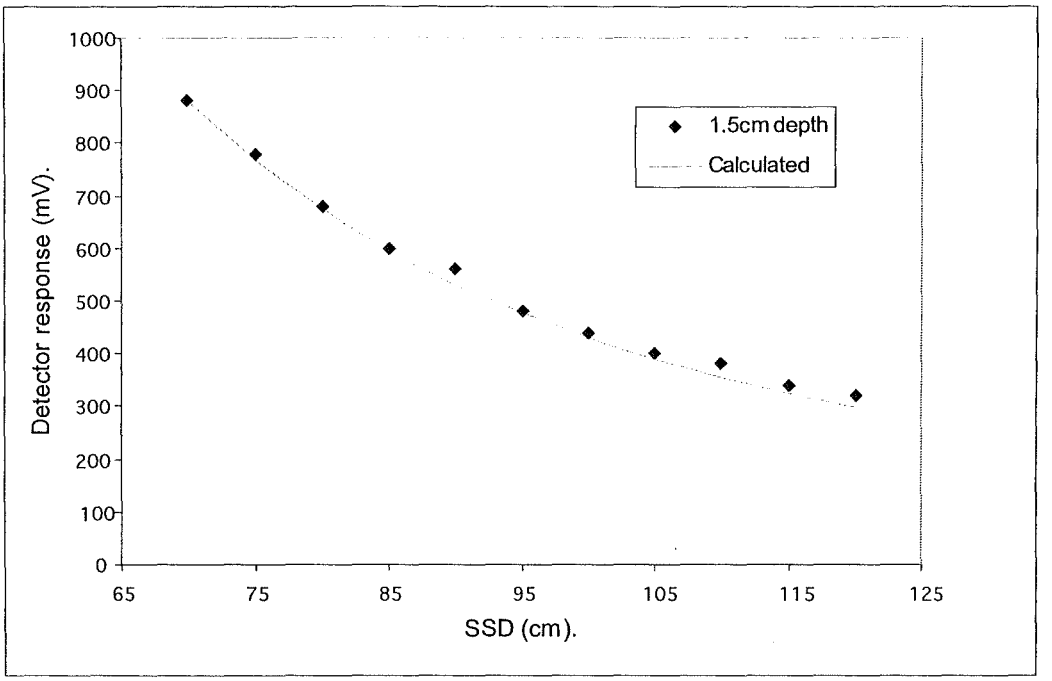

Figure 4.1: Response of the plastic scintillator detector (signal) compared to calculated response using inverse square law when exposed to a 6 MV x-ray beam at 1.5cm depth in the water tank.

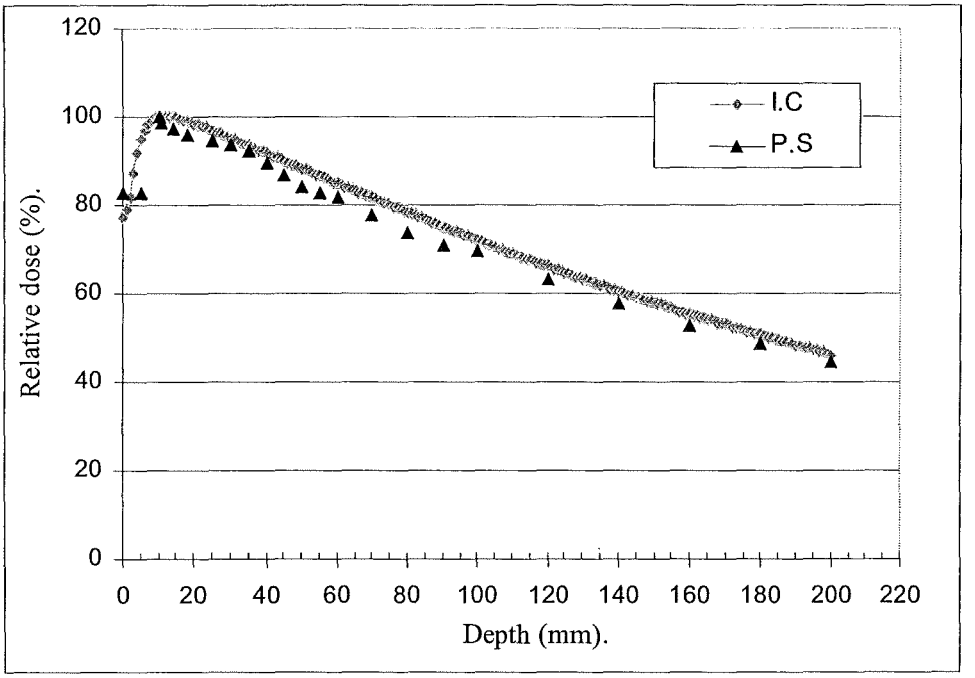

Figure 4.2: Percent depth dose in water phantom tank using plastic scintillator (P.S) and compared to the depth dose obtained using ionisation chamber (I.C) for 6 MV x-ray beam, 40X40cm^2 as field size, 250MU, and 100cm as source to surface distance.

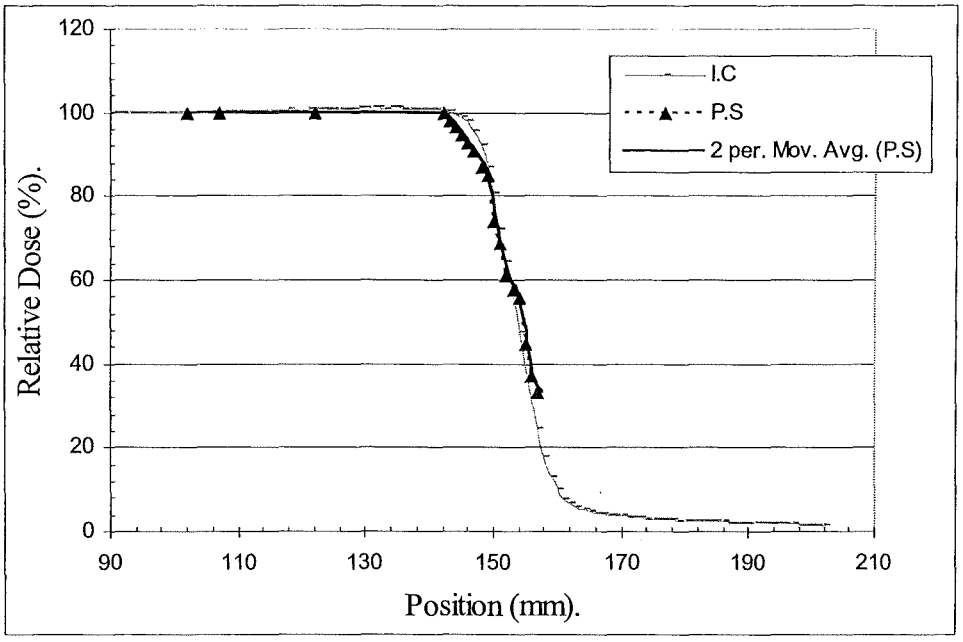

Figure 4.3: 6 MV x-ray beam linear accelerator x-ray half beam profile in water tank phantom using prototype plastic scintillator (P.S) and compared to ionisation chamber (I.C). The line between the plastic scintillator points is a straight line calculated from a 2 point running average.

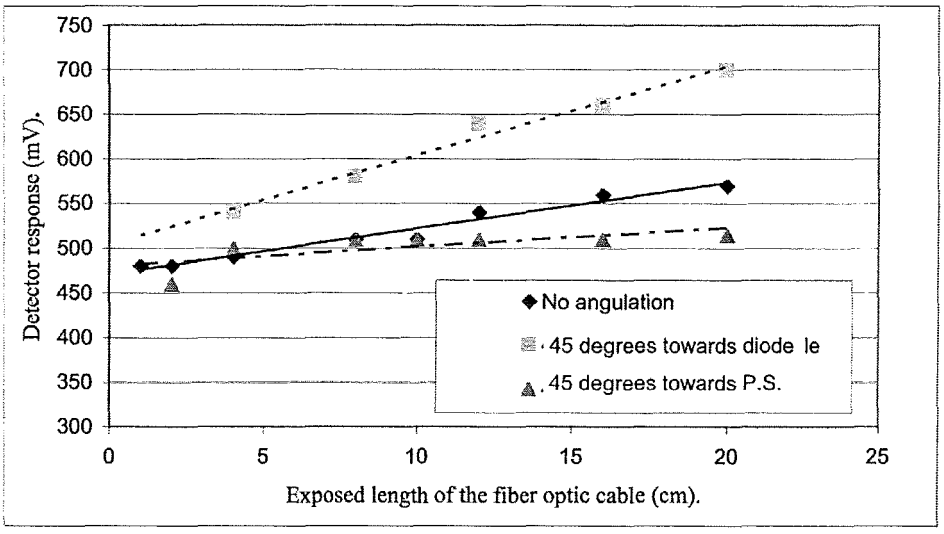

Figure 4.4: Prototype plastic scintillator (P.S) as a main signal and plastic fibre guide (background) detector response from three different 6 MV x-ray beam angles. 0°, -45° (towards plastic scintillator) and 45° (towards photodiode), as the length of fibre optic cable under the beam has increased. The lines are drawn to guide the eye.

The effect of beam size on detector response was studied as well. This experiment was a good indicator of the contribution due to stem effects and of backscatter response with increasing beam size. Field sizes of 2×2, 4×4, 6×6, 8×8, 10×10, 15×15, 20×20, 25×25, 30×30, 35×35 and 40×40 cm^2 were selected for this study. The result shows a parallel response between depths of 15mm and 100mm in the water tank phantom as shown in figure 4.5.

4.6 Photographic detection experiments

Photographic detection experiments represent important experiments to give preliminary results about the system design, efficiency and amount of light emitted by the plastic scintillator. Moreover, permanent documentation, with no contribution from electronic noise, may be obtained for discussion and evaluation. Plastic scintillation light signals can be recorded easily without any interference from radiofrequency or any other electronic in the accelerator area. Also, we may record small light signals due to stem effects of the fibre optic cable that are otherwise not easily detected unless special high sensitivity electronics are used and noise is suppressed.

Although the exposure of the film is related to the amount of light, the film cannot be used as a calibrated detector for the absolute amount of light. The film response is not linear and is modified by the age of the film and the processing. Therefore, we can only gain qualitative and gross comparisons with the film. Nonetheless, this is important information to help us in the final system design.

Many exposures were performed with and without a plastic scintillator as the main signal source. A 25 cm length of the light guide was exposed to two different beam angles; 40° toward the photodiode and 40° toward the plastic scintillator. Irradiation parameters of 6 MV, SSD = 100 cm, 25×25 cm^2 field size and 400-800MU were used. The distal end of the fibre optic cable was positioned against X-Omat V therapy verification film in a light tight box. The tip of the fibre optic was positioned vertically against the film using a polished heavy object,

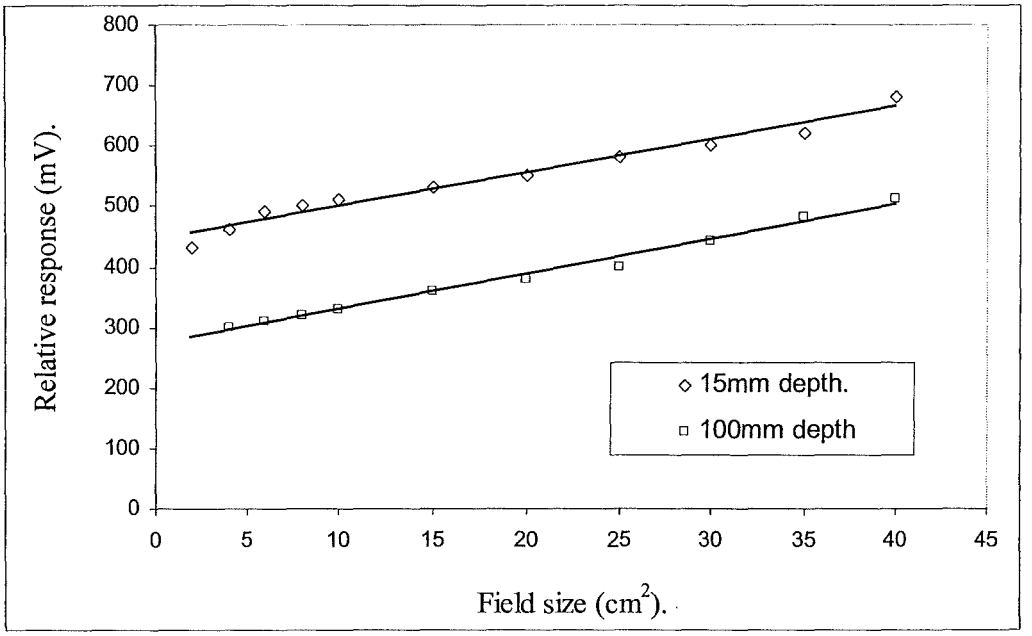

Figure 4.5: Prototype plastic scintillator (signal) and plastic fibre guide (background) detector response from different irradiation beam sizes using 6 MV x-ray beam, 250MU, at 100cm source to surface distance (SSD) with 15 & 100 mm depths in water tank.

maintaining a distance of 3mm between the tip of the fibre and the sensitive film. Automatic film processors were used to process the film of all experiments.

Other experiments were performed to record the stem effect light arising from fluorescence and Cerenkov radiation. Part of the fibre optic was looped vertically on the radiation field area and exposed to a 40° beam angle. The beam produces more fluorescence from one side and more Cerenkov from the other side. This experiment was repeated two times: one with and one without an optical filter. These experiments give information about the effectiveness of the optical filter to filter all noise light corning from stem effects. At the same time, another experiment was performed to assess the interference of the optical filter on plastic scintillator signals.

The density of spots recorded at all exposures was evaluated using a densitometer with a 1 mm window hole. The densitometer was reset against the film base background. The densitometer readings are tabulated in table 4.1.

These results evaluate the light contribution due to stem effects and the plastic scintillator. Also evident is the effect of beam angle on the production of fluorescence and Cerenkov radiation within the fibre optic. This in turn indicates the relative contribution from the main plastic scintillator signal and the background signal. Nevertheless, there is a good filtration response for unwanted stem light. This is an important factor towards manufacture of a miniature detector system without any need for a reference fibre cable [1].

Table 4.1: Densitometer reading for irradiated detector at two different beam angles, with and without plastic scintillator.

Densitometer reading with beam angle at 40° toward photodiode.				Densitometer reading with beam angle at 40° toward plastic scintillator.			
With Plastic Scintillator		Without Plastic Scintillator		With Plastic Scintillator		Without Plastic Scintillator	
400MU	800MU	400MU	800MU	400MU	800MU	400MU	800MU
3.05	3.48	1.41	2.04	2.88	3.28	0.36	0.43

4.7 Detector system efficiency

4.7.1 Intrinsic efficiency

The intrinsic efficiency (η) of a given scintillator is defined as the ratio of the light energy (E_L) generated in the scintillator to the kinetic energy (E_K) dissipated by the charged particles, and is given by:

$$\eta = E_L / E_K \qquad (4.1)$$

The remaining fraction of the particle energy is dissipated in radiationless transitions. The intrinsic efficiency depends on the scintillator material and incident energy of the ionising particle [33].

4.7.2 Light coupling efficiency

The light coupling efficiency depends strongly on the quality of the optical coupling of the different parts of a given scintillator detection system. For stable light collection systems, the overall light collection efficiency (ε_{light}) is equal to the product of several partial collection efficiencies as defined by the following equation [30].

$$\varepsilon_{light} = \varepsilon_{accept} \times \varepsilon_{couple1} \times \varepsilon_{transmit} \times \varepsilon_{focus1} \times \varepsilon_{filter} \times \varepsilon_{focus2} \qquad (4.2)$$

where:

(ε_{accept}) represents the fraction of light photons produced in the scintillator travelling in the direction of the fibre optic cable that would potentially fall within the acceptance cone of the fibre core.

($\varepsilon_{couple1}$) represents the fraction of incident photons that are transmitted through the coupling interface between the scintillator and the fibre light guide.

($\varepsilon_{transmit}$) represents the transmission efficiency of the fibre light guide.

($\varepsilon_{focus\,in\,g1}$) represents the fraction of incident photons from the scintillator that are transmitted through the PCX $lens_1$.

(ε_{filter}) represents the fraction of incident photons from the scintillator that are transmitted through the optical filter.

($\varepsilon_{focus\,in\,g2}$) represents the fraction of incident photons from the scintillator that are transmitted through the PCX $lens_2$.

4.7.3 Scintillator size

In order to determine the absorbed dose in the plastic scintillator, it is important to know whether the detecting volume behaves as a small cavity (Bragg-Gray cavity) [2], or a large cavity, or something in between [33]. For the small cavity condition, the ratio of the absorbed dose $\overline{D_{sci}}$ in the cavity to that of the surrounding medium D_{med} in the absence of the "plastic scintillator" cavity is equal to the ratio of the average unrestricted mass stopping powers of the cavity to that of the medium. In the case of a large cavity condition, assuming that charged particles are generated completely by photon interactions occurring in the cavity and their energy is deposited completely inside the cavity. The ratio of the dose in the cavity to that of the medium is equal to the ratio of the average mass energy-absorption coefficients of the cavity to that for the medium [33]. Burlin's generalized cavity theory bridges between the two extremes. The Burlin cavity relation can be written in a simple form as:

$$\frac{\overline{D_{sci}}}{D_{med}} = d \times S_{med}^{sci} + (1-d) \times \left(\frac{\mu_{en}}{\rho}\right)_{med}^{sci} \qquad (4.3)$$

where:

$\overline{D_{sci}}$ is the average absorbed dose in the cavity (scintillator).

D_{med} is the absorbed dose in the medium surrounding the cavity under charge particle equilibrium (CPE).

S_{med}^{sci} is the mean ratio of mass collision stopping powers for the scintillator and the surrounding medium.

$\left(\frac{\mu_{en}}{\rho}\right)_{med}^{sci}$ is the mean ratio of the mass energy-absorption coefficients for scintillator and surrounding medium.

d is a parameter related to the scintillator size (cavity) that approaches unity for small cavities and zero for large ones. It accounts for the attenuation of the electrons entering the cavity and the build up of electrons generated inside the cavity [33]. If the equilibrium charged particle fluence is approximately the same in the plastic scintillator and surrounding medium, d is given by:

$$d = (1 - e^{-\beta L}) / \beta L \qquad (4.4)$$

where:

$\beta(\text{cm}^{-1})$ is the effective absorption coefficient of the electrons in the cavity.

L(cm) is the mean path length of the electrons across the cavity.

According to Burlin cavity theory, the evaluation of parameter d provides information concerning the source of the electrons detected in the plastic scintillator (cavity). β is evaluated using Burlin's suggested formula, while t_{max} is arbitrarily taken as the depth when the secondary fluence is attenuated to 4% of its original value and determined from a text book [3].

L in equation 4.4 is defined as the average chord length and is taken as being equal to:

$$L = 4V / S \qquad (4.5)$$

where:

V is the volume of the plastic scintillator (cavity).

S is the surface area of the plastic scintillator (cavity).

Equation 4.5 is for convex cavities and diffuse electron fields [33]. In this study, the cavity (plastic scintillator) is a right angle circular cylinder with its axis at right angles to the x-ray beam and surrounded by a polystyrene cap.

Equation 4.3 was evaluated for the plastic scintillator (as the cavity) and with one limiting assumption about the polystyrene cap wall which we approximate with zero thickness. The parameter d was estimated from equation 4.4 for the mean free path length L. Table 4.2 shows values of d as a function of photon energy for cylindrical plastic scintillators of 1.0 mm and 2.0 mm in diameter, both of which are 10.0 mm in length.

Figure 4.6 shows parameter d versus monoenergetic photons for two sizes of plastic scintillators (1.0 mm and 2.0 mm in diameter, both 10.0 mm in length). Also, figure 6.6 shows that a d value of 0.5 at approximately 1.31 MeV and 1.83 MeV for the 1.0 mm and 2.0 mm diameter scintillator, respectively. In the energy ranges of 1.31 MeV and 1.83 MeV, these scintillator sizes (cavities) are expected to behave as intermediate cavities, justifying the application of Burlin theory. If the detector is used in the orthovoltage x-ray range (<250 KeV), the detecting volume can be considered as a large cavity. Small cavity behaviour is attained only if the mean beam energy is above 20 MeV [33].

Table 4.2: *d* parameter as a function of energy for plastic scintillators of 1.0 mm and 2.0 mm in diameter, both 10.0 mm in length, for which $L = 4V/S$ = 0.95 mm and 1.81 mm respectively.

Photon energy (MeV)	t_{max} * (g/cm^2)	β * (cm^{-1})	*d* (1.0 mm dia.)	*d* (2.0 mm dia.)
0.1	4.38 E-4	7.58 E+3	0.0014	0.00073
0.2	3.18 E-3	1.04 E+3	0.0100	0.00531
0.3	9.47 E-3	3.51 E+2	0.0300	0.01570
0.4	1.96 E-2	1.69 E+2	0.0620	0.03200
0.5	3.34 E-2	9.96E+1	0.1060	0.05500
0.6	5.05 E-2	6.59 E+1	0.1600	0.08400
0.8	9.18 E-2	3.62 E+1	0.2810	0.15200
1.0	1.42 E-1	2.35 E+1	0.3990	0.23200
2.0	4.52 E-1	7.35	0.7200	0.55300
3.0	8.10 E-1	4.10	0.8280	0.70600
4.0	1.19	2.81	0.8780	0.78400
5.0	1.57	2.11	0.9060	0.83100
6.0	1.97	1.69	0.9230	0.86100
8.0	2.76	1.20	0.9450	0.89900
10.0	3.57	0.929	0.9570	0.92000
15.0	5.62	0.591	0.9720	0.94800
20.0	7.62	0.436	0.9790	0.96200

* Estimated t_{max} and β from Beddar et al [20], for same photon energy but for different scintillator sizes.

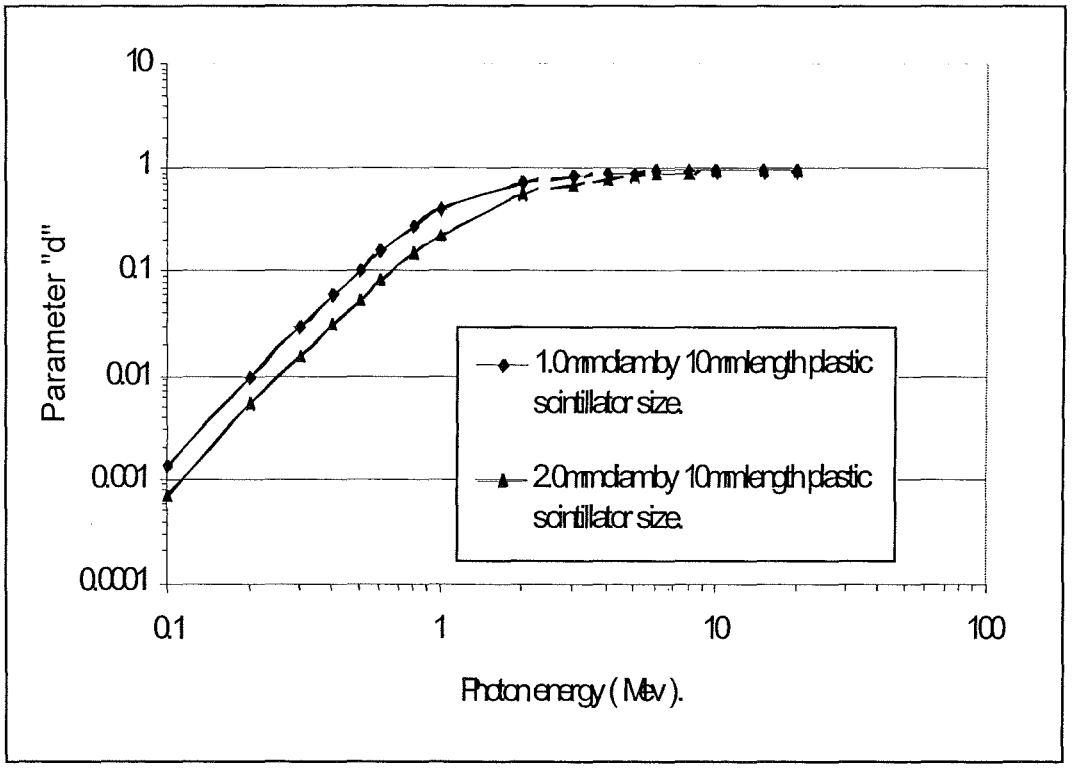

Figure 4.6: Parameter *d* as a function of photon energy for two cylindrical plastic scintillators of 1.0 mm and 2.0 mm in diameter, both 10.0 mm in length.

Practically, we studied three different plastic scintillator diameters; namely 1.0 mm, 2.0 mm and 3.0 mm and three different lengths of scintillator; namely 5.0 mm, 10.0 mm and 15.0 mm respectively.

The experiment set-up has the polished ends of the scintillators facing the X-Omat V radiotherapy verification sensitive film to ensure that detection represents the actual scintillator light emitted through the fibre light guide. The entire scintillator surfaces were covered with reflector paint except the polished end spliced to the fibre light guide. A calibrated densitometer was used to evaluate the densities of the light spots created by each scintillator. Irradiation parameters were: 6MV, SSD=100cm, field size = $10x10cm^2$, no angulations and three different monitor units (16MU, 8MU, 4MU) were used in this experiment.

Figures 4.7, 4.8 and 4.9 show the response of the plastic scintillators of different dimensions. As the diameter and length increase the amount of light created within the plastic scintillator.

4.8 Signal to noise (S/N) definition

In order to establish reasonable criteria to quantify the adequacy of the response and the sensitivity of this category of detectors, there is a need to define a signal to noise ratio that is relevant in the context of scintillation dosimetry and suitable for radiotherapy applications. In order to meet this objective, all components contributing to the signal to noise ratio need to be clearly identified.

The signal in the system is defined as the light output produced in the scintillator that will be measured by the photo detection system (photodiode). The source of noise is first, the natural response of the fibre optic cable to high energy radiation and second, the dark current of the photodiode [34]. The magnitude of dark current of the photodiode is generally of the order of pico amperes, and is

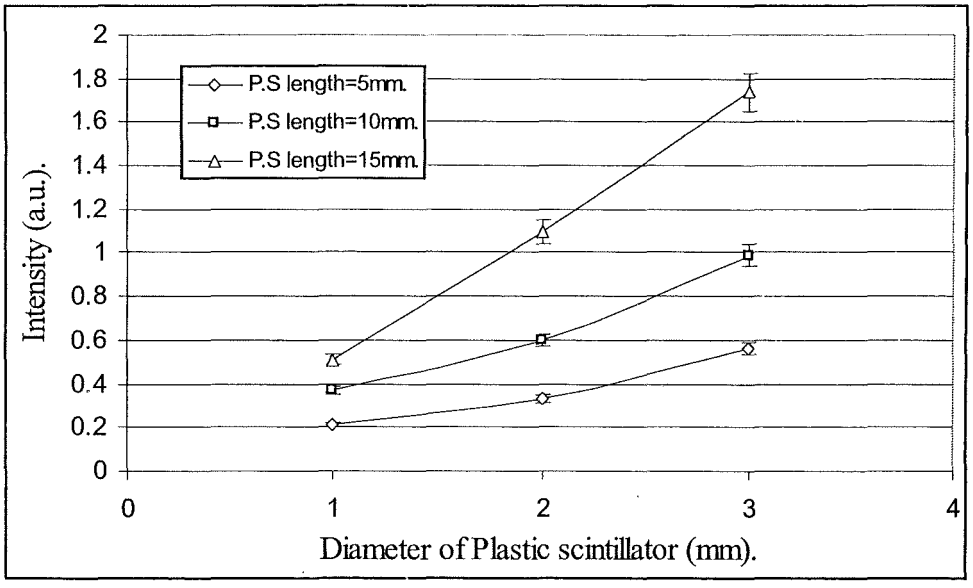

Figure 4.7: Optical response of plastic scintillators (P.S) of lengths 5.0 mm, 10.0 mm, and 15.0 mm and of diameters 1.0 mm, 2.0 mm, and 3.0 mm on irradiation by 16MU beam. The lines are drawn to guide the eye.

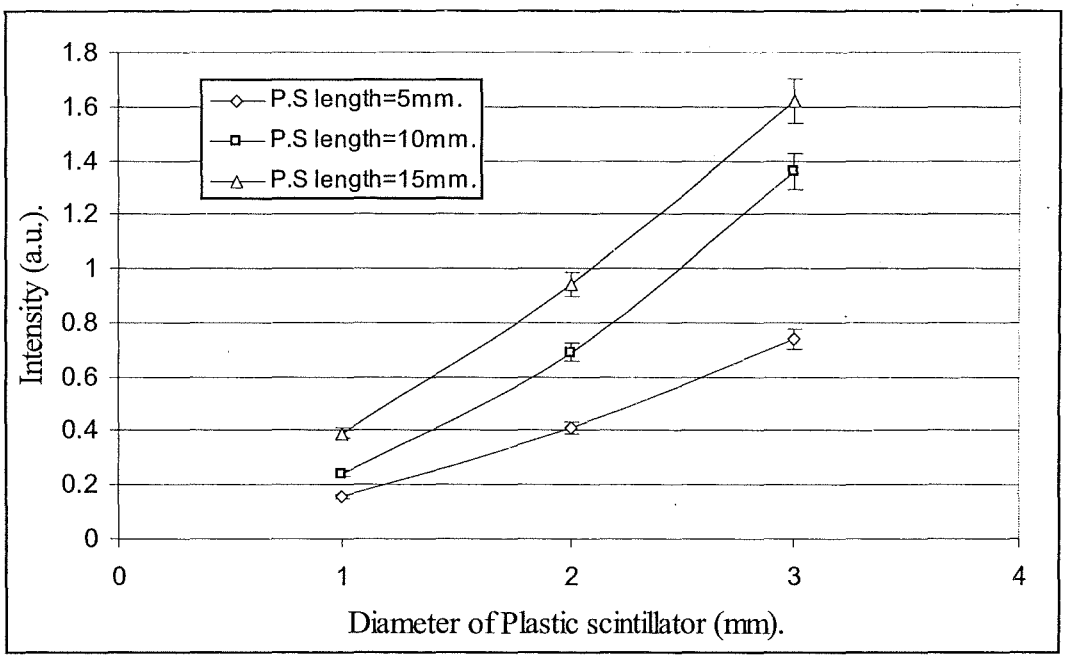

Figure 4.8: Optical response of plastic scintillators (P.S) of lengths 5.0 mm, 10.0 mm, and 15.0 mm and of diameters 1.0 mm, 2.0 mm, and 3.0 mm on irradiation by 8MU beam. The lines are drawn to guide the eye.

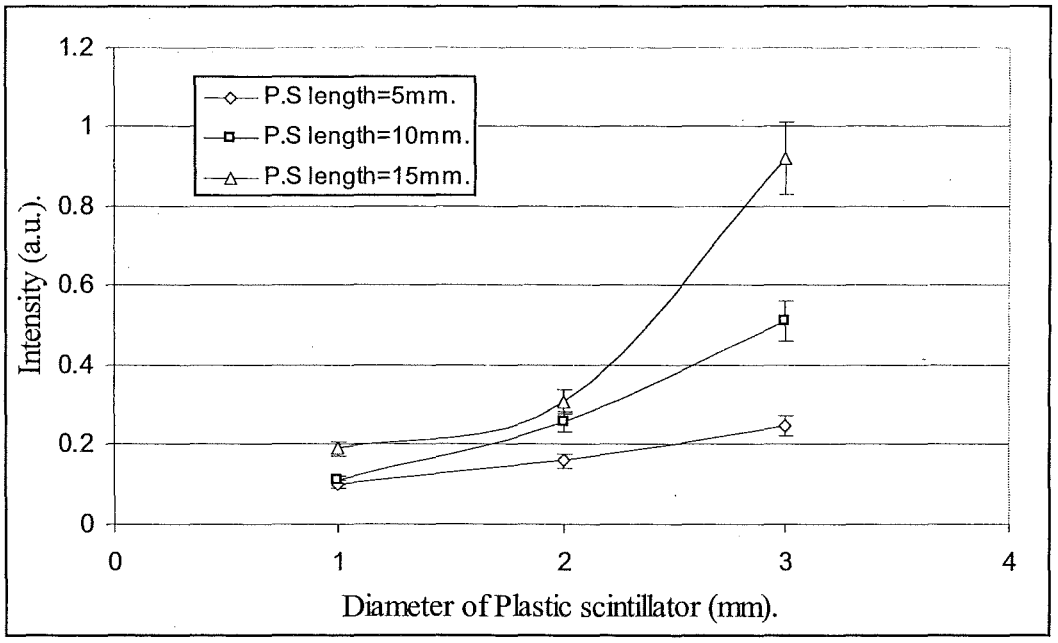

Figure 4.9: Optical response of plastic scintillators (P.S) of lengths 5.0 mm, 10.0 mm, and 15.0 mm and of diameters 1.0 mm, 2.0 mm, and 3.0 mm on irradiation by 4MU beam. The lines are drawn to guide the eye.

negligible compared to scintillator signals and to background light signal induced in the portion of fibre optic cable directly exposed to irradiation beam.

Because the dark current of the photodiode is negligible, the detector under investigation detects only "noise" that arises from the background signals created by the fibre optic cable exposed to direct irradiation. This noise (or background) can be filtered using a Corion "narrow band pass optical filter" [31]. The scintillator signal is then the total signal measured by the photodiode positioned behind the optical filtration system.

Use of the narrow band pass optical filter will ensure that most of the signal created within the fibre optic is blocked, and primarily the main signal light that is centred on a wavelength of 425nm is detected. The filter will allow primarily the light detection within the detection range of 407nm and 442nm. In this detection range the light signal arises mainly from the plastic scintillator and may also contain a small amount of the Cerenkov tail. Jelley [32] deduced that the number of photons emitted by an electron within a spectral region defined by wavelengths $\lambda 1$ and $\lambda 2$ can be found using equation 4.6.

$$N = 2\pi\alpha\ell \left(\frac{1}{\lambda 2} + \frac{1}{\lambda 1}\right) \left(1 - \frac{1}{\beta^2 n^2}\right) \qquad (4.6).$$

where:

α is the fine structure constant = $e^2/hc = 1/137$.
n is the average refractive index of the medium.
β is the ratio of velocity in the medium to that of light in vacuum.

Taking, for example, 500 KeV electrons moving through a depth of 1.0 mm of pure silica and plastic fibre materials, it can found from equation 4.6 that between 407nm and 442 nm, approximately 0.04 photons (for silica fibre) and 0.05 (for plastic fibre) are emitted by a single electron of this energy, for β^2=1.02

and n=1.458 (for silica fibre) and n=1.492 (for plastic fibre). β is taken as the ratio of velocity of electrons in the medium to that of light in the vacuum, using relativistic energy and mass equation.

From the above example, we can conclude that Cerenkov emitted light background, which represents most of the background in the system, essentially does not pass through the optical filter within the bandwidth and can be considered near zero.

CHAPTER 5

Characteristics of scintillator with SiO_2 & PMMA fibres for detectors of the x-ray beam

5.1 Introduction

In this chapter, the general characteristics of the SiO_2 and PMMA optical fibres used with the scintillation detectors when irradiated by high energy photon beams is assessed. The two types of fibre optic materials used have different physical and mechanical characteristics. The optical fibres chosen for this investigation are from Edmund Optics Ltd. [26]. The first fibre (SiO_2) is a high OH content radiation resistant hard-core silica fibre type NT57-071, having a core diameter of 1000 μm with a cladding thickness of 100 μm. The fibre numerical aperture is 0.22 (core refractive index = 1.458, cladding refractive index = 1.441, continuous minimum bend radius = 275mm, acceptance angle = 25.4°). The numerical aperture of 0.22 is an f-number of 2.3. Therefore, all the light emitting from this fibre will be collected by the f-number 1.0 collection lens. The fibre cladding is surrounded with a 1400 μm nylon buffer for greater protection. The outer jacket was covered with a polyvinylchloride shrinkable tubing to make the fibre light proof from external sources.

The second fibre is Eska acrylic fibre optics type VO2-536, having a core diameter of 980μm and sheathed with a special thin layer of fluorine polymer that has a lower refractive index than the fibre core. The PMMA fibre numerical aperture is 0.51 (core refractive index = 1.492, cladding refractive index = 1.402, continuous minimum bend radius = 55mm, acceptance angle =61.0°). This numerical aperture of 0.51 is an f-number of 0.98. Therefore, the fibre nearly matches the f-number 1.0 collection lens. The fibre cladding is surrounded by a black polyethylene jacket for greater protection and to be light proof from external sources.

The light from the scintillators was transmitted through the optical fibres and then detected using a photosensitive device (BPW21 photodiode from R.S) [35], which converts the light into an electrical signal. This photodiode is one of the most sensitive devices among semiconductor detectors in the blue region. The BPW21 relative spectral sensitivities were 0.4 at 425nm wavelength and 0.12 at 375nm. The sensitivity decreased with decreasing wavelength from 375 nm. Therefore, the sensitivity of the BPW21 photodiode was approximately 25% or less for the maximum Cerenkov light compared to the peak scintillator emission.

The SiO_2 and PMMA optical fibre coupled scintillation detectors were exposed to high energy photon beams using a Varian CLINAC 2100C linear accelerator. The electrical signals from the photodiodes were evaluated using two channel digital storage oscilloscopes from Tektronix [36], with a software product designed to interface the oscilloscope data to the computer. This option allows for remote control, capture, analysis and document waveform and measurement data. Readings from both the SiO_2 and PMMA optical fibre coupled scintillation detectors were measured simultaneously to for an accurate result comparison.

5.2 Reproducibility and stability of detector signals

Two prototype plastic scintillation detectors composed of two small plastic scintillators measuring 10mm in length and 3mm in diameter, spliced into two different fibre optic cables (SiO_2 and PMMA) was used to study reproducibility and stability of the system signals. The distal ends of the fibres were connected into an electronics box containing the focusing optics, the optical filter, and the photodiodes that were connected to the digital oscilloscope described in 5.1. The measurements were performed in a solid water phantom, using a 6 MV single energy linear accelerator [37]. The irradiation rate was 250MU/min at a distance of 100 cm between the source and surface of the phantom. The field size was set to be 10×10 cm^2 and the point of measurement was set at d_{max} = 15 mm. The oscilloscope trace showed the intensity of light from a single radiation pulse from

the LINAC, as opposed to the signals accumulated and averaged over a longer period of time. Figure 5.1 shows that the relative readings of the SiO_2 detector are contained well within ± 3.5%. A percentage standard deviation of 0.74% was obtained for a series of 10 readings using the SiO_2 fibre.

Under similar irradiation parameters, a percentage standard deviation of 0.87% was obtained for a series of 10 consecutive readings using the PMMA fibre optic. Figure 5.2 shows that the relative readings of the PMMA detector are contained well within ± 3.96%.

5.3 Dose rate proportionality

The dose rate proportionality of the miniaturized plastic scintillation detectors (10mm in length and 3mm in diameter) were tested using Varian linear accelerator (Varian CLINAC 2100C) at different dose rate settings; namely 50, 100, 150, 200 and 250 MU/min. These dose rates are specified at d_{max} = 15 mm for 6MV beam energy (15 mm) for a field size equal to 10×10 cm^2 and an SSD equal to 100 cm, so that 1 MU corresponds to 1.0 cGy in water. The monitor chamber is calibrated at the 250MU/min settings for 6MV photon energy. A Farmer ion chamber was used to calibrate the other dose rate settings (MU/min) in terms of the actual delivered dose rate expressed in cGy/min for 6MV photon energy.

The responses of the miniaturized plastic scintillation detectors using SiO_2 and PMMA fibre optic cables were determined by simultaneous photodiode response to an irradiation of 50, 100, 150, 200 and 250 cGy/min. The mean response for a single radiation pulse is equal to 1780 mV for the SiO_2 fibre optic cable ± 1.66 % and is equal to 2160 mV for the PMMA fibre optic cable ± 1.9 %. This shows that the detector responses are independent of dose rate in the range investigated as shown in figure 5.3 for the SiO_2 fibre optic cable and figure 5.4 for the PMMA fibre optic cable.

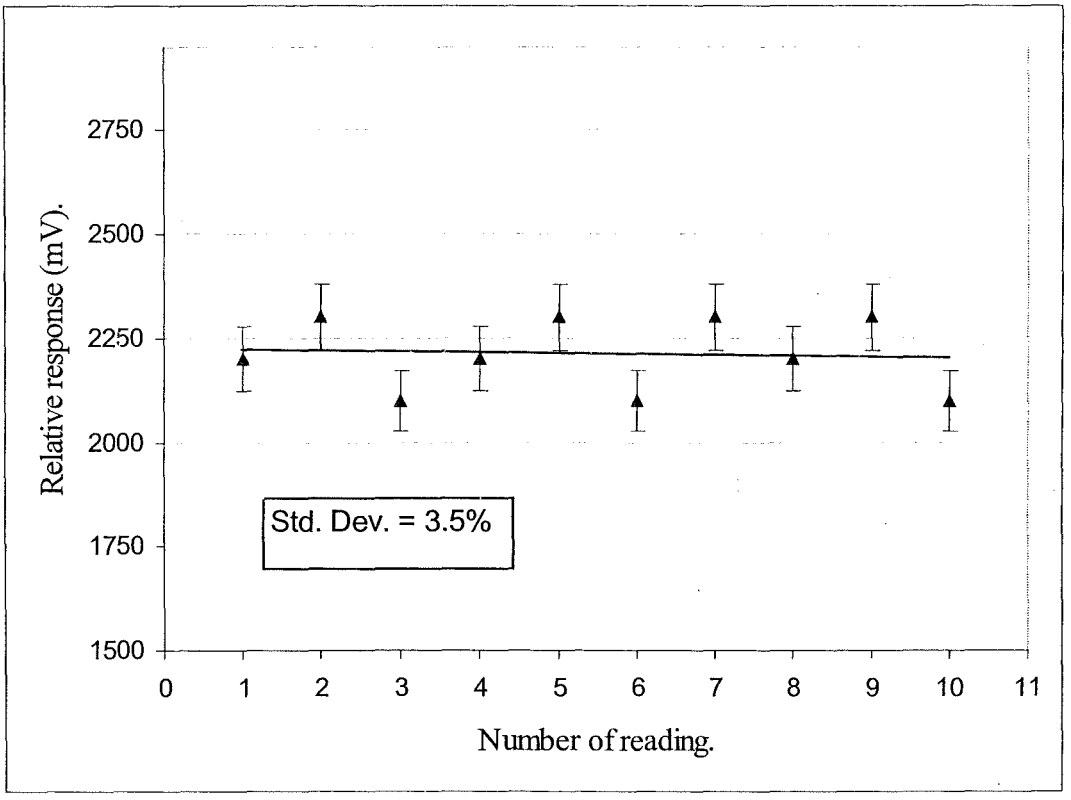

Figure 5.1: Response of miniaturized plastic scintillation detector using SiO_2 fibre in a 6 MV x-ray beam, with 10X10cm^2 field size, 250MU/min and 100cm source to phantom distance. The line shows the mean value and the error bars show the standard errors of the mean.

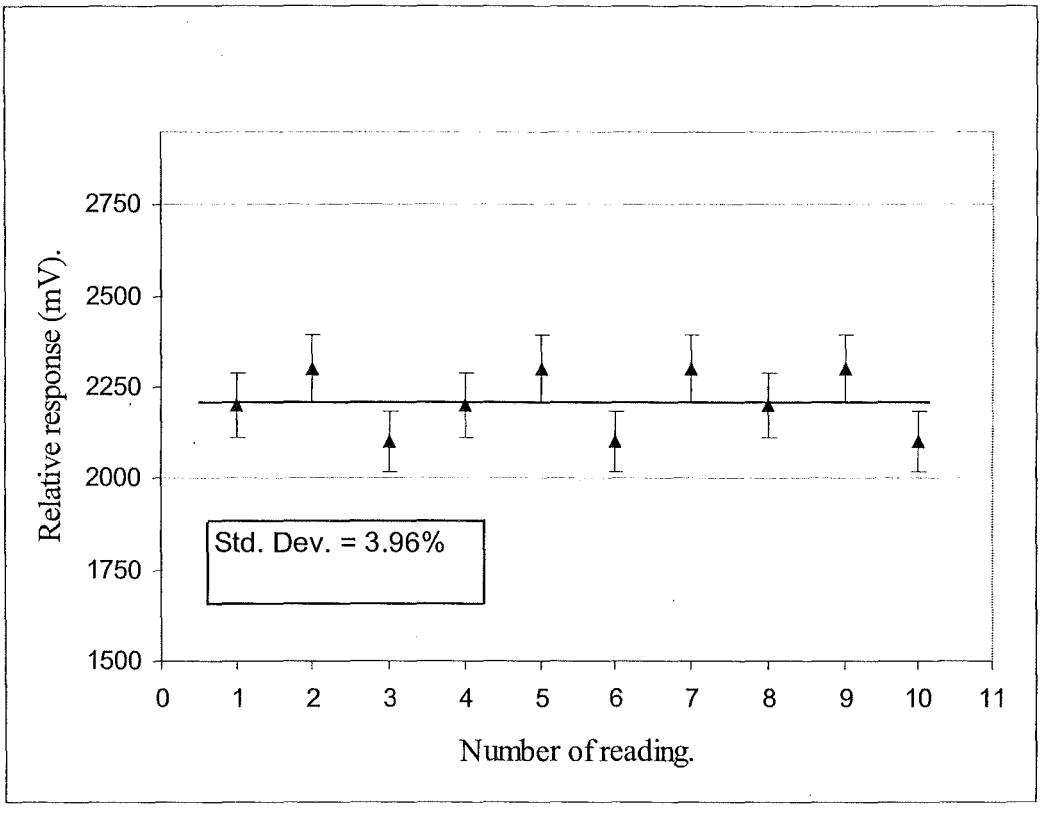

Figure 5.2: Response of miniaturized plastic scintillation detector using PMMA fibre in a 6 MV x-ray beam, with 10X10cm^2 field size, 250MU, and 100cm source to phantom distance. The line shows the mean value and the error bars show the standard errors of the mean.

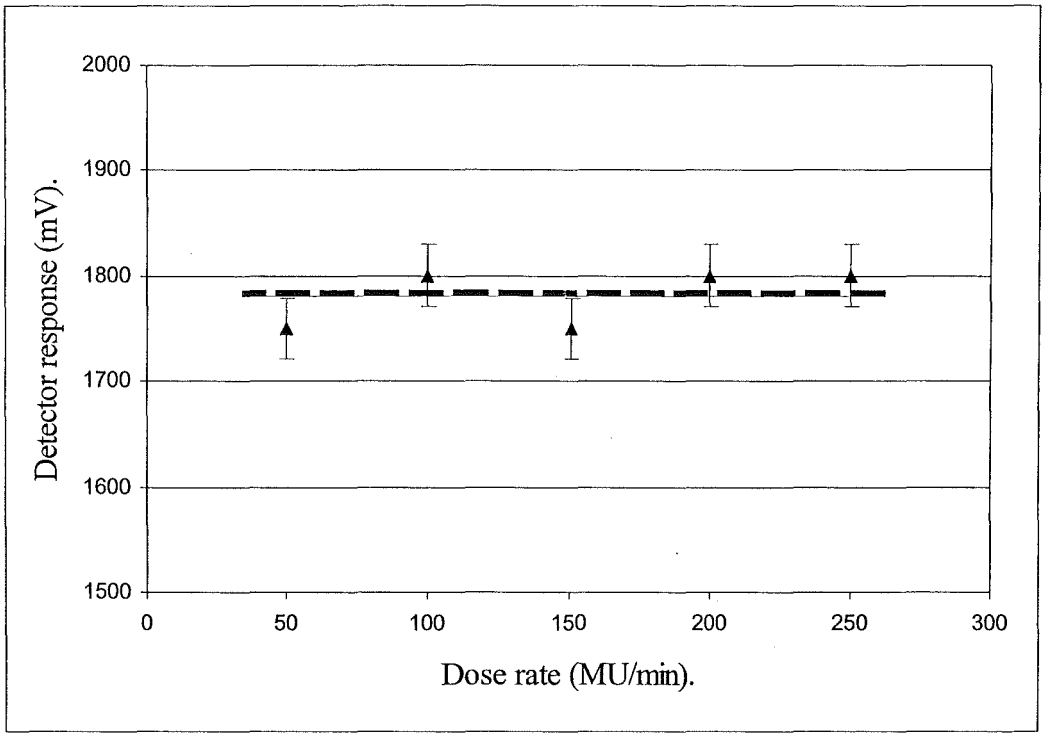

Figure 5.3: Detector response vs. dose rate of miniaturized prototype scintillation detector 10mm in length and 3mm in diameter at 6 MV photon energies using SiO_2 fibre optic light guide cable. The dashed line shows the mean value and the error bars show the standard errors of the mean.

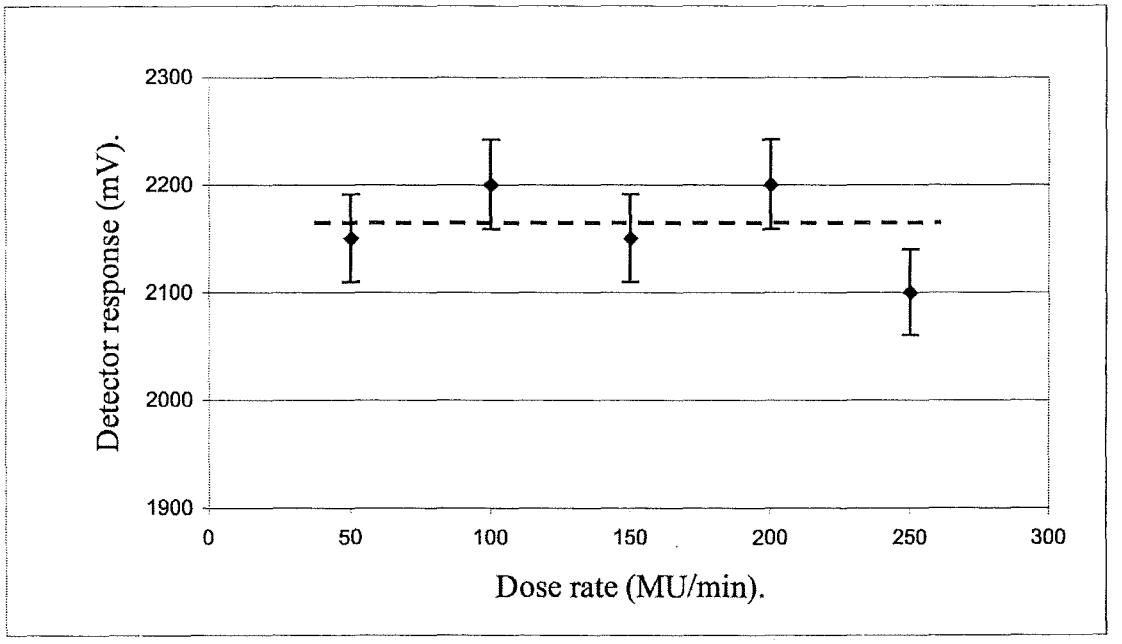

Figure 5.4: Detector response vs. dose rate of miniaturized prototype scintillation detector 10mm in length and 3mm in diameter at 6 MV photon energies using PMMA fibre optic light guide cable. The dashed line shows the mean value and the error bars show the standard errors of the mean.

5.4 Depth dose distribution in water

Depth dose measurements in water were performed using the miniaturized plastic scintillation prototype detectors. The scintillators are 10mm in length and 3mm in diameter and are spliced into two different fibre optic cables namely, SiO_2 fibre optic cable and PMMA fibre optic cable. The measurements were compared with the depth dose curves obtained using ionisation chambers. The measurements were performed on a Varian linear accelerator providing a 6MV photon beam.

These measurements were made using an automatic water phantom tank system that was controlled by computer software from PTW [38] for a 10×10 cm^2 field size at an SSD of 100 cm for the 6 MV photon beam. Figure 5.5 and figure 5.6 compare the depth dose measurements obtained with an ion chamber and the depth dose obtained with the miniaturized plastic scintillation detectors. First, a Farmer ion chamber was used to generate the depth dose profile for the 6 MV photon beam for a 10×10 cm^2 field size. Then, the experiment was repeated with the SiO_2 and PMMA optical fibre coupled scintillators to generate the depth dose profile for the same 6 MV photon beam and same field size and under the same irradiation parameters.

On the whole, the correlations between the measurements from the ion chamber and scintillation detectors are good. In particular, the depth dose profile of the scintillation detector with the SiO_2 fibre optic cable overlaps nearly exactly with that of the ion chamber. But, when the PMMA fibre optic cable material was used, there is a small deviation from the ion chamber profile as the depth of the detector increases. These deviations may be attributed to the stem effect within the PMMA fibre optic cable (Cerenkov contribution), which was exposed to larger field sizes as distance increased.

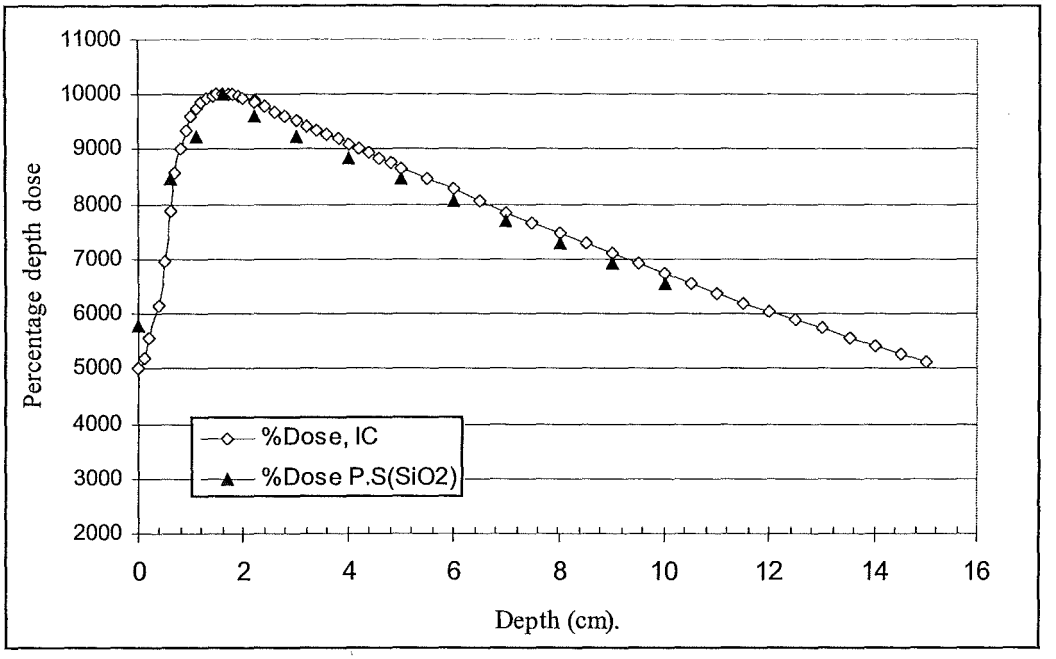

Figure 5.5: Percentage depth dose in water obtained using the miniaturized prototype plastic scintillation detector (P.S), using SiO_2 fibre optic cable. The results are compared to the depth dose obtained using 0.125 cm^3 PTW Semiflex chambers (IC) for a 6 MV photon beam. The line is drawn to guide the eye.

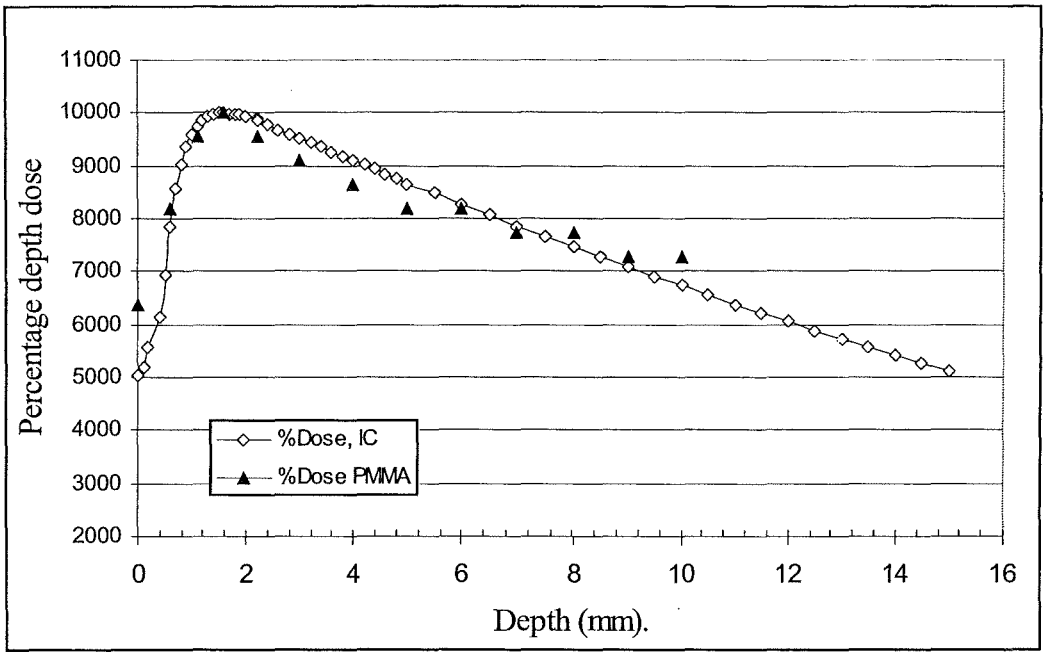

Figure 5.6: Percentage depth dose in water obtained using the miniaturized prototype plastic scintillation detector (P.S), using PMMA fibre optic cable. The results are compared to the depth dose obtained using 0.125 cm^3 PTW Semiflex chambers (IC) for a 6 MV photon beam. The line is drawn to guide the eye.

Figure 5.5 and figure 5.6 show the good agreement between the depth dose profiles of the ion chamber and the miniaturized plastic scintillation detectors. Also, these figures show the effects due to larger field size and the stem effect in the PMMA fibre optic cable. Moreover, these figures clearly show that the SiO_2 fibre optic cable has a good tolerance to radiation, while the PMMA fibre optic cable shows more sensitivity to radiation as a greater length of fibre is irradiated. The larger numerical aperture (or equivalently, the larger acceptance angle) of the PMMA fibre compared to the SiO_2 fibre makes it more susceptible to Cerenkov radiation. So, this result is expected.

Absorbed dose is the mean energy absorbed in a medium due to photon interactions per unit mass. The dose can be assessed at any point using the dosimetry protocols. A reference dose is usually assessed at the depth of the maximum dose (d_{max}), where the percentage relative dose is normalized to $D(d_{max}, f, S, E)$ or D_{max}. The dose within the body is then used in computer treatment planning calculations in terms of percentage depth dose, which is the ratio, expressed as a percentage, of the absorbed dose at any point to the dose at D_{max} [39] as shown in equation 5.1:

$$\%D(d_{10},f,S,E) = \frac{D(d_{10},f,S,E)}{D(d_{\max},f,S,E)} \times 100 \qquad 5.1$$

where,

$\%D$	represents percentage depth dose.
d_{10}	represents depth dose at 10 cm inside the phantom.
$d_{\max}$	represents maximum depth dose inside the phantom.
f	represents distance between the beam source and phantom surface.
S	represents field size.
E	represents photon beam energy.

Values of D_{10}/D_{max} for the SiO_2 and PMMA miniaturized plastic scintillation detectors were compared with D_{10}/D_{max} obtained using the CADSCAN dosimetry system at the research centre of King Faisal Specialist Hospital in Saudi Arabia. The measurements were made in water with a 6 MV photon beam and a 10×10 cm^2 field size. The miniaturized plastic scintillation detector using the SiO_2 fibre optic cable shows a 6.4% deviation from the data obtained using the CADSCAN dosimetry system, while the detector using the PMMA fibre optic cable shows better matching with only a 3.2% deviation from the results obtained using the CADSCAN dosimetry system.

These results were corrected for background noise using a narrow band optical filter to reject most of the light arising from the stem effect. The background signal arises mainly from the inherent dark current of the photodiode and from the Cerenkov light generated in the fibre. With good optical coupling, the Cerenkov contribution is small when compared to the light output of the scintillators. In our case, the Cerenkov contribution to the total output signal of the detector (for a field size of 10×10 cm^2 and for 6 MV x-ray beam) was equal to 5.4% for the miniaturized plastic scintillation detector using PMMA fibre optic cable material.

In comparison with the results obtained from the ion chamber, a maximum deviation of approximately 1.9% is observed for the scintillation detector with the SiO_2 fibre optic cable. In the case of the PMMA scintillation detector the maximum deviation is approximately 4.6%. These percentages are valid for responses in water of depth 50 mm. The percentage divergence of the PMMA scintillation detector is greater than that for the SiO_2 detector at all depths. As the depth increases the percentage divergence of the SiO_2 detector decreases, especially along the descending tail of the ion chamber curve. The Cerenkov light output induced in the PMMA fibre varies smoothly with depth. When the Cerenkov signal starts to contribute to the overall signal it is due to the gradually increasing diffuseness of the angle of secondary electron transport, allowing more light to enter the acceptance cone of the fibre. This is valid only for photon beams

and only when the stem of the miniaturized plastic scintillation detector is perpendicular to the central axis of the radiation beam. These deviations might increase with increasing irradiation field sizes and with beam angulations.

5.5 Photon beam profiles

The miniaturized plastic scintillation detectors were used in measurements of the penumbral region of 6 MV photon beam profiles. The results were compared to those obtained using a 0.125 cm^3 PTW Semiflex ionisation chamber. Both the ion chamber and the miniaturized plastic scintillation detectors were oriented perpendicular to the radiation beam. Their longitudinal axes were perpendicular to the beam central axis and to the scanning direction.

Transverse and radial dose profiles were measured for a 6 MV photon beam in a 10×10 cm^2 field size at d_{max} for the above energy in a PTW-MP3-S automatic water phantom system. These measurements were compared to the results obtained from a PTW-MP3-S ion chamber system. The same software (PTW-Freiburg Mephysto Export V.6.0) was used for measurements of both the miniaturized plastic scintillation detector and the PTW ion chamber. Continuous movement of the miniaturized plastic scintillation detectors during irradiation could not be achieved due to the different electronic system of the scintillation system compared with the ion chamber system.

The spatial resolution of a detector depends on the size and the shape of the detecting volume and also on the orientation of the detector relative to the scan direction. The SiO_2 and PMMA optical fibres coupled to miniaturized plastic scintillation detectors both show superior similar resolution compared to the 0.125 cm^3 ion chamber. The SiO_2 and PMMA fibre optic cables have different radiation resistances with the SiO_2 fibre optic able to withstand more radiation.

In spite of different resistances to radiation, both SiO_2 and PMMA detectors exhibit similar spatial resolution compared with the 0.125 cm^3 PTW ion chamber. The response of the PMMA fibre optic cable is very good and shows no effect due to background signal such as Cerenkov radiation. This result justifies recommendation of PMMA fibre optic cable. Another main advantage of the PMMA cable that makes it more suitable for in vivo measurements is its flexibility.

Figure 5.7 and figure 5.8 show full transverse and radial dose profiles respectively of a 6 MV photon beam for a 10×10 cm^2 field size at d_{max} in a water tank phantom using the miniaturized plastic scintillation detector that is spliced with a SiO_2 fibre optic cable. The results are compared with those from a 0.125 cm^3 PTW ionisation chamber. Figure 5.9 and figure 5.10 show full transverse and radial dose profiles respectively of a 6 MV photon beam for a 10×10 cm^2 field size at d_{max} in a water tank phantom using the miniaturized plastic scintillation detector that is spliced into PMMA fibre optic cable. The results are compared with those from a 0.125 cm^3 PTW ionisation chamber.

The same irradiation parameters; including 10×10 cm^2 field size, 250 MU/min as dose rate, SSD=100 cm and d_{max} = 15 mm, were used for all dose profile investigations.

5.6 Intensity linearity of the miniaturized detector

The miniaturized plastic scintillation detectors were tested for intensity linearity signatures with a 6 MV LINAC photon beam. These studies were performed using Perspex as a build up phantom, with d_{max} = 15 mm. The intensity linearity was measured at different distances between the source and the surface of the phantom: 85, 95, 105, 115, 125, 135 and 145 cm.

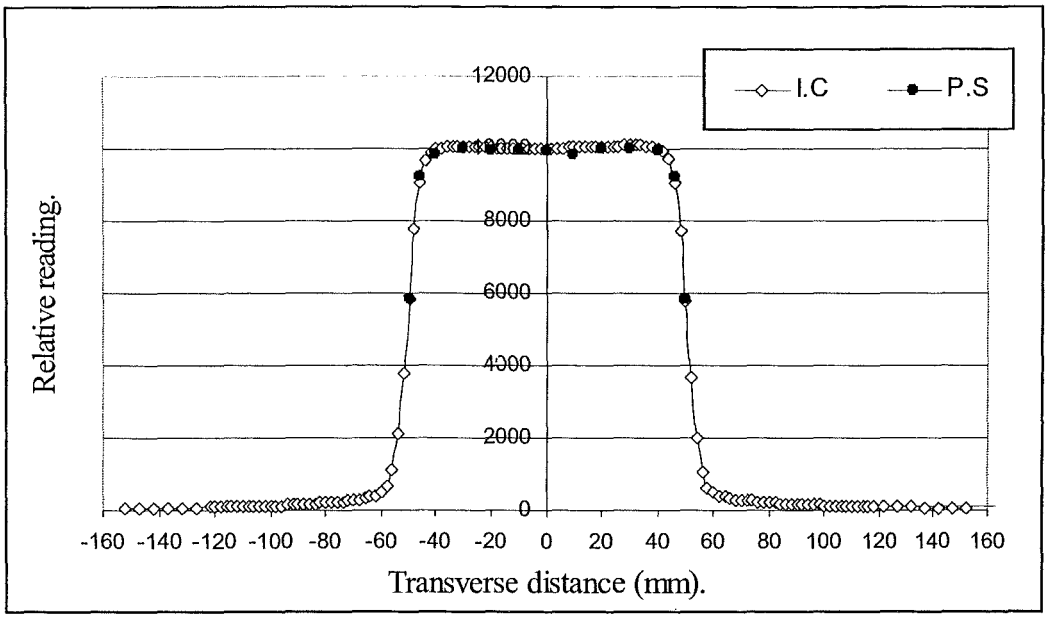

Figure 5.7: Transverse dose profile of a 6 MV photon beam for 10x10cm^2 field size at 15mm depth in water tank phantom using miniaturized plastic scintillation detector (P.S) that is spliced into SiO_2 fibre optic material and compared with 0.125 cm^3 PTW Semiflex ionisation chambers (I.C). The line is drawn to guide the eye.

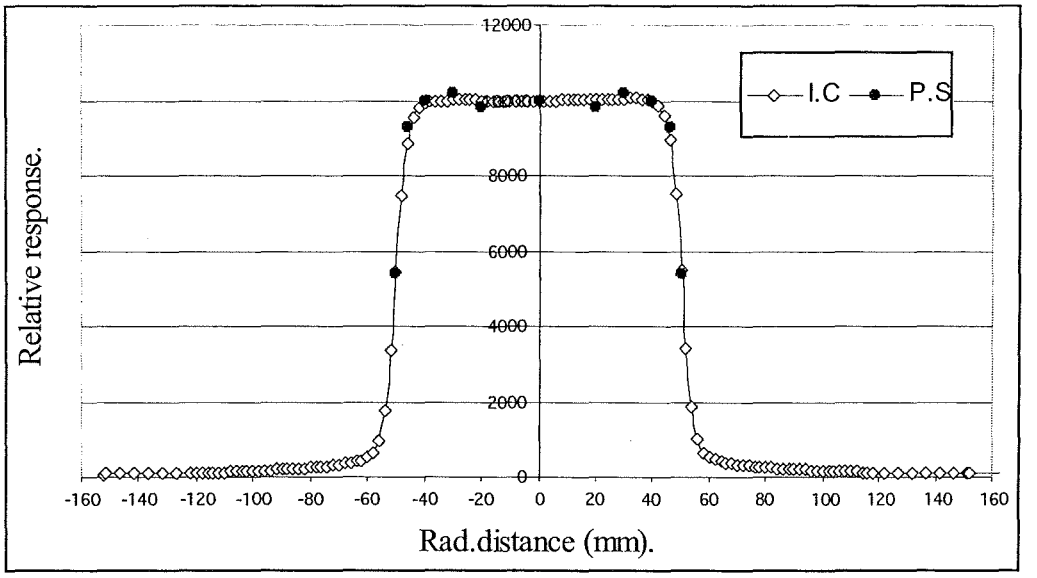

Figure 5.8: Radial dose profile of a 6 MV photon beam for 10x10 cm^2 field size at 15 mm depth in water tank phantom using miniaturized plastic scintillation detector (P.S) that is spliced into SiO_2 fibre optic material and compared with 0.125 cm^3 PTW Semiflex ionisation chambers (I.C). The line is drawn to guide the eye.

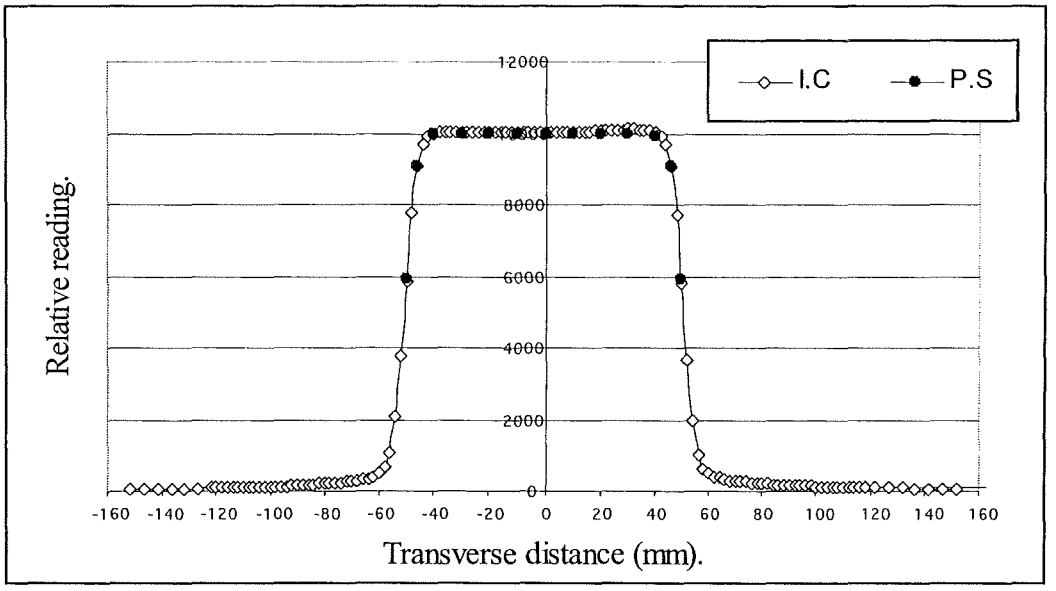

Figure 5.9: Transverse dose profile of a 6 MV photon beam for 10x10 cm^2 field size at 15 mm depth in water tank phantom using miniaturized plastic scintillation detector (P.S) that is spliced into PMMA fibre optic material and compared with 0.125 cm^3 PTW Semiflex ionisation chambers (I.C). The line is drawn to guide the eye.

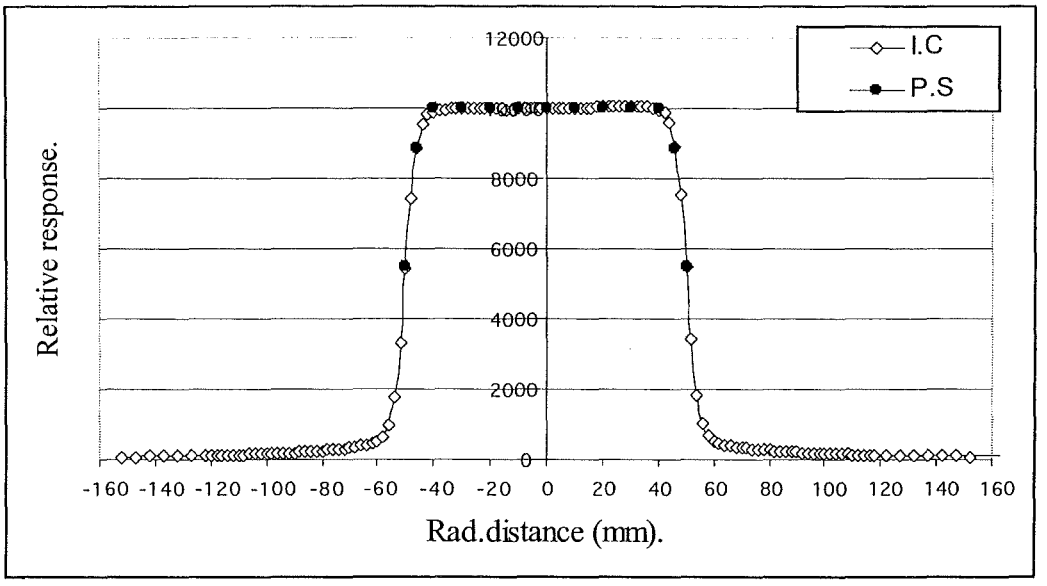

Figure 5.10: Radial dose profile of a 6 MV photon beam for 10x10 cm^2 field size at 15 mm depth in water tank phantom using miniaturized plastic scintillation detector (P.S) that is spliced into PMMA fibre optic material and compared with 0.125 cm^3 PTW Semiflex ionisation chambers (I.C). The line is drawn to guide the eye.

Figure 5.11 shows the response of the detector as a function of increasing distance from the source. The tails of the curves are affected by background contribution especially in the case of the PMMA fibre optic. The background contribution was expected to be greater with the PMMA detector due to wide acceptance angle and decreased radiation resistance compared with the SiO_2 detector. Moreover, with both fibre materials the length of fibre exposed increases as the distance between the source and surface of the phantom increases. This may contribute to increased interference in the tail regions of the curve.

5.7 Dependence on irradiation fibre length

The optical fibre light guide used in these studies consists of two types of fibre optic materials; SiO_2 fibre optic cable and PMMA fibre optic cable. Both were shielded from non-plastic scintillator light by a plastic jacket. The miniaturized plastic scintillation detectors were exposed to a 6 MV photon beam. The measurements were performed in a Perspex phantom at the corresponding d_{max} for a 6 MV photon beam. The dose rate in these conditions was 2.5 Gy/min. The miniaturized plastic scintillation detectors were positioned perpendicularly with respect to the radiation beam, so that their longitudinal axes were orthogonal to the beam central axis. The system responses with cable length are shown in figure 5.12.

In general, the percentage increase in response for the PMMA fibre optic cable was approximately 10% greater than that for the SiO_2 fibre optic cable over the range of fibre lengths studied. The different response is expected due to different properties and different acceptance angles of the two materials.

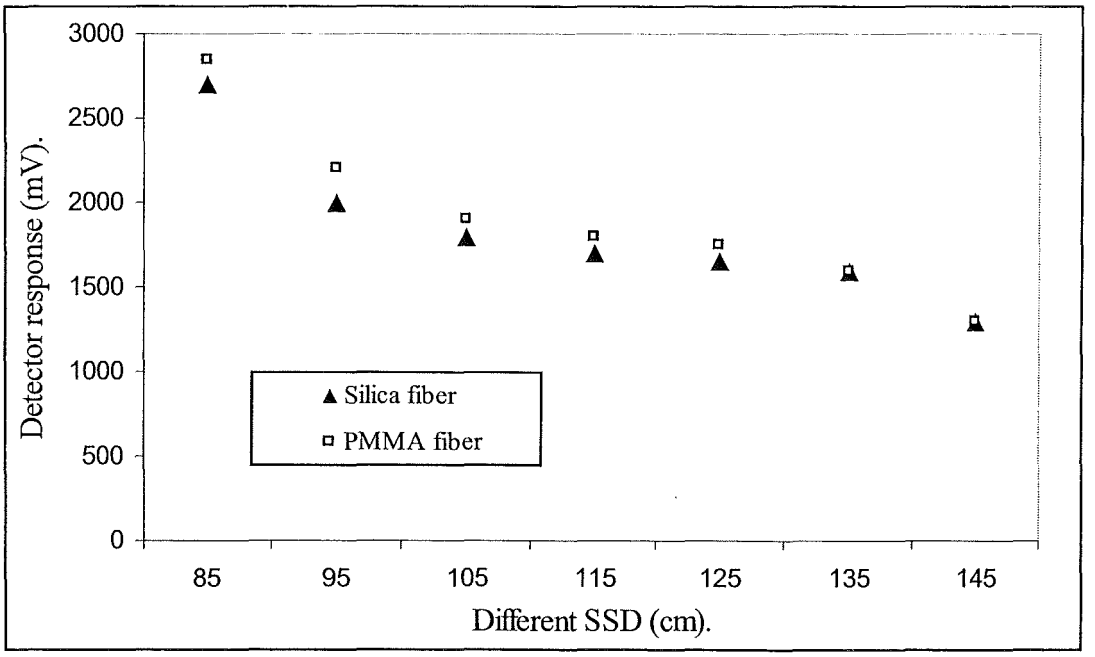

Figure 5.11: Detector response using SiO_2 (Silica) and PMMA fibre optic light guides for 6MV photon beam at different source to surface distances, using 100MU, SSD=100 cm, d_{max} = 15 mm on solid water phantom and dose rate equals 250MU/min.

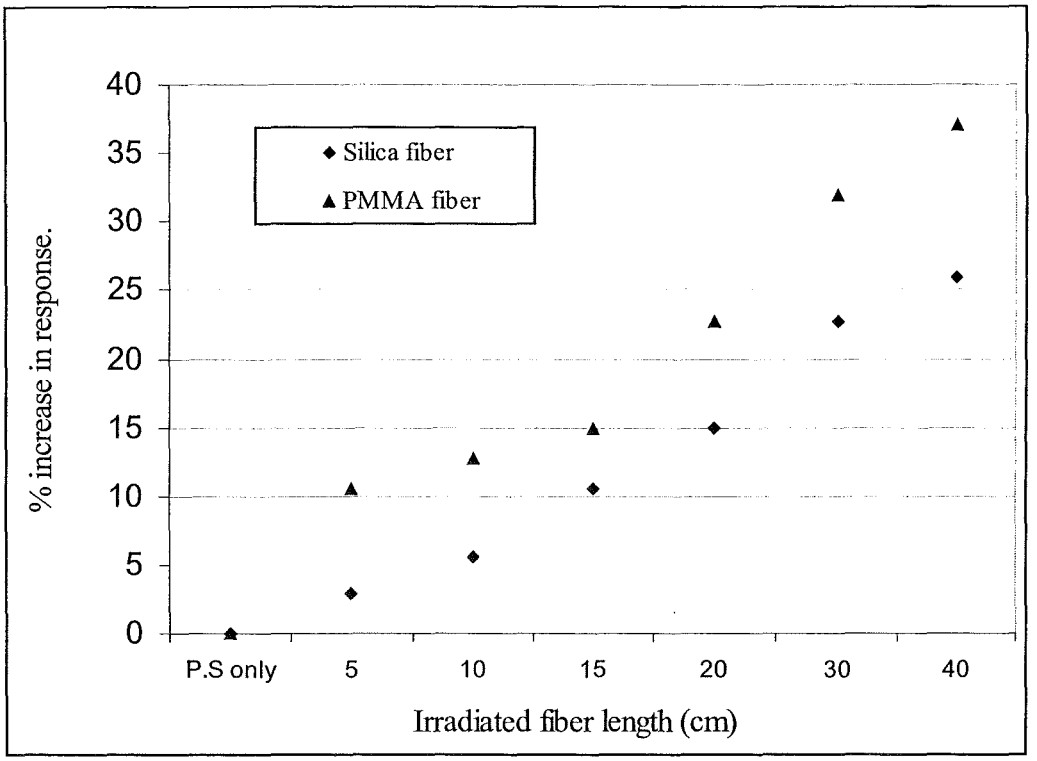

Figure 5.12: Percentage increase in detector response due to irradiation of the fibre optic cables compared with plastic scintillators response only. Irradiation made using 6MV photon beam, 100MU, SSD=100 cm, d_{max}=15 mm with a Perspex phantom and dose rate of 250MU/min.

5.8 Dependence on irradiation field size

The miniaturized plastic scintillation detectors were exposed to a 6 MV photon beam using five beam sizes of 5x5 cm^2, 10x10 cm^2, 15x15 cm^2, 20x20 cm^2, 30x30 cm^2 and 40x40 cm^2. The measurements were performed in a Perspex phantom at the corresponding d_{max} for a 6 MV photon beam. The miniaturized plastic scintillation detectors were positioned perpendicularly with respect to the radiation beam, so that their longitudinal axes were orthogonal to the central axis of the beam. SiO_2 and PMMA detector responses as a function of irradiated field sizes were obtained for a 6 MV photon beam as shown in figure 5.13.

Over the range of field sizes investigated, the SiO_2 fibre optic material shows less variation in detector response relative to the response of the PMMA fibre optic detector. However, the increase in detector response at larger field sizes may arise from scattering and multi scattering of radiation. Figure 5.13 clearly shows the effect of beam size on detector response for the two different optical fibre materials.

5.9 Beam directional dependence

Beam directional dependence was measured for the prototype plastic scintillation detectors spliced into the two different fibre optic cables (SiO_2 and PMMA) using a 6 MV photon beam in a solid water phantom at d_{max} corresponding to a 6 MV photon beam. A 5 cm length of the end of the fibre light guide (SiO_2 and PMMA) was positioned parallel to the plane of the gantry rotation at the isocentre. The 5 cm length was fixed, pointing sidewards as shown in figure 5.14. The angle of the central axis of the photon beam was varied from 45° toward the photodiode to 45° toward the plastic scintillator. A fixed field size of 10×10 cm^2 was selected to ensure full irradiation of the scintillator material at all gantry angles and to maintain the same fibre length within the field size, which was constantly irradiated at a 0° angle. The results are shown in figure 5.15. As

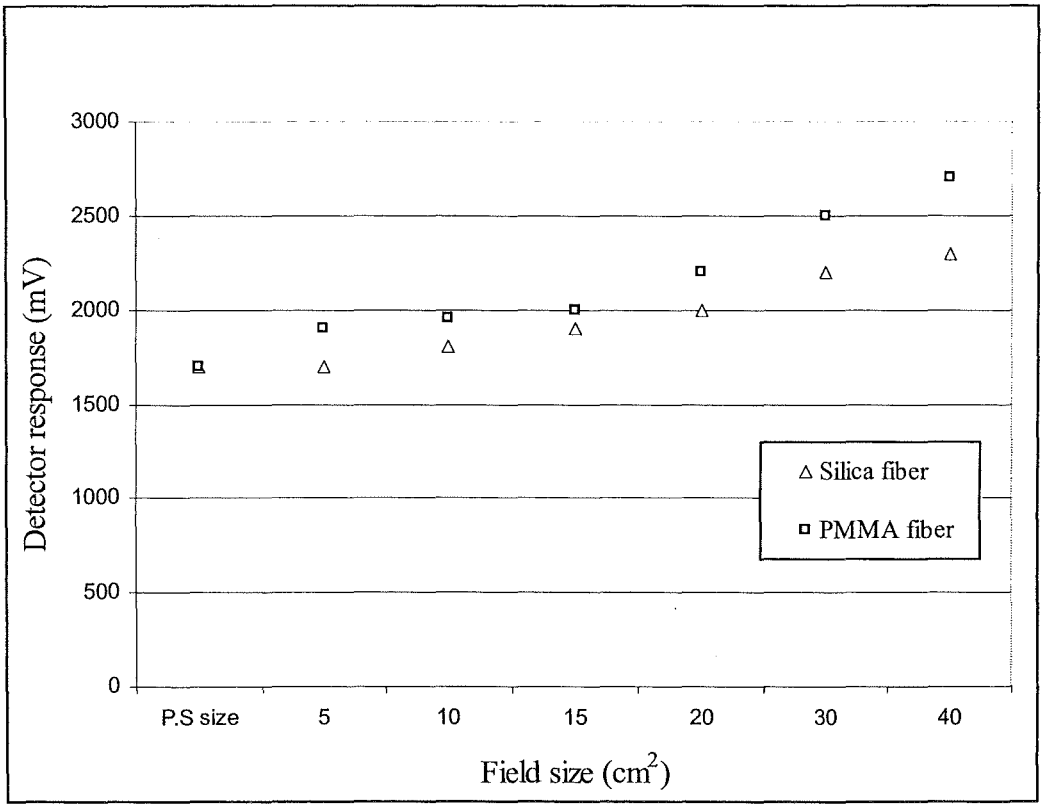

Figure 5.13: Effect of beam size on miniaturized plastic scintillation detector response using SiO_2 (Silica) and PMMA fibre optic light guide for 6MV photon beam with 100MU, SSD=100 cm, d_{max} = 15 mm at Perspex phantom and dose rate of 250MU/min.

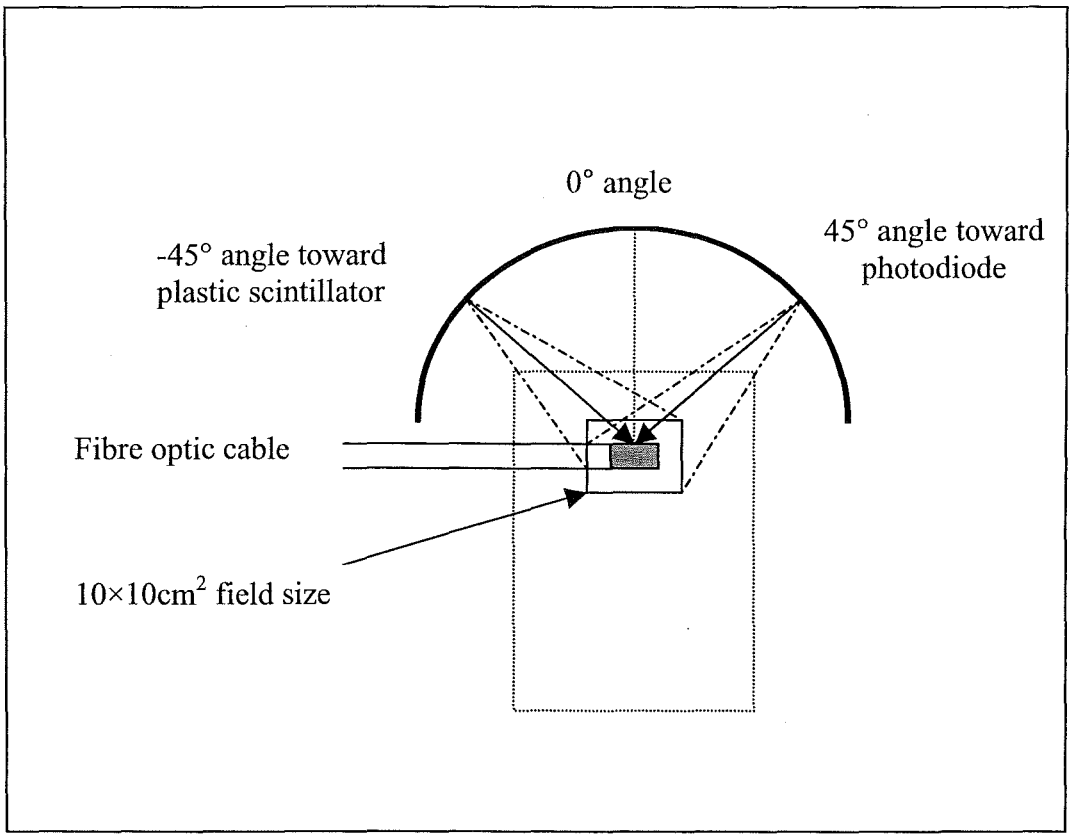

Figure 5.14: Experimental set-up and definition of angles for the fibre optic light guide in the photon beam to study the effect of beam angle on detector response. The beam size was fixed to be 10×10 cm^2 during all experiments.

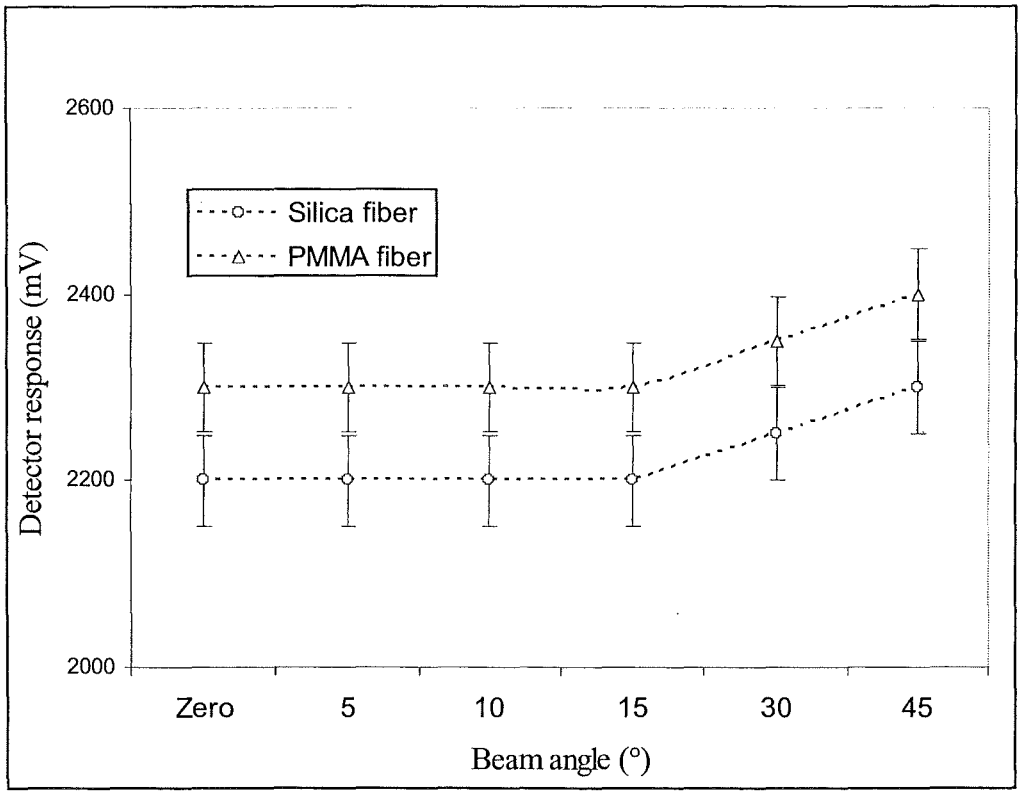

Figure 5.15: The radiation induced light intensity for SiO_2 (Silica) and PMMA fibre optic light guide at different photon beam angles irradiated toward photodiode as in set-up shown in figure 5.14. The dashed lines are to guide the eye.

the angle toward the photodiode are varies from 0° to 15° the light induced in both SiO_2 and PMMA fibres does not show any significant change in response. However beyond a 15° angle towards the photodiode the induced light for both the SiO_2 and PMMA fibres increases gradually to a peak at an angle of 45° toward the photodiode. Figure 5.16 shows that as the angle of rotation toward the plastic scintillator varies from 0° to 45°, the SiO_2 and PMMA detectors show flat responses with no significant increases.

The dominant background light generating process can be confidently identified as Cerenkov, in view of the angular dependence. The scintillation process and fluorescence in the optical fibres should be isotropic. As expected the PMMA fibre optic material again shows more angular dependence compared to the SiO_2 fibre optic material. The different acceptance angles, 61° for PMMA and 25.4° for the SiO_2 fibre optic material accounts for this difference in angular dependence.

On the basis of angular dependence, SiO_2 is the preferred fibre optic material. On the other hand the greater flexibility of PMMA is an advantage for therapeutic applications.

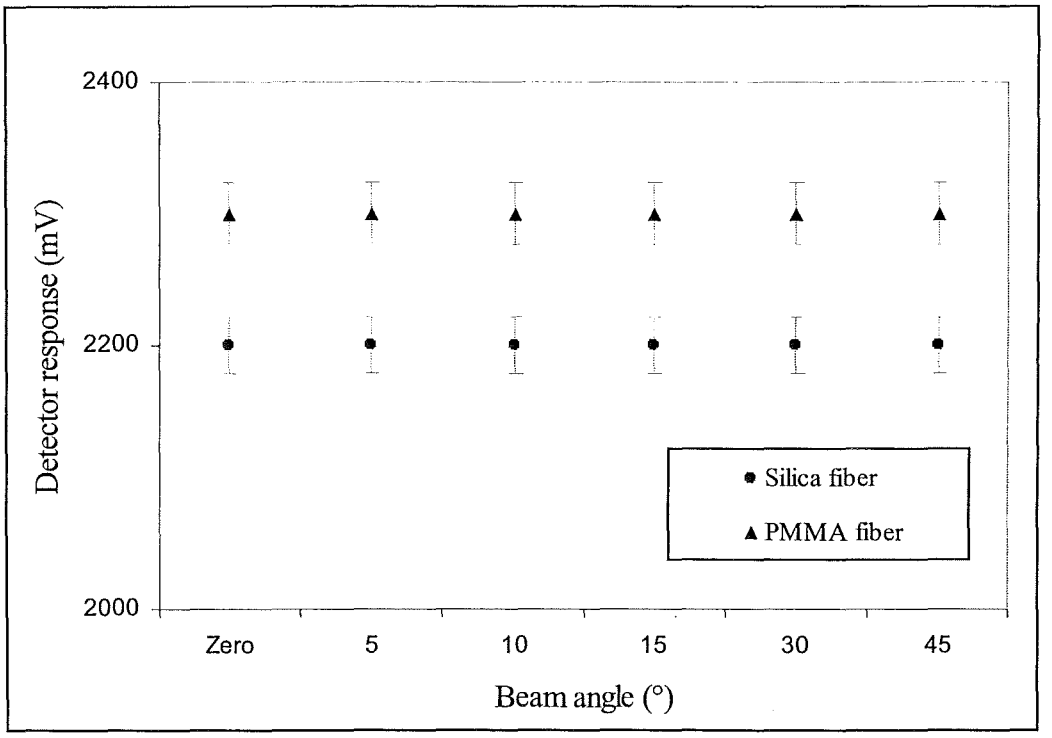

Figure 5.16: The radiation induced light intensity for SiO_2 (Silica) and PMMA fibre optic light guide at different photon beam angles irradiated toward plastic scintillator as in figure 5.14 set-up. The error bars are standard errors of the mean.

CHAPTER 6

Ultimate design characteristics of the detectors

6.1 Introduction

This chapter presents an evaluation of the general characteristics of the SiO_2 and PMMA optical fibre coupled detectors upon irradiation by high energy photon beams. The evaluation is based on use of a specially designed integrator and digital counting system (Appendix B). The dual dosimeter electronic system consists of two identical channels: one channel for SiO_2 scintillation detection and another channel for PMMA scintillation detection. The details of the integration and counting system are described previously in chapter 3. The integration system represents the final trial toward reducing the amount of interference light on detectors response. The circuits in Appendix B are design to suit the linear accelerator that used for this study.

6.2 Linearity of the detector signals at the integrator

To evaluate the linearity of the output signals at the integrator digital screen the prototype plastic scintillator detectors with both optical fibres were exposed to a 6MV x-ray beam linear accelerator Varian CLINAC 2100C [37]. The irradiation was performed using a water phantom at d_{max} = 15 mm and SSD = 100 cm. Figure 6.1 and figure 6.2 show the response of the SiO2 optical fibre coupled scintillation detector exposed to beam sizes of 10x10 cm^2 and 20x20 cm^2 respectively while figure 6.3 and figure 6.4 show the response of PMMA optical fibre coupled scintillation detector exposed to beam sizes of 10x10 cm^2 and 20x20 cm^2 respectively. Note that, the linearity of the output signals generated within the scintillator and coupled with the SiO_2 and PMMA fibre optic cables was evaluated using similar irradiation parameters. Figure 6.5 and figure 6.6 compare the linear response of the scintillator coupled with SiO2 fibre irradiated at a beam size of

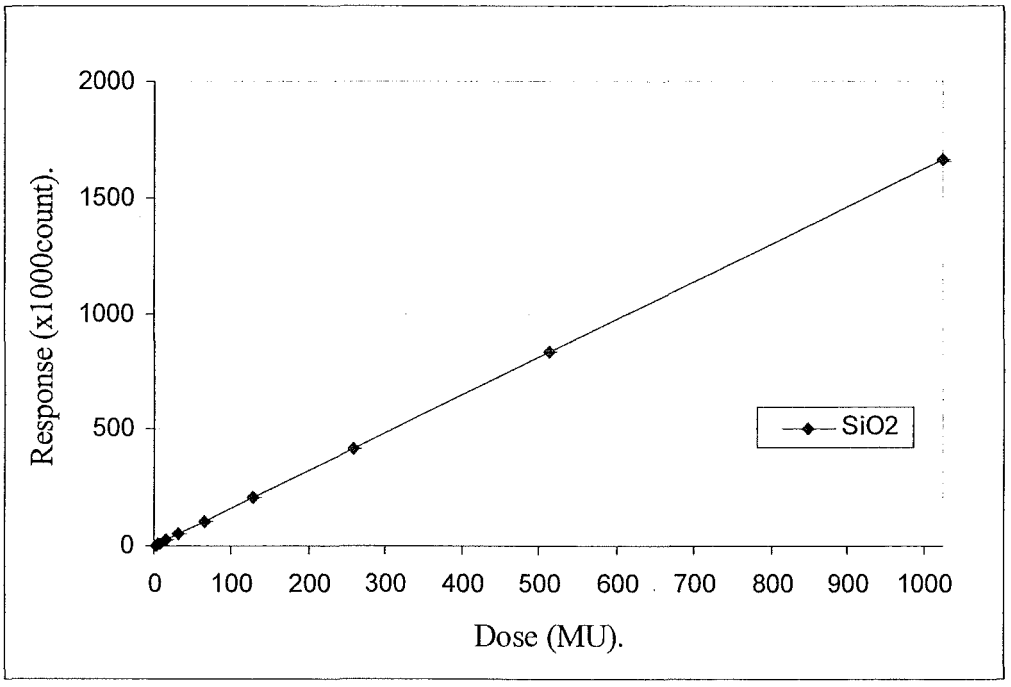

Figure 6.1: Response using a pulse integrator of the SiO_2 cable coupled scintillation detector 3 mm in diameter and 10 mm long exposed to 6MV x-ray photon beam, at field size of 10x10 cm^2. The line is a straight line least squares fit passing through the origin.

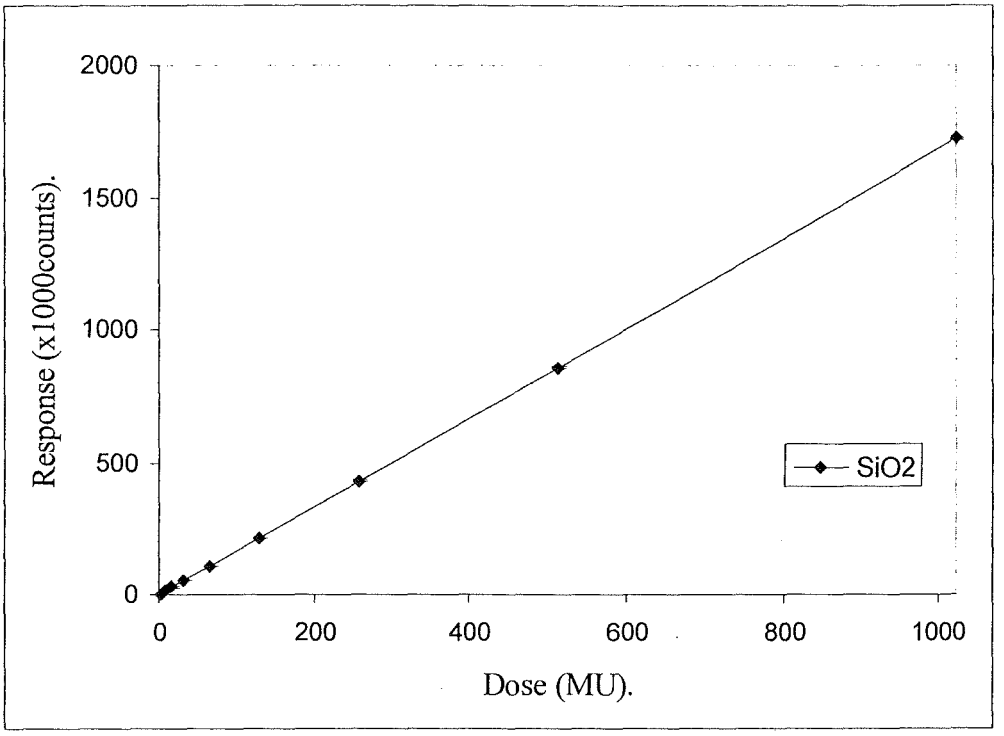

Figure 6.2: Response using a pulse integrator of the SiO_2 cable coupled scintillation detector 3 mm in diameter and 10 mm long exposed to 6MV x-ray photon beam, at field size of 20x20 cm^2. The line is a straight line least squares fit passing through the origin.

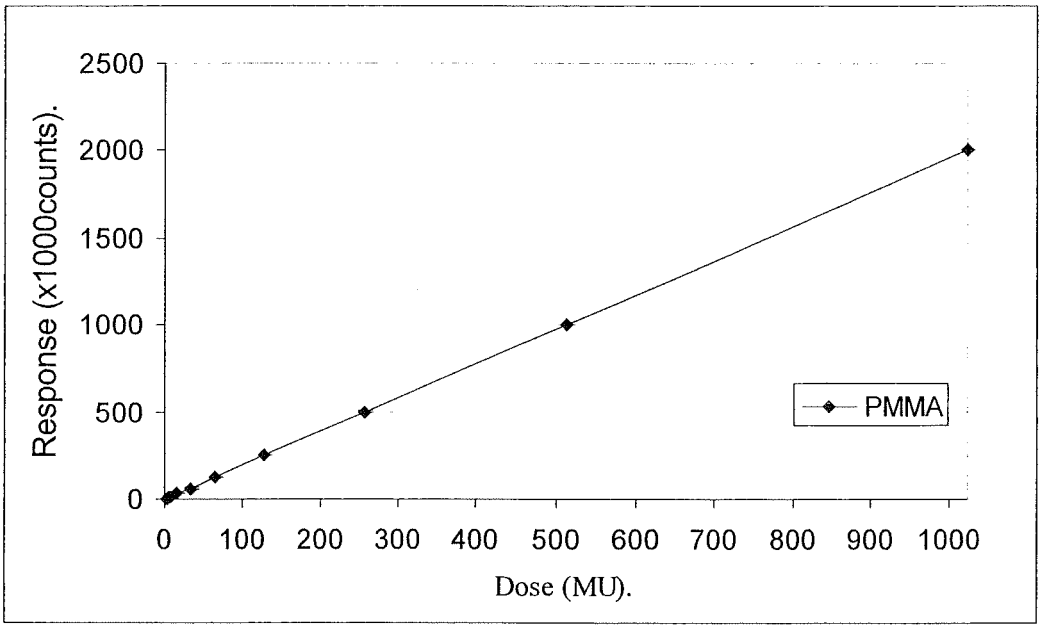

Figure 6.3: Response using a pulse integrator of the PMMA cable coupled scintillation detector 3 mm in diameter and 10 mm long exposed to 6MV x-ray photon beam, at field size of 10x10 cm^2. The line is a straight line least squares fit passing through the origin.

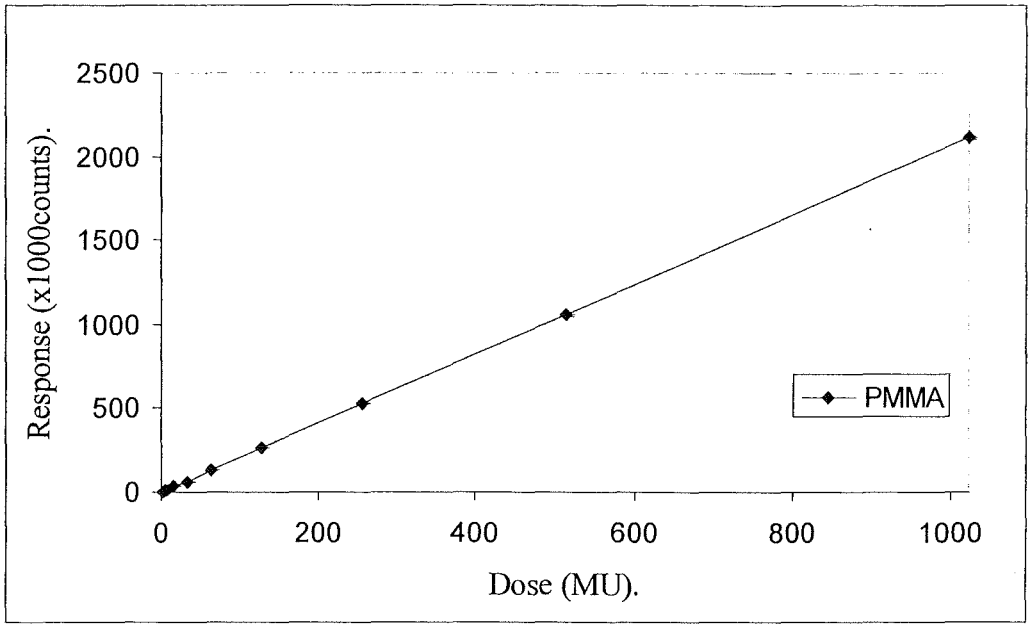

Figure 6.4: Response using a pulse integrator of the PMMA cable coupled scintillation detector 3 mm in diameter and 10 mm long exposed to 6MV x-ray photon beam, at field size of 20x20 cm^2. The line is a straight line least squares fit passing through the origin.

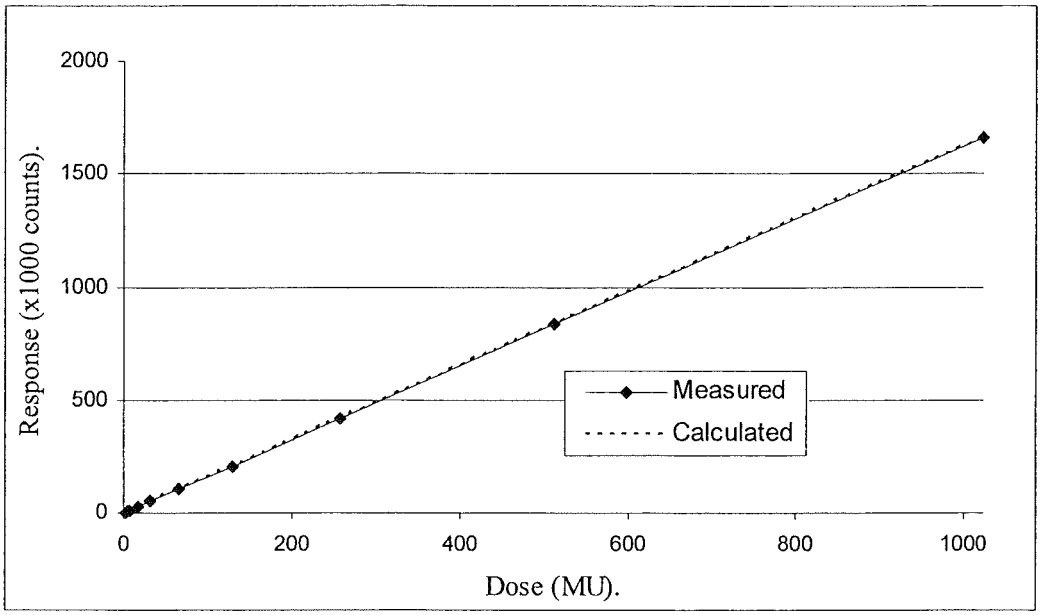

Figure 6.5: Response of SiO_2 fibre coupled scintillator detector irradiated by 6MV x-ray beam, field size of 10x10 cm^2. The solid line is a least squares fit of the data through the origin. The dashed line is a comparison of the values calculated by multiplying the first measured reading by the same factor by which the doses were increased.

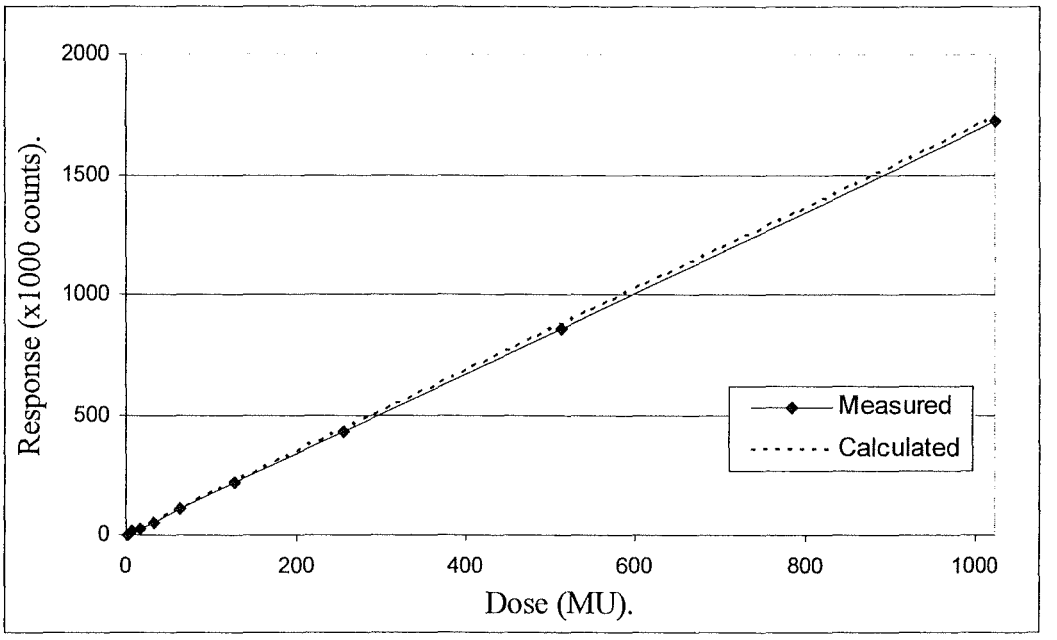

Figure 6.6: Response of SiO_2 fibre coupled scintillator detector irradiated by 6MV x-ray beam, field size of $20x20cm^2$. The solid line is a least squares fit of the data through the origin. The dashed line is a comparison of the values calculated by multiplying the first measured reading by the same factor by which the doses were increased.

10x10 cm^2 and 20x20 cm^2 respectively with a calculated response obtained by multiplying the first measured reading by the dose increase factor. Analogously figure 6.7 and figure 6.8 compare the linear response of the scintillator coupled with the PMMA fibre irradiated at a beam size of 10x10 cm^2 and 20x20 cm^2 respectively, with the corresponding calculated values. The irradiation time was varied from 0.01 minutes to 4.1 minutes corresponding to a dose range varying from 2cGy up to 1024cGy. The integrated detector output signals were found to be linear as a function of dose within the dose range indicated. Both fibre detectors show very good agreement between the measured and multiplied doses. No significant fatigue affecting the accumulated doses was observed for either the SiO_2 or the PMMA optical fibre coupled scintillation detectors.

6.3 Detector sensitivity to field factor

Output of therapy machines is measured in R/min (coulomb/kg/min) in air for low energy x-rays and ^{60}Co beams. For linear accelerator beams, however, the output is expressed in cGy at d_{max} in a phantom per monitor unit (MU). The cGy/MU value for a given therapy beam varies with the field size [40]. The larger the field, the greater the output per monitor unit for linear accelerator beams. The reason is that as the field size increases, the amount of radiation scattered to the phantom or patient increases. Also, there is increased forward scattering by the jaws and changes in backscattering to the monitor chamber. Field size correction factor (C_{fs}) describes the effects due to forward–backward scattering as shown in equation 6.1.

$$C_{fs} = \frac{\text{dose at } d_{max} \text{ for a field size (fs)}}{\text{dose at } d_{max} \text{ for a standard field size (10x10cm}^2\text{)}} \qquad (6.1)$$

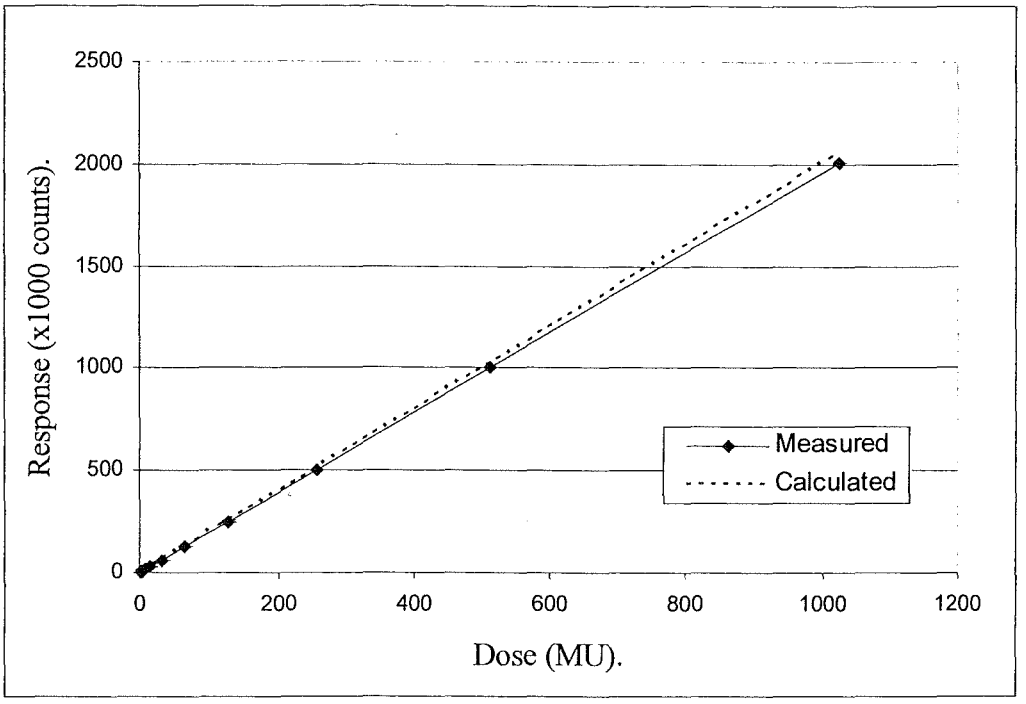

Figure 6.7: Response of PMMA fibre coupled scintillator irradiated by 6MV x-ray beam, field size of 10x10 cm^2. The solid line is a least squares fit of the data through the origin. The dashed line is a comparison of the values calculated by multiplying the first measured reading by the same factor by which the doses were increased.

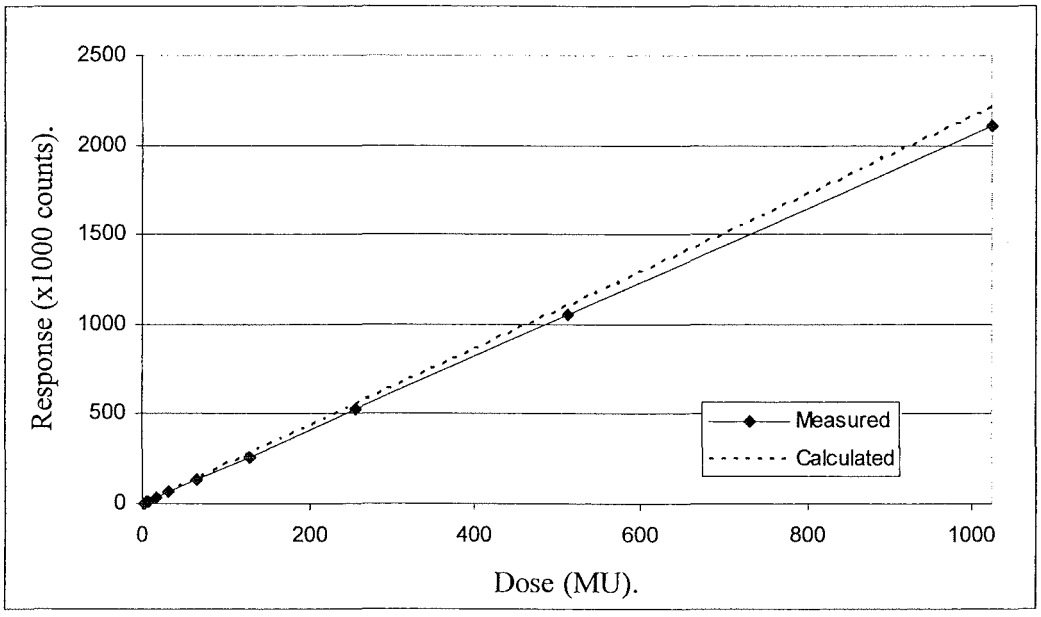

Figure 6.8: Response of PMMA fibre coupled scintillator irradiated by 6MV x-ray beam, field size of 20x20cm^2. The solid line is a least squares fit of the data through the origin. The dashed line is a comparison of the values calculated by multiplying the first measured reading by the same factor by which the doses were increased.

To evaluate sensitivity to field factors the prototype plastic scintillation detectors were irradiated by a 6MV x-ray beam linear accelerator Varian CLINAC 2400C [37]. In reference to the treatment machine used in this study, the field size factor of the beam used was found to be 1.0 for a field size of 10x10 cm^2 and 1.041 for a field size of 20x20 cm^2. Figure 6.9 and figure 6.10 show the responses of the SiO_2 and PMMA scintillation detectors, respectively, for these field sizes. A 3.94% increase in response was calculated for the SiO_2 and PMMA optical fibre coupled scintillation detectors using the tabulated field factor values of the machine employed in our investigation. Increased field size is responsible for this increase in response. There is a strong correlation with tabulated values with no more than ±0.92% deviation. This is indicative of the sensitivity of the scintillation detectors to small changes in the field strength or field size.

6.4 Reproducibility and stability of the integrator signal

The final prototype scintillation detectors were tested for reproducibility and stability. The results obtained from these prototype detectors were different from the one described in section 5.1. The distal ends of the fibre are connected into a light tight optics and electronic circuit box containing the focusing system, optical filtering system, and the photo detection system. The output from this optical system is connected to a two channel digital integrator and counting system specific for the scintillation detectors. The output from the two detectors can be read simultaneously. At the same time the digital integrator is connected with modulator triggering (MOD TRIG) of the linear accelerator. The measurements are performed in a solid water phantom, using a Varian 2400C [37] linear accelerator. The irradiation energy is 6MV with a dose rate equal to 250MU/min at SSD equal to 100 cm. The field size is set at 10×10 cm^2 and the point of measurement is set at d_{max} equal 15mm.

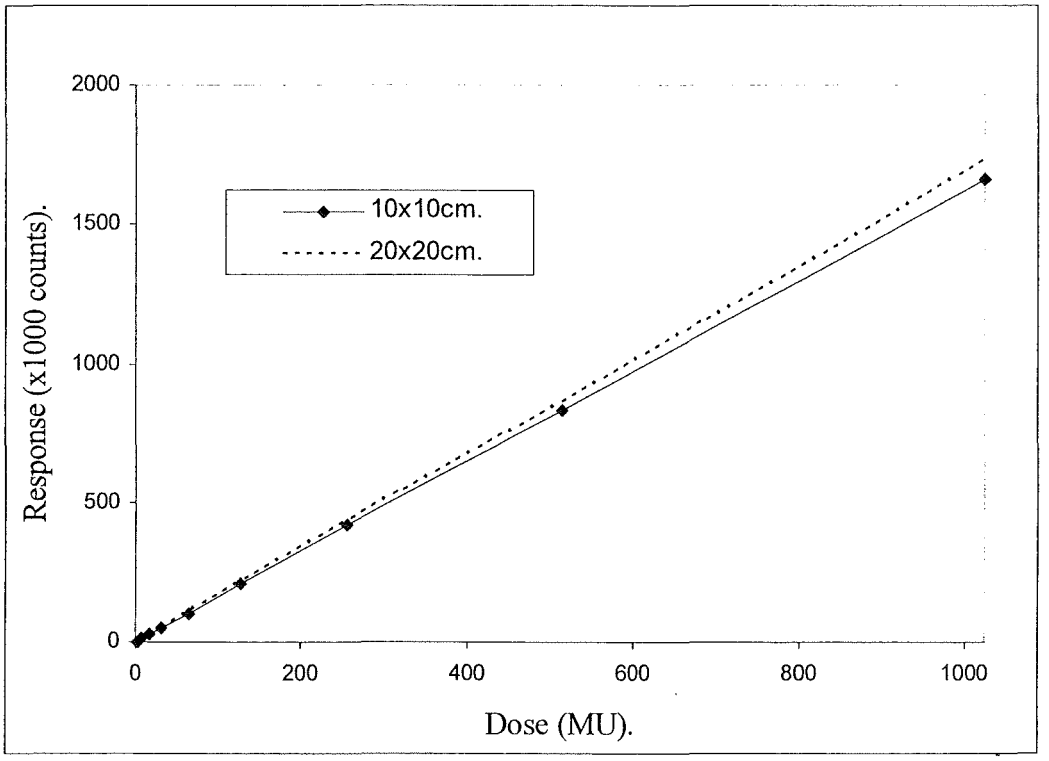

Figure 6.9: Response of SiO_2 scintillation detector irradiated by 6MV x-ray beam size of 10x10 cm^2 and 20x20 cm^2. The solid line is a least squares fit of the data through the origin. The dashed line is a comparison of the values calculated by multiplying the first measured reading by the same factor by which the doses were increased.

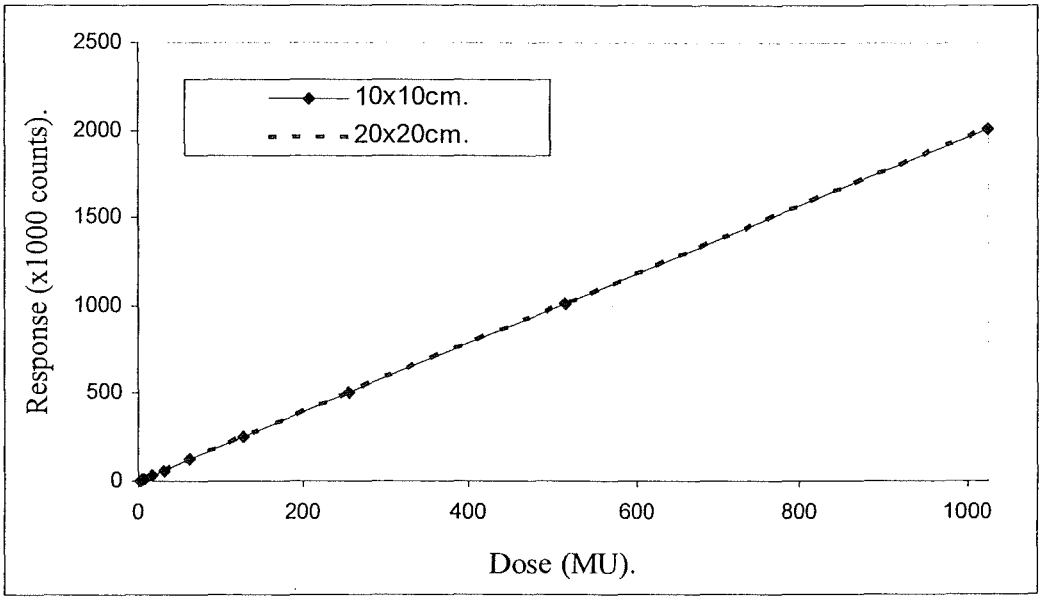

Figure 6.10: Response of PMMA scintillation detector irradiated by 6MV x-ray beam size of $10x10cm^2$ and $20x20cm^2$. The solid line is a least squares fit of the data through the origin. The dashed line is a comparison of the values calculated by multiplying the first measured reading by the same factor by which the doses were increased.

The output reading presenting the signals is integrated over a constant dose of 20cGy. A percentage standard deviation of 1.49% was obtained for a series of twelve consecutive readings when using the SiO_2 fibre. Figure 6.11 shows that the readings of the SiO_2 fibre coupled detector are contained well within ± 1.49% standard deviation.

Simultaneously, under similar irradiation parameters, a percentage standard deviation of 0.94% was obtained for a series of twelve consecutive readings using the PMMA fibre. Figure 6.12 shows that the relative readings of the PMMA fibre coupled detector are contained well within ± 0.94% standard deviation.

6.5 Dose rate proportionality

The dose rate proportionality of the SiO_2 and PMMA fibre coupled scintillation detectors was evaluated using a Varian 2400C [37] linear accelerator with a single energy equal to 6MV at different dose rate settings of 50, 100, 150, 200 and 250 MU/min. These dose rates are specified at d_{max} equals 15 mm for a 6MV beam energy, a field size equal to 10x10 cm^2 and SSD equal to 100 cm. The response of the SiO_2 and PMMA fibre coupled scintillation detectors determined by integrating signals corresponding to an irradiation of 20cGy is shown in figure 6.13 and figure 6.14, respectively. The responses when using the SiO_2 fibre are independent of dose rate with an uncertainty of ±1.2%. On the other hand the responses when using the PMMA fibre are independent of dose rate with a smaller uncertainty of ±0.82%. These results show that the response of the SiO_2 and PMMA fibre coupled scintillation detectors are independent of dose rate in the range investigated.

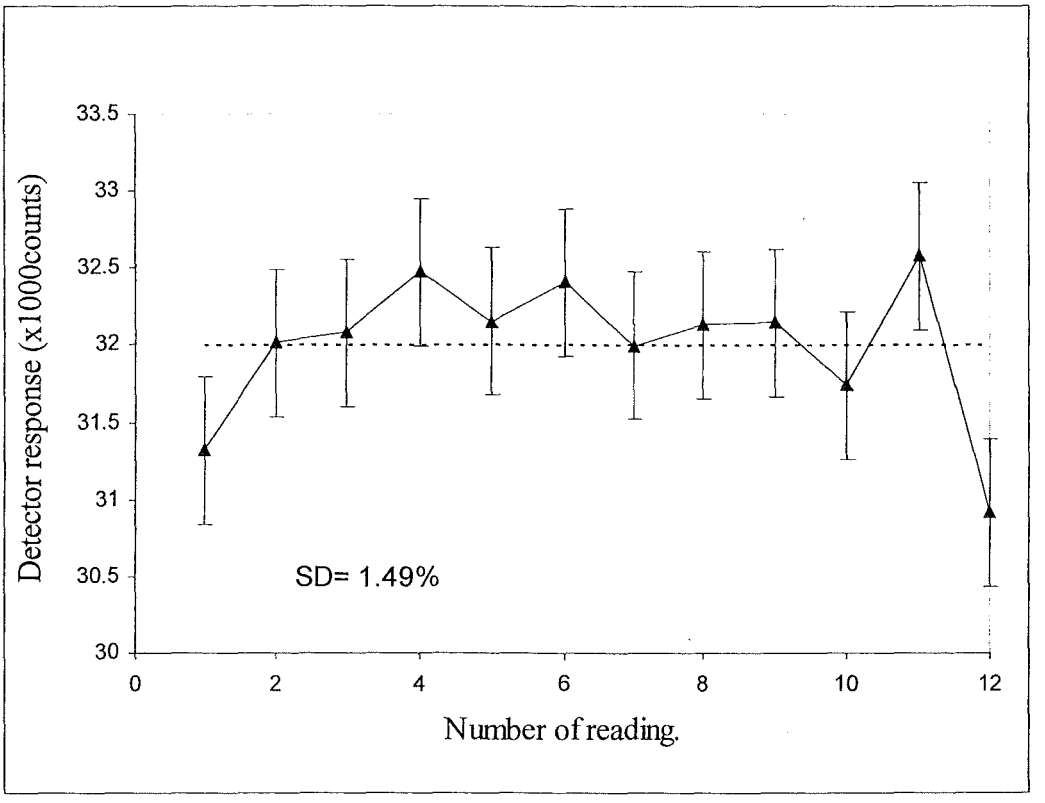

Figure 6.11: Response of plastic scintillation detector using SiO_2 fibre in a 6 MV x-ray beam, 10x10 cm^2 as field size, 250MU/min dose rate, dmax=15mm, and 100 cm source to surface distance in water phantom vs. number of readings for a total dose of 20cGy. The dashed line is the mean of all the measurements. The error bars are standard errors of the mean.

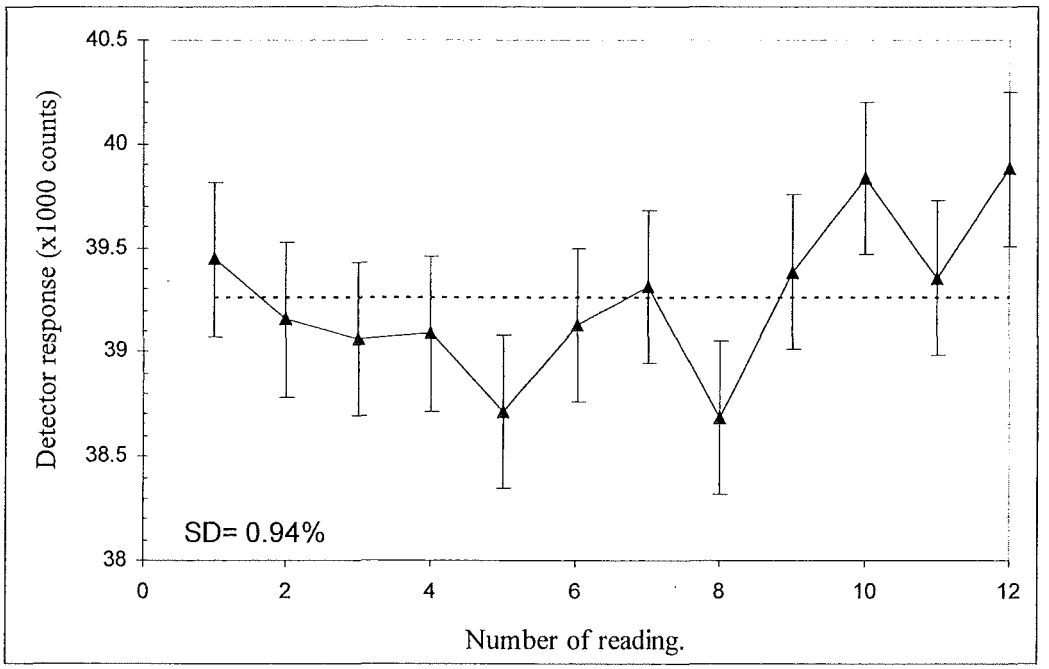

Figure 6.12: Response of plastic scintillation detector using PMMA fibre in a 6MV x-ray beam, 10x10 cm^2 as field size, 250MU/min dose rate, dmax=15mm, and 100 cm source to surface distance in water phantom vs. number of readings for a total dose of 20cGy. The dashed line is the mean of all the measurements. The error bars are standard errors of the mean.

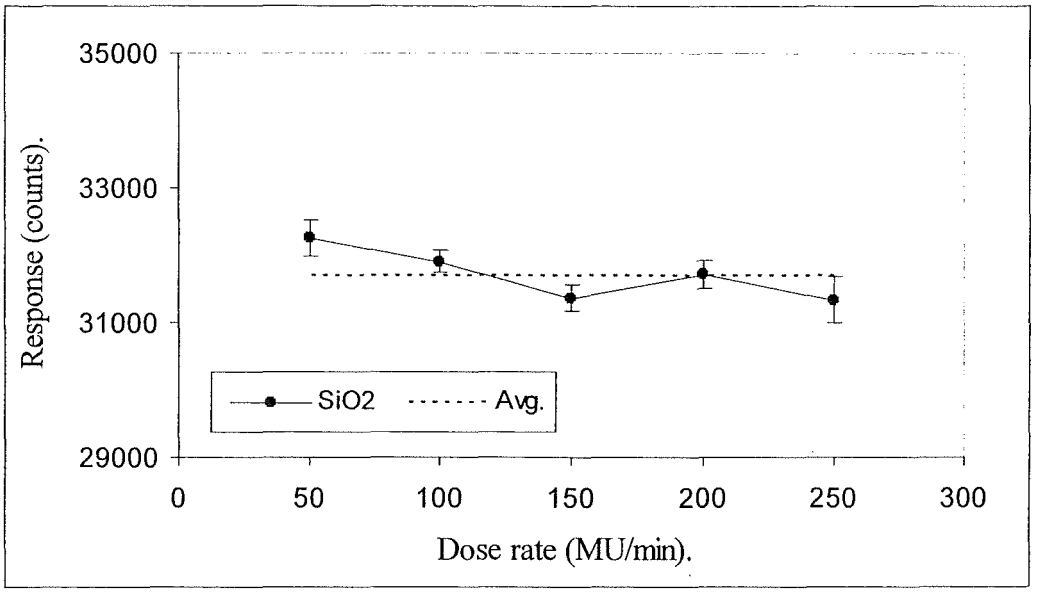

Figure 6.13: Dose rate independence of SiO_2 scintillation detector, at 6 MV photon energy, 10x10 cm^2 field size, SSD of 100 cm and d_{max} = 15mm in water phantom for a total dose of 20cGy. The dashed line is the mean of all the measurements. The error bars are standard errors of the mean. The solid line is drawn to guide the eye.

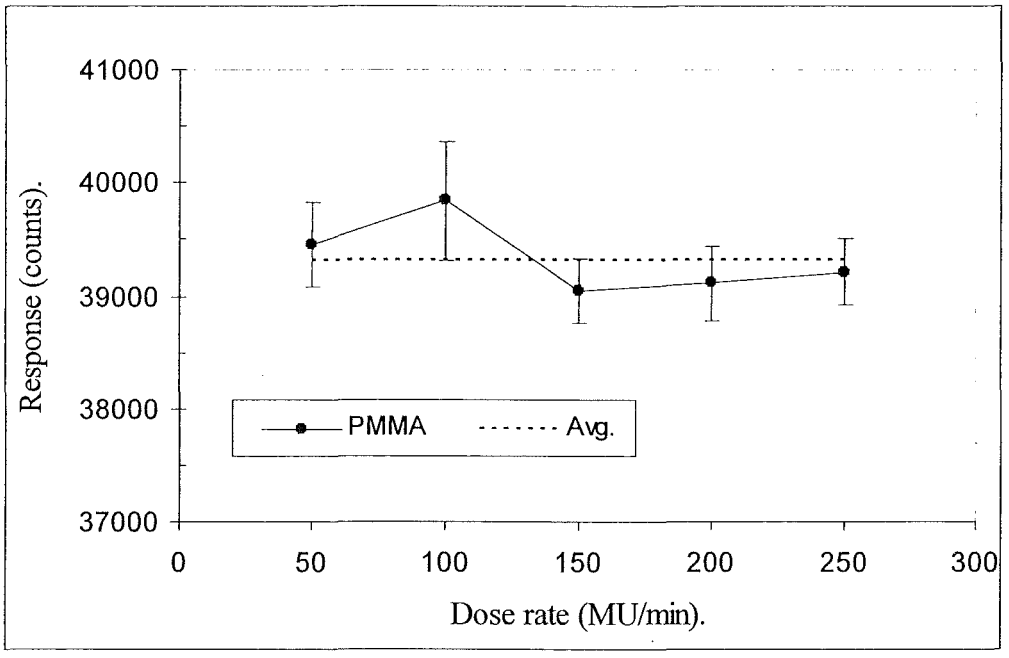

Figure 6.14: Dose rate independence of PMMA scintillation detector, at 6 MV photon energy, 10x10 cm^2 field size, SSD of 100 cm and d_{max} = 15mm in water phantom for a total dose of 20cGy. The dashed line is the mean of all the measurements. The error bars are standard errors of the mean. The solid line is drawn to guide the eye.

6.6 Intensity with distance

The SiO_2 and PMMA fibre coupled scintillation detectors were evaluated for intensity linearity signatures using digital integration and the counting system. These studies were performed using a water phantom, with d_{max} = 15mm. The intensity linearity measurements were made at varying distance points between the source and surface of the phantom while the field size was kept constant. The selected distance points were 90, 100, 110, 120, 130 and 140 cm.

Figure 6.15 shows the response when using the SiO_2 fibre as a function of corresponding source-surface distance (SSD). There is good agreement between the measured responses and the responses calculated using the inverse square law ($D_1=D_2\ [SSD_2]^2 / SSD_1]^2$). The responses when using the PMMA fibre are shown in figure 6.16. In the case when using the PMMA fibre, there is a greater degree of divergence between the calculated and observed responses than occurs when using the SiO_2 fibre and this is attributed to the wider acceptance angle of PMMA fibre optics.

6.7 Effect of incident beam angle on detector response

The SiO_2 and PMMA fibre cable response to different irradiation beam angles was evaluated to assess the amount of signal arising from interference, particularly Cerenkov radiation. Also, the response of the SiO_2 and PMMA fibre coupled scintillation detectors to the irradiation angle was evaluated to assess the overall flatness of the detector responses with respect to beam angle. Cerenkov light collected by the optical fibres is highly dependent on the angle between the long axis of the fibre cable and the incident photon direction [8]. When the beam angle is positioned vertically at 90° to the long axis of the fibre optic, there is minimum signal contribution from Cerenkov radiation [11]. For all measurements of the effect of beam incident angle on fibre and detector responses, a constant fibre length was irradiated to ensure observations are a function of beam angle only.

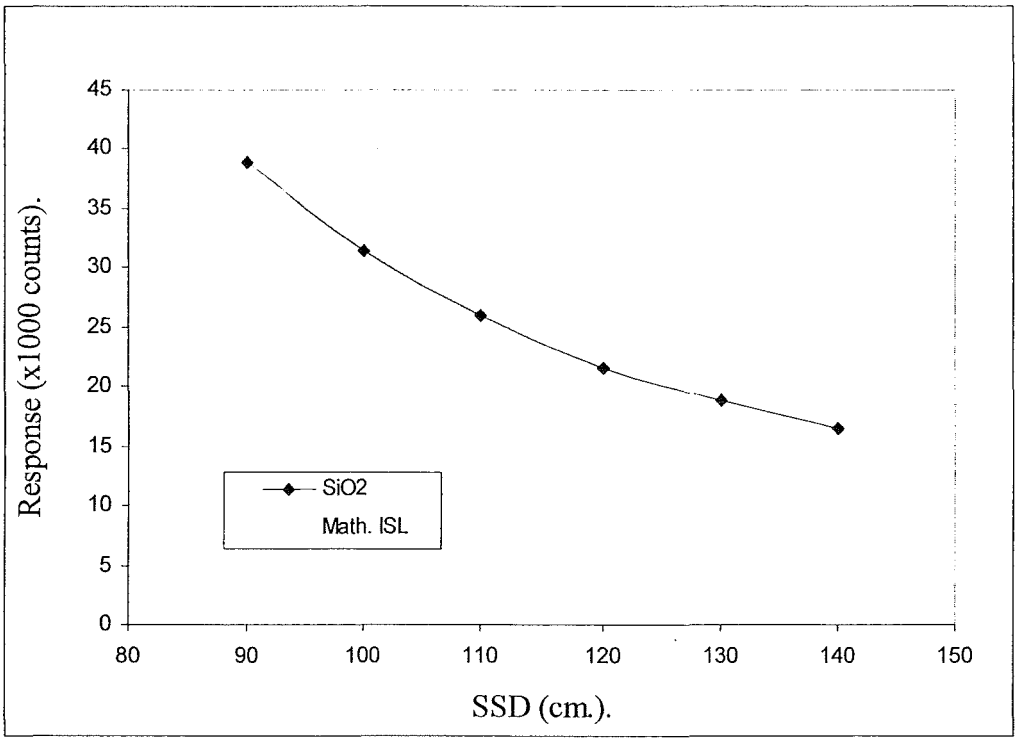

Figure 6.15: Measured response of SiO_2 scintillation detector at different SSD and calculated response due to inverse square law (ISL) for a total dose of 20cGy, d_{max}=15mm, dose rate of 250M/min at water phantom. The diamonds represent the measured response and the line is a least squares fit of the inverse square law.

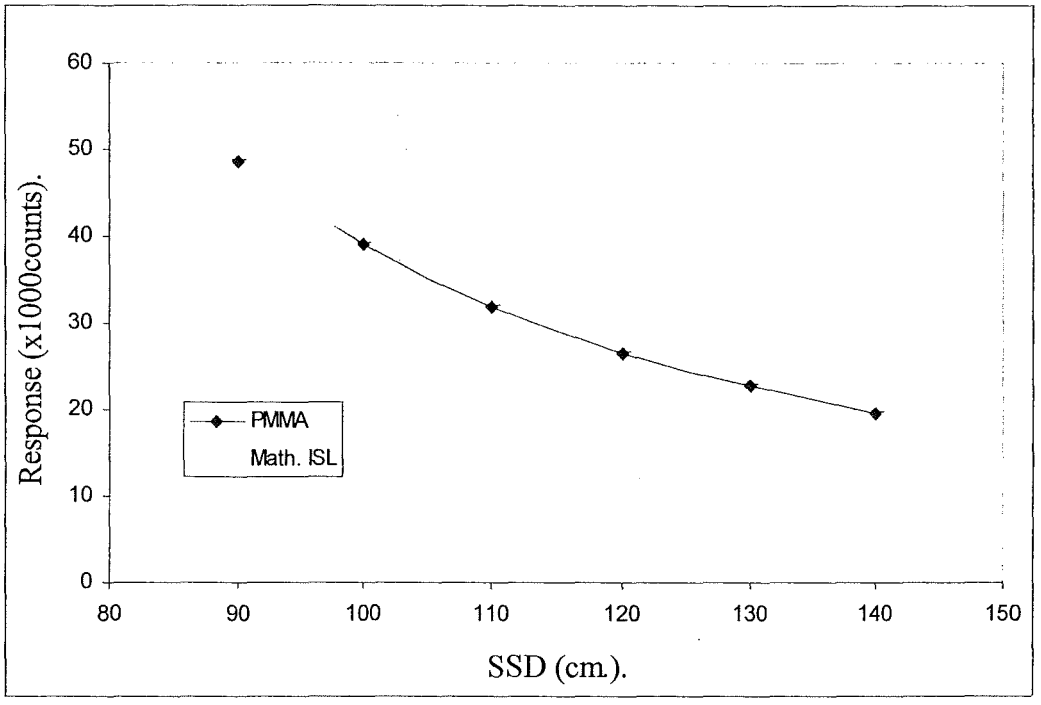

Figure 6.16: Measured response of PMMA scintillation detector at different SSD and calculated response due to inverse square law (ISL) for a total dose of 20cGy, d_{max}=15mm, dose rate of 250M/min at water phantom. The diamonds represent the measured response and the line is a least squares fit of the inverse square law.

6.7.1 Effect of incident beam angle on fibre optics response

To evaluate the effect of incident beam angle on light guide response, SiO_2 and PMMA fibre optic light guides were positioned in the centre of a 20x20cm^2 photon beam and coupled to the optical filtration, digital integration and a counting system. Due to the importance of maintaining a constant fibre length under the irradiation beam and to make the SiO_2 and PMMA results useful for comparison, the same experiment set-up was used for both the SiO_2 and the PMMA fibre optic cables and the field size was arranged to be a constant 20x20 cm^2 half field to avoid any effects arising from divergence of the incident beam. The photon central axis was varied from -50° (toward the plastic scintillator) to +60° (toward the photodiode). Figure 6.17, 6.18 and 6.19 shows that as the angle varies from -50° to +60° there is no significant increase in the incident light in the SiO_2 and PMMA fibres.

The irradiation parameters for these experiments were selected as 20cGy, SSD equal to 100 cm, d_{max} equal to 15mm, dose rate equal to 250MU/min and 6MV was the selected energy using the Varian 2400C [37]. An interesting result is that the response of the SiO_2 fibre optic is greater than that of the PMMA fibre (when comparing the signals from the fibres alone). When the plastic scintillator was attached to these fibres the response of PMMA and scintillator is greater than the SiO_2 and scintillator response. This reflects the strong attenuation of PMMA fibre of light with shorter wavelengths, yet the large acceptance angle of the PMMA fibre.

6.7.2 Effect of incident beam angle on SiO_2 scintillation detector response

The effect of incident beam angle on SiO_2 fibre coupled scintillation detector response was evaluated using the technique described in section 6.7.1. Two field sizes of 10x10 cm^2 and 20x20 cm^2 were selected for this study. For the field size of 20x20 cm^2, the fibre length under irradiation is fixed at 10 cm, which

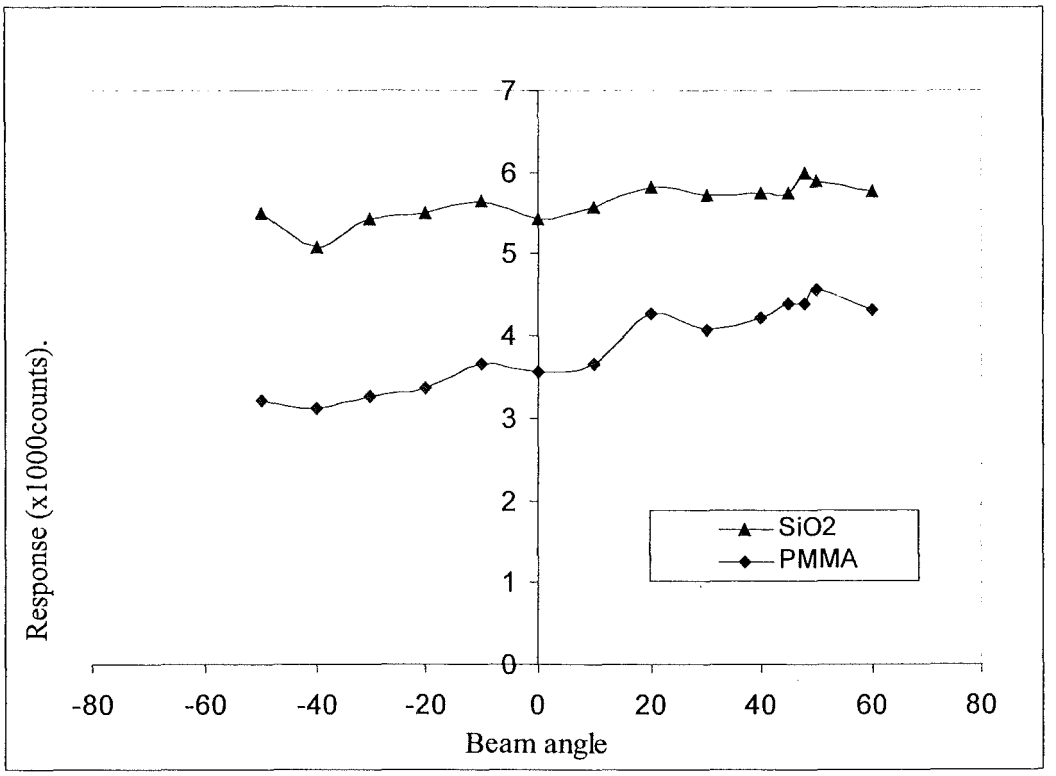

Figure 6.17: Effect of incident beam angle on SiO_2 and PMMA fibre optic (with the scintillator) response for 20x20 cm^2 half field, using Varian 2400C 6MV linear accelerator. The lines are drawn to guide the eye.

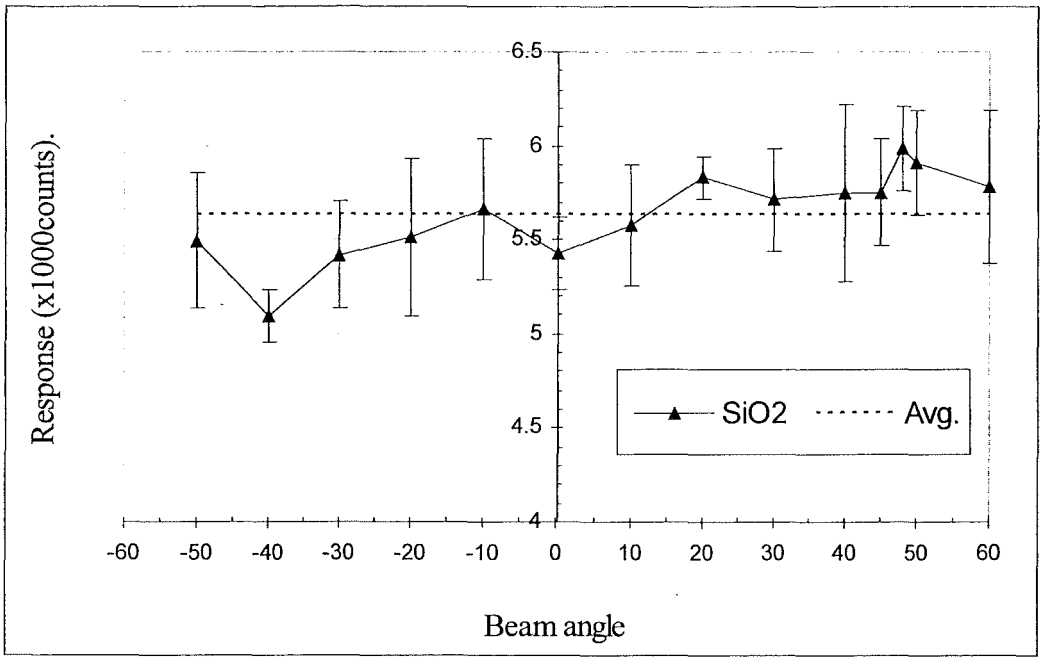

Figure 6.18: Effect of incident beam angle on SiO_2 fibre optic response for 20x20 cm^2 half field, using Varian 2400C 6MV linear accelerator. The dashed line is the mean of the measurements. The error bars are standard errors of the mean and the solid line is drawn to guide the eye.

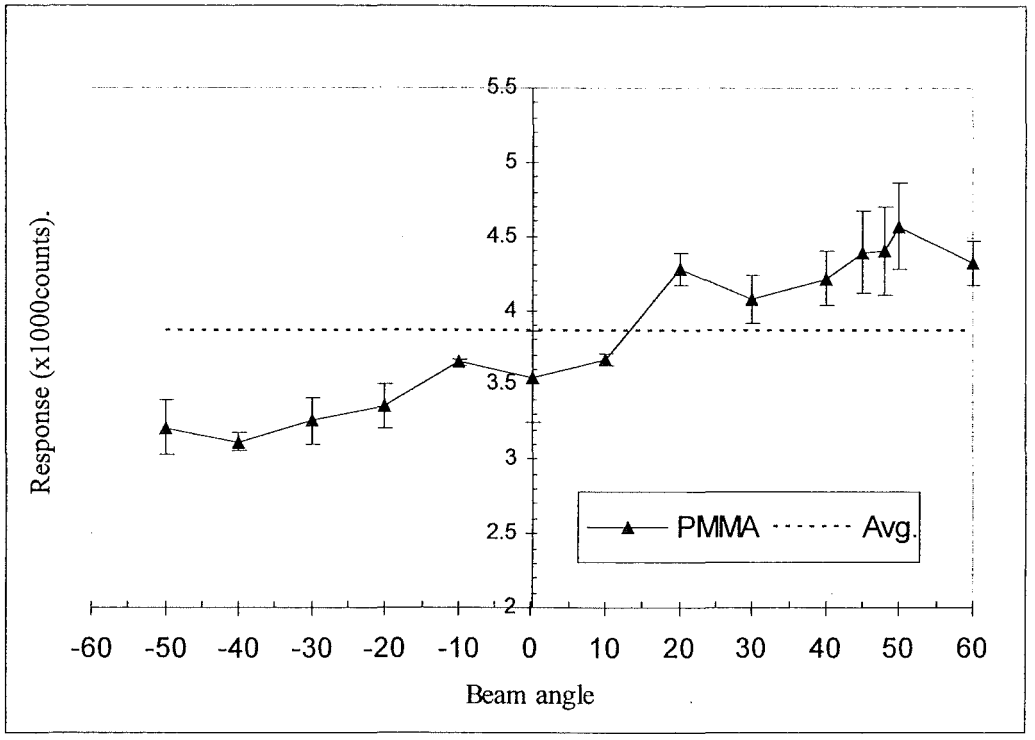

Figure 6.19: Effect of incident beam angle on PMMA fibre optic response for 20x20 cm^2 half field, using Varian 2400C 6MV linear accelerator. The dashed line is the mean of the measurements. The error bars are standard errors of the mean and the solid line is drawn to guide the eye.

is equivalent to the irradiated length as described in section 6.7.1. Thus it is possible to compare beam angle dependence with and without plastic scintillator.Figure 6.20 shows the relatively flat response of the SiO_2 fibre coupled scintillation detector to different beam angles ranged between -60° and +60° for 10x10 cm^2 field sizes. Likewise, figure 6.21 shows a similar constant response of the SiO_2 fibre coupled scintillation detector irradiated over the same range of beam angles by a 6MV photon beam with the field size increased to 20x20cm^2. With the field size doubled, good independence of the SiO_2 fibre coupled scintillation detector on beam angle was observed. This is an encouraging indication of optimized optical filtration of interference light.

6.7.3 Effect of incident beam angle on PMMA scintillation detector response

Applying the techniques described in section 6.7.1, the effect of beam incident angle on the response of the PMMA fibre coupled scintillation detector was evaluated. Two field sizes were selected as for the when the SiO_2 fibre was used. The acceptance angle of the PMMA fibre is more than double than the SiO_2 fibre acceptance angle. Nevertheless, the PMMA scintillation detector shows a very good flat response over the beam angle range described in section 6.7.2 and shown in figure 6.22 for a 10x10 cm^2 field size and in figure 6.23 for a 20x20 cm^2 half field size. The response of the PMMA scintillation detector was relatively independent of beam angle in the 20x20 cm^2 field for the range of beam angles investigated.

Comparison of the above results when the SiO_2 and PMMA fibre optic were used shows that detected light with the SiO_2 fibre is more dependent to beam angle than with the PMMA fibre. When the same comparison is made for the SiO_2 and PMMA optic fibres spliced to plastic scintillators, the PMMA fibre and scintillator show a greater dependence with beam angle. Figure 6.24 and figure 6.25 compare the responses of the SiO_2 and PMMA fibre coupled scintillation detectors in 10x10 cm^2 and 20x20 cm^2 fields respectively.

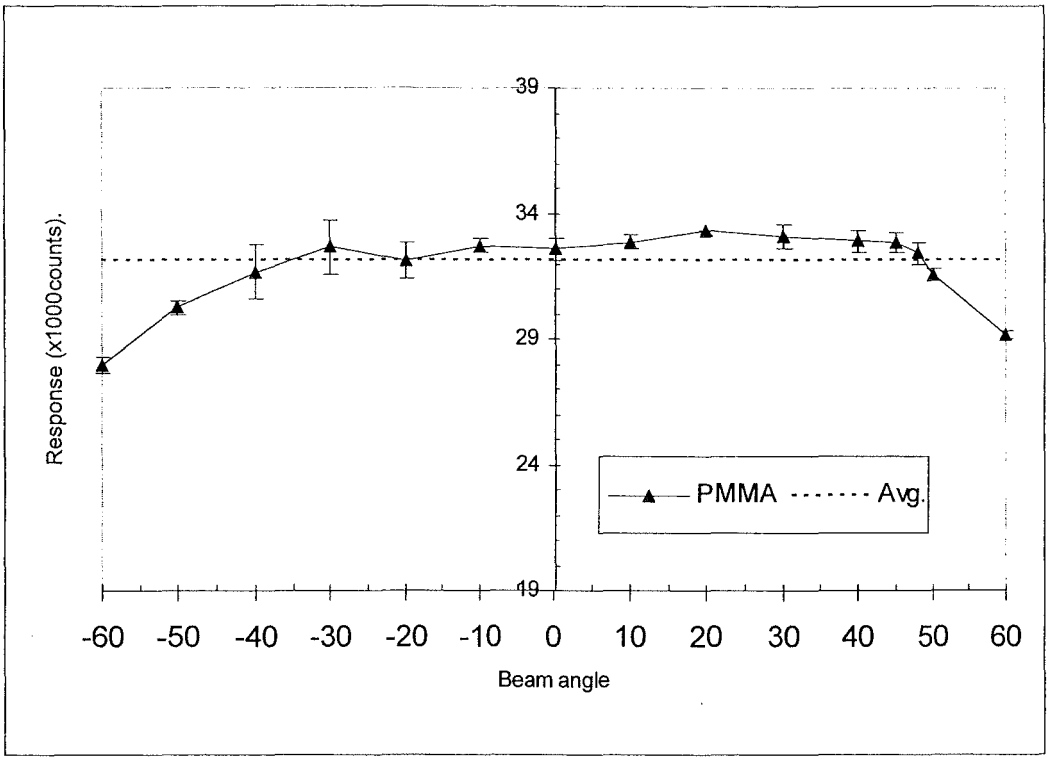

Figure 6.20: Effect of incident beam angle on SiO_2 fibre coupled scintillation detector response for 10x10 cm^2 half field, using Varian 2400C 6MV linear accelerator. The dashed line is the mean value of the measured response. The error bars are standard errors of the mean. The solid line is drawn to guide the eye.

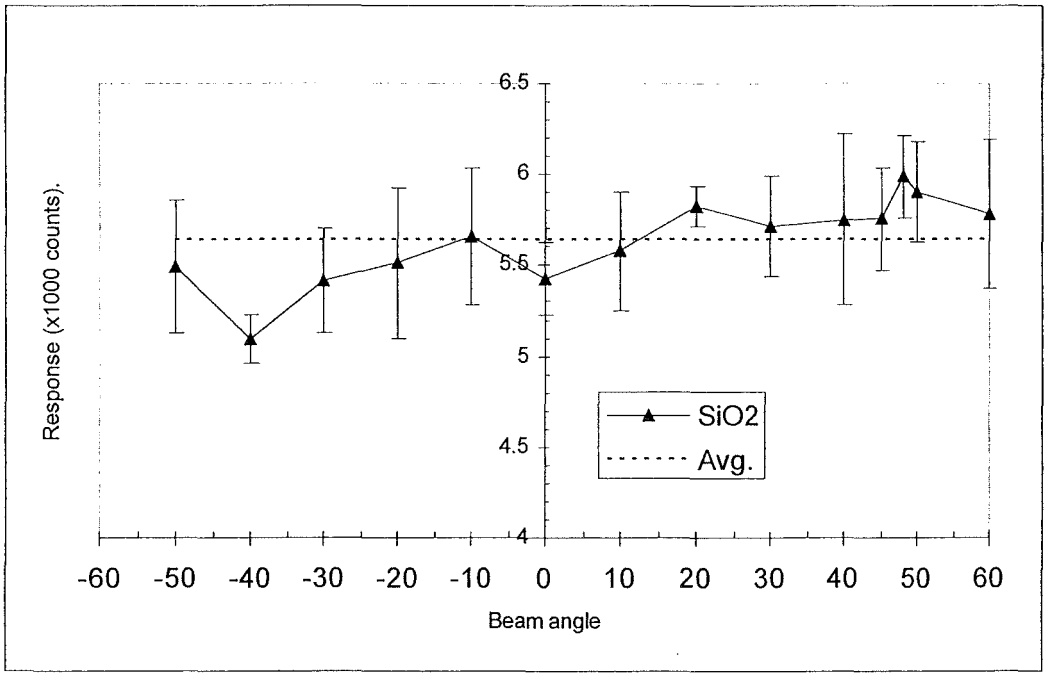

Figure 6.21: Effect of incident beam angle on SiO_2 fibre without the scintillator for 20x20 cm^2 half field, using Varian 2400C 6MV linear accelerator. The dashed line is the mean value of the measured response. The error bars are standard errors of the mean. The solid line is drawn to guide the eye.

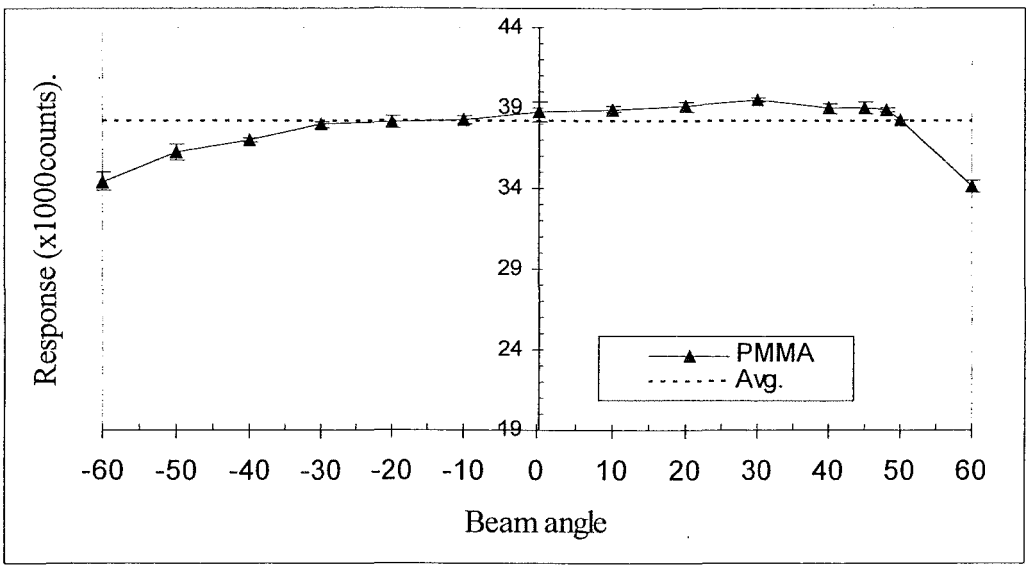

Figure 6.22: Effect of incident beam angle on PMMA fibre coupled scintillation detector response for 10x10 cm^2 half field, using Varian 2400C 6MV linear accelerator. The dashed line is the mean value of the measured response. The error bars are standard errors of the mean. The solid line is drawn to guide the eye.

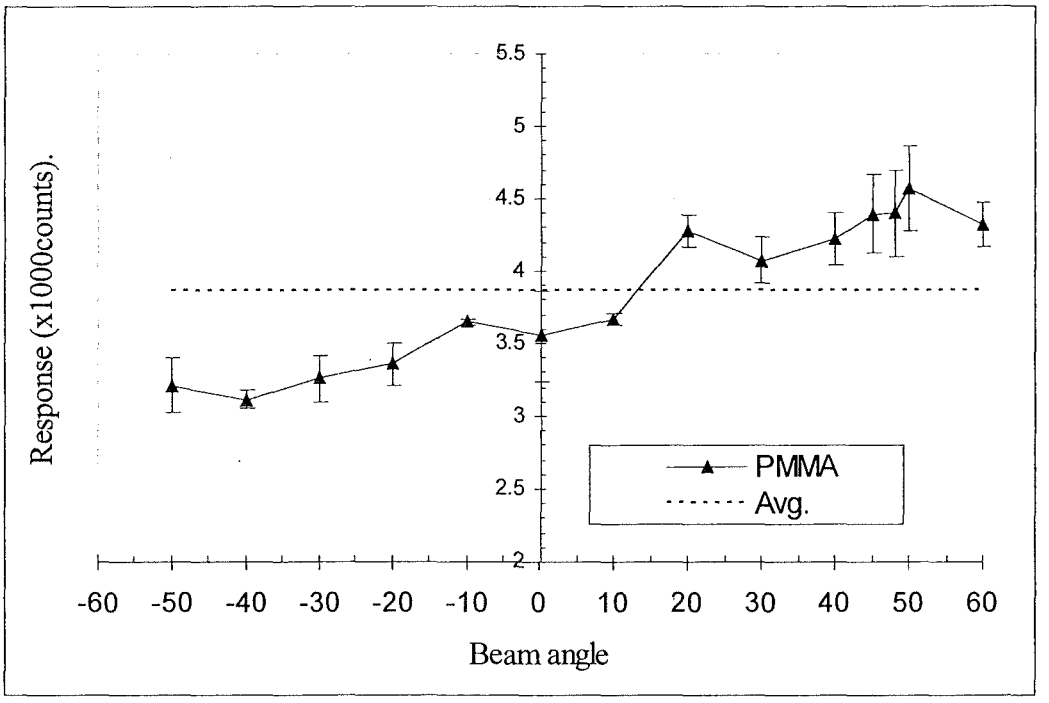

Figure 6.23: Effect of incident beam angle on PMMA fibre coupled without the scintillator for 20x20cm^2 half field, using Varian 2400C 6MV linear accelerator. The dashed line is the mean value of the measured response. The error bars are standard errors of the mean. The solid line is drawn to guide the eye.

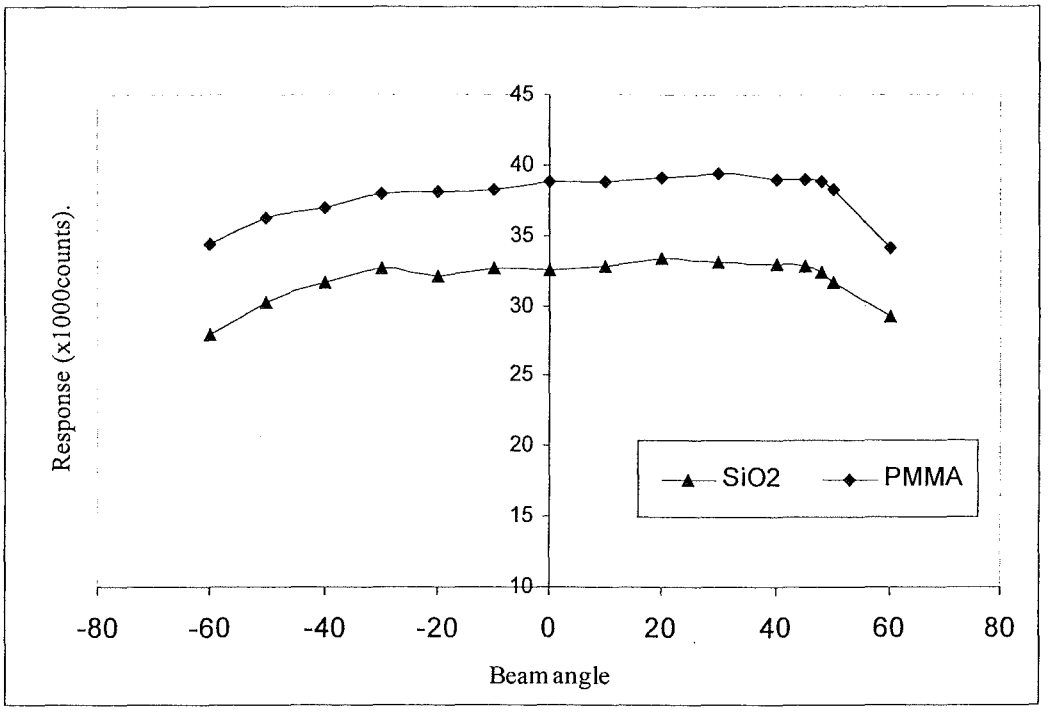

Figure 6.24: Effect of incident beam angle on SiO_2 and PMMA fibre coupled scintillation detector response for 10x10 cm^2 half field, using Varian 2400C 6MV linear accelerator. The lines are drawn to guide the eye.

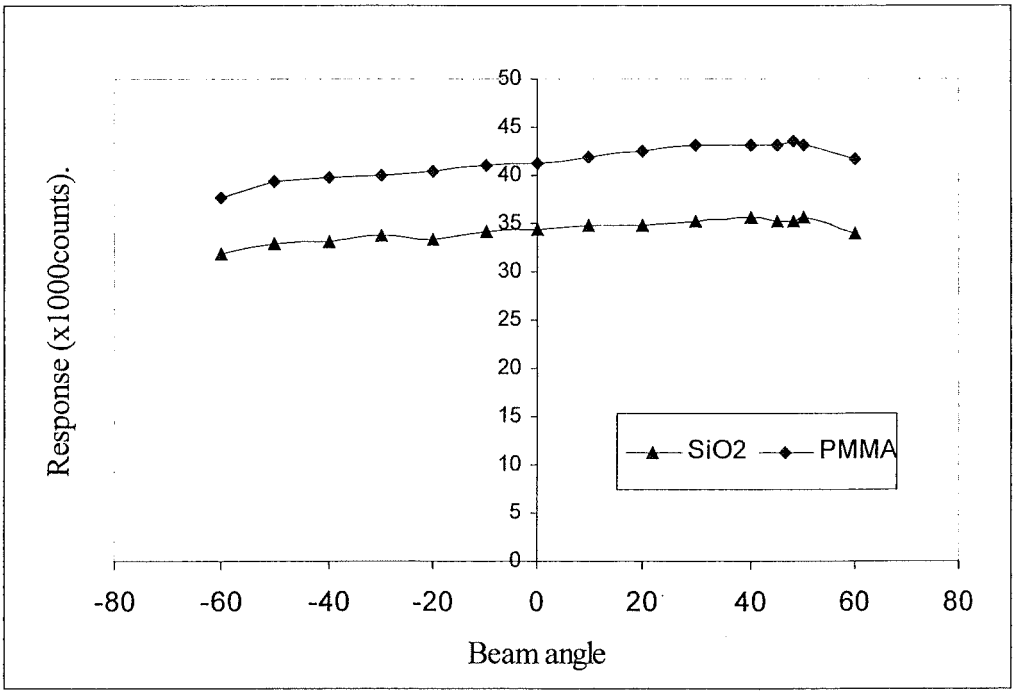

Figure 6.25: Effect of incident beam angle on SiO_2 and PMMA scintillation detector response for 20x20 cm^2 half field, using Varian 2400C 6MV linear accelerator. The lines are drawn to guide the eye.

The PMMA fibre coupled detector is potentially more suited to medical applications than the SiO_2 fibre coupled detector. Detection of a background signal via a second optical fibre is probably unnecessary with PMMA. Another advantage with respect to medical applications is the flexibility of the PMMA fibre optic.

6.8 Efficiency of optical filtration on fibre response

The main interference light in the plastic scintillation detection systems is mainly due to Cerenkov radiation and fluorescence of the fibre optic cable. Fluorescence generated by the radiation may not be as significant a problem as expected [28], and the collection efficiency of the scintillation emissions can be increased relative to interference radiation collection by coating the plastic scintillator material with an optical reflector [41]. This coat should be thin enough so that the water equivalence of the plastic scintillator is maintained. One of the aims of this study is to minimize the contribution of interference radiation to the total probe light output when using tissue equivalent plastic scintillators for high energy dosimetry. Thus, it is very important to assess the amount of interference radiation compared with scintillation radiation on irradiation by a high energy photon beam. Fluorescence radiation predominates when the long axis of the fibre optic light guide is positioned at right angles with photon beam direction [39]. Also, Beddar et al [42] reported that for photon beam energy, the stem effect could be neglected at particular depths and when the fibre optic light guide is positioned at right angles to the direction of the beam.

Whenever the fibre optic light guide is positioned at a non-zero degree angle with respect to the beam direction, Cerenkov radiation may contribute, especially at angles greater than the Cerenkov emission angle. The Cerenkov emission angle is dependent on the refractive index of the fibre optic cable and is approximately 45° for the SiO_2 fibre and 48° for the PMMA fibre. Cerenkov radiation may occur in either of two situations: First, when the photon beam is directed toward the

plastic scintillator (negative contribution); second, when it is directed toward the photo detection system (positive contribution). The following subchapter assesses the contribution of Cerenkov radiation to the SiO_2 and PMMA detector responses at beam angles of -45°, 0° and 45°. We limit our discussion to these three angles because we want to ignore the more complex angular dependence of the Cerenkov intensity. Instead, we want to only focus on instances with minimal and maximal contributions from Cerenkov radiation. Field sizes of 10x10 cm^2 and 20x20 cm^2 were selected. Moreover, comparison of results from investigations at beam angles of 0° and 45° (toward photo detection system) will give us a clear indication of the efficiency of the optical filtration in blocking interference radiation.

6.8.1 Efficiency of optical filtration on SiO_2 fibre coupled response

In order to evaluate both the efficiency of optical filtration and also the amount of interference occurring in the absence of optical filtration, experiments were conducted in which the SiO_2 fibre light guide was positioned in the centre of 10x10 cm^2 and 20x20 cm^2 fields and irradiated by a photon beam. The amount of light reaching the detector was measured with the digital integration and counting system. A constant length of the fibre optic was irradiated during the entire investigation. The photon central axis angle with respect to the fibre optic light guide was varied. We limit our discussion to three angles, namely -45° (direction toward plastic scintillator), +45° (direction toward photodiode) and 0°. The irradiation parameters for these experiments were selected to be 20cGy, SSD equal to 100 cm, d_{max} equal to 15mm in water phantom, dose rate equal to 250MU/min and selected energy equal to 6MV using the Varian 2400C [37].

Figure 6.26 and figure 6.27 show the response in 10x10 cm^2 and 20x20 cm^2 field sizes respectively, for the SiO_2 fibre with and without optical filter in the detection system. These figures show that in the absence of optical filtration

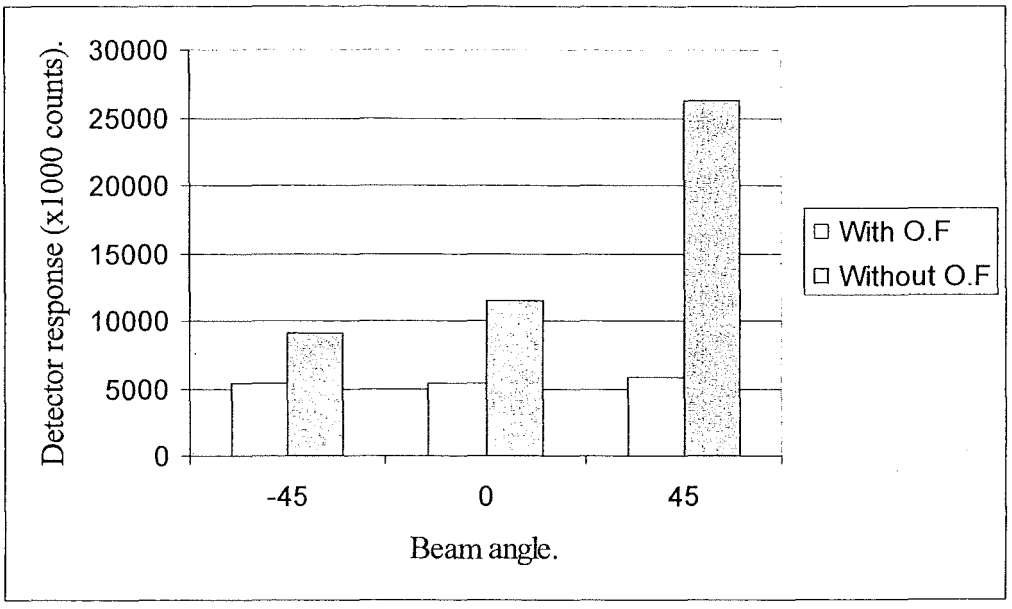

Figure 6.26: Radiation detected from irradiating the SiO_2 fibre without the scintillator with a 10x10 cm^2 field size. The lighter shaded columns are with the optical filter in the detector system. The darker shaded columns are without the optical filter in the detector system.

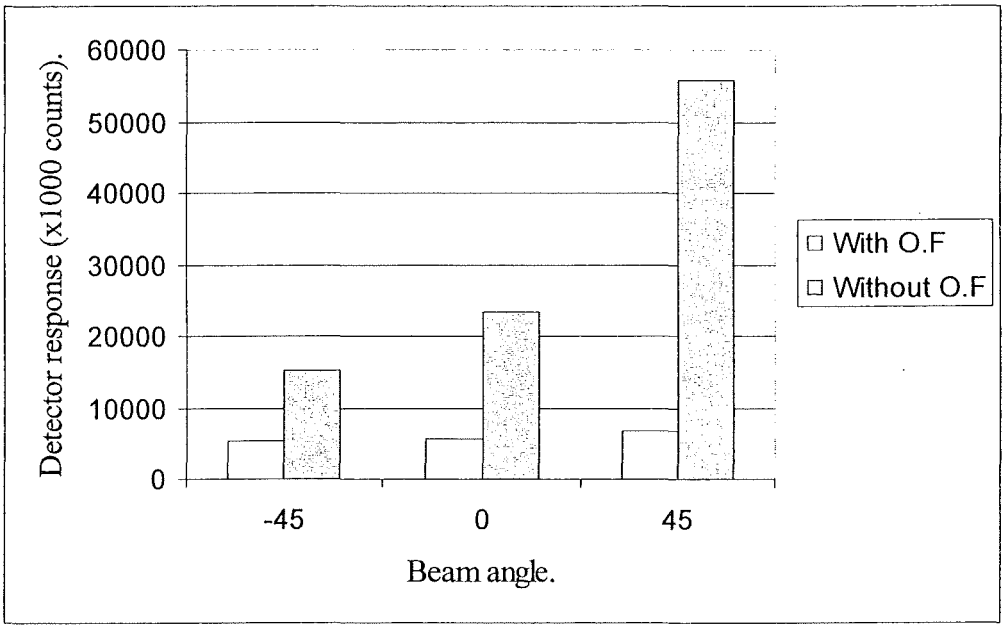

Figure 6.27: Radiation detected from irradiating the SiO_2 fibre without the scintillator with a 20x20 cm^2 field size. The lighter shaded columns are with the optical filter in the detector system. The darker shaded columns are without the optical filter in the detector system.

there is a significant increase in response at +45° (direction toward photodiode), in field sizes of both 10x10 cm^2 and 20x20 cm^2.

Looking at figure 6.26, we see with the SiO_2 fibre and the 10x10 cm^2 field that about 50% of the fibre fluorescence will pass through the optical filter and little, if any Cerenkov light passes through the filter. At -45° and 0° there should be very little Cerenkov light. Most of the light reaching the detector without the filter in place is, therefore, fibre fluorescence. This signal decreased to about 50% when the filter is added. Thus the filter blocks about 50% of the fibre fluorescence. The 2.5 times greater signal at +45° compared to -45° and 0° without the filter. This indicates that the Cerenkov light is much greater than fibre fluorescence. When the filter is place, the light signal is the same size, independent of the angle. Therefore, we conclude that little, if any, of the Cerenkov light passes through the filter.

Now looking at figure 6.27, we a similar result. With twice the length of fibre irradiated, there is about two times more fibre fluorescence (note the signal without the filter at -45° and 0°). The amount of light is now decreased to 33% with the optical filter. These signals are very small, so it is within our noise to have the signal decreases to 33% at this field size and to 50% with a smaller field size. Similar to figure 6.26, it appears that very little, if any of the Cerenkov light is transmitted by the optical filter.

6.8.2 Efficiency of optical filtration on PMMA fibre response

The efficiency of optical filtration on the response of the PMMA fibre light guide was evaluated using the same procedure described in 6.8.1 for the SiO_2 fibre. Thus the PMMA fibre light guide was positioned in the centre of 10x10 cm^2 and 20x20 cm^2 fields and irradiated by a photon beam. A digital integration and counting system was used. A constant length of the fibre optic was irradiated at three different beam angles: (-45°, 0°, and +45° angle). The same irradiation

parameters and same accelerator machine (Varian 2400 C) were used in the investigations with PMMA as were used in section 6.8.1 with SiO_2 fibre to allow comparison between responses of the PMMA and SiO_2 fibres.

Figure 6.28 and figure 6.29 show the relative response in 10x10 cm^2 and 20x20 cm^2 field sizes respectively, for the PMMA fibre with and without optical filtration. These figures show that in the absence of an optical filter, there is less fluorescence from the PMMA than from the SiO_2 fibre that reaches the detector. Similar to the SiO_2 fibre, about 50% of the fluorescence from the PMMA fibre is filtered out by the optical filter.

One slight difference between the SiO_2 fibre and the PMMA is the slight increase in light (without the optical filter in place) at 0° compared to -45°. It is reasonable to assume that a bit more Cerenkov light would couple down the fibre at 0° with the PMMA fibre. The Cerenkov cone is greater (48° compared to 45° for SiO_2). Also, the acceptance angle of the PMMA fibre is more than twice as wide as the SiO_2 fibre. Correspondingly, there is about 5 times more Cerenkov light than fluorescence in the PMMA fibres at 45°.

Still, when the optical filter is added to the detector system, the response is roughly independent of the three wavelengths. Therefore, the optical filter appears to work similar with the PMMA fibre. About 50% of the fibre fluorescence is filtered out with the filter and the larger Cerenkov component is nearly completely filtered out.

The measurements appear to be consistent. When the length of fibre irradiate, the amount of light created by both fluorescence and the Cerenkov effect doubles.

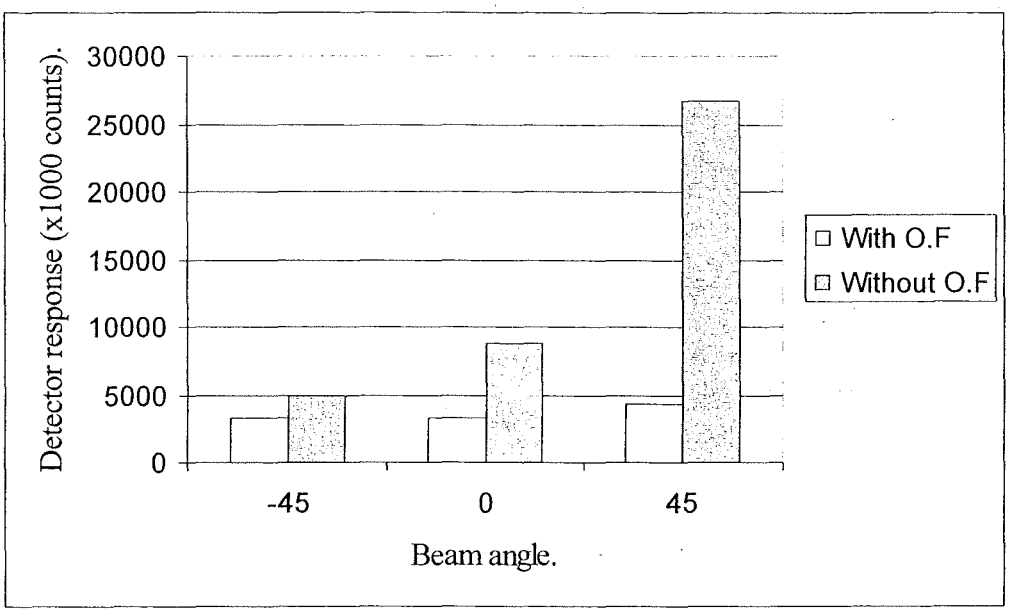

Figure 6.28: Radiation detected from irradiating the PMMA fibre without the scintillator with a 10x10 cm^2 field size. The lighter shaded columns are with the optical filter in the detector system. The darker shaded columns are without the optical filter in the detector system

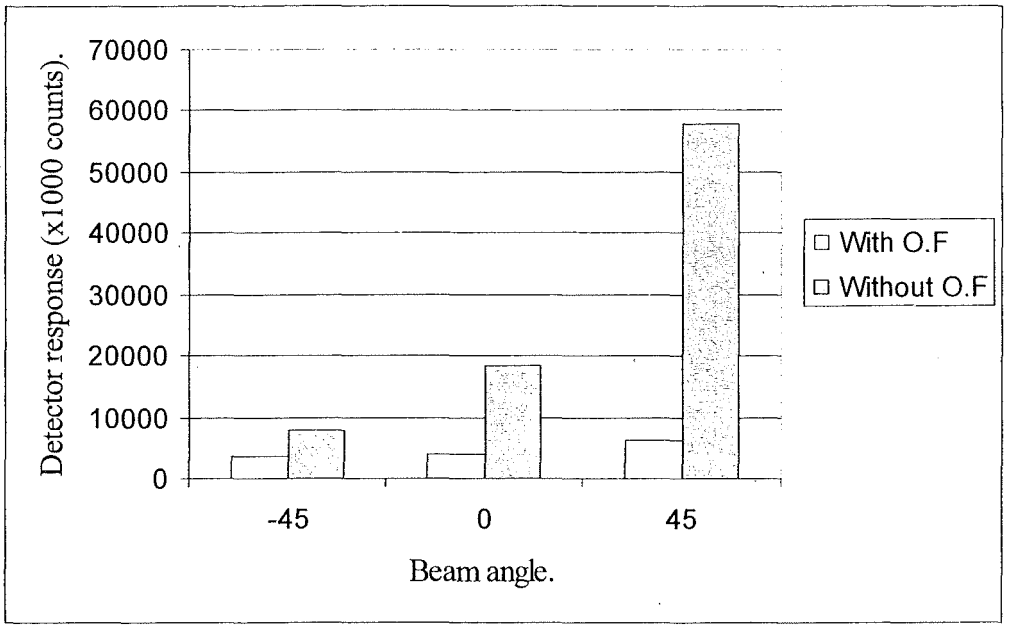

Figure 6.29: Radiation detected from irradiating the PMMA fibre without the scintillator with a 20x20 cm^2 field size. The lighter shaded columns are with the optical filter in the detector system. The darker shaded columns are without the optical filter in the detector system

6.8.3 Assessment of amount of unfiltered interference radiation

Based on the results of 6.8.1 and 6.8.2 in the 10x10cm^2 field, SiO_2 and PMMA fibre light guide responses were compared. Figure 6.30 shows the response of the SiO_2 and PMMA fibre optic light guides, with and without optical filtration. Within the bounds of experimental error, the response of the SiO_2 and PMMA fibres, in the absence of the optical filter, show the same intensity of light at a beam angle of 45° which is the angle yielding maximum Cerenkov radiation. The light at 45° is a combination of Cerenkov light and fibre fluorescence.

But when the incident radiation was at right angles with to long axis of the fibre optics (0°), the fluorescence of SiO_2 fibre was more than for the PMMA fibre. This result may award some advantage to the PMMA fibre optic although SiO_2 is the optimum fibre optic light guide due to the radiation resistance and high transmission characteristic [43].

The data replotted in figure 6.30 allows easier comparison between the fibres. Even though more Cerenkov radiation couples into the PMMA fibre, it is generally a better fibre to use. The optical filter seems to be very efficient in removing the Cerenkov light, therefore the extra Cerenkov light in the PMMA fibre is no problem. The fluorescence in the PMMA fibre is less than the fluorescence in the SiO_2 fibre. About 50% of the fluorescence does pass through the filter, so the using the PMMA with less fluorescence is better. The overall result is that the optical filter is an effective means of minimizing interference radiation for both SiO_2 and PMMA fibres.

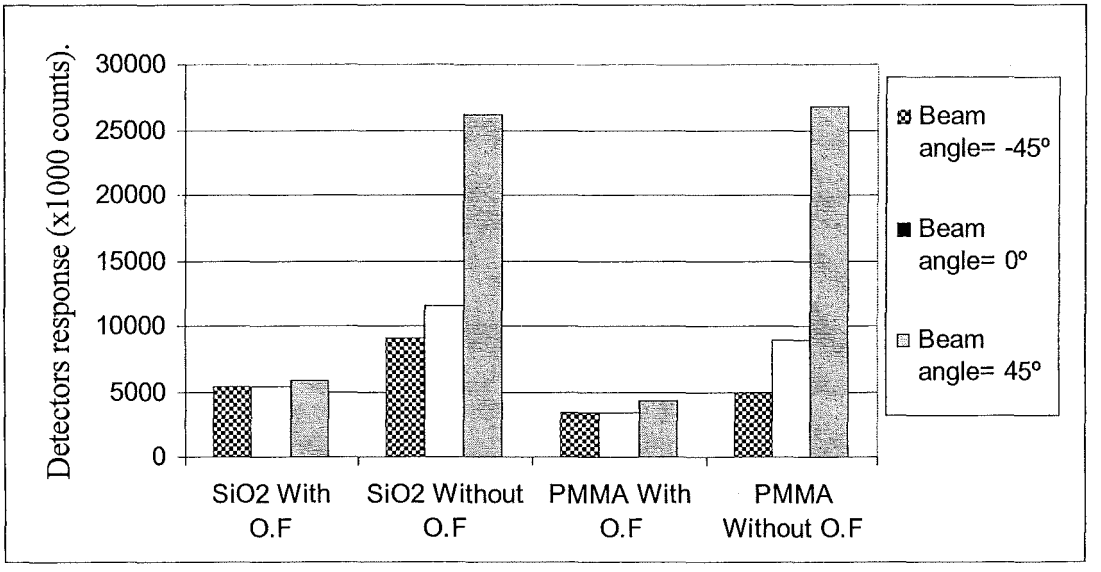

Figure 6.30: Effect of optical filter on SiO_2 and PMMA fibre optic light guide response for 10x10cm^2 field size.

6.9 Threshold of SiO_2 and PMMA scintillation detectors

From a physics point of view, a radiation detector for radiotherapy should be designed to measure energy absorbed per unit mass [16]. Plastic scintillation detectors absorb energy directly and indirectly, and other effects of radiation are used to assess the impact of radiation on tissues. Most dosimeters are large and are not tissue equivalent and are therefore not suitable for *in-vivo* dosimetry. SiO_2 and PMMA scintillation detectors are small in size and are tissue equivalent and they have potential uses for *in-vivo* dosimetry in radiation therapy applications. SiO_2 and PMMA detectors are able to accurately measure a physical dose with accuracy limited only by minor errors. The precision of the measurements of SiO_2 and PMMA scintillation detectors is indicated by the consistent results for investigations described in section 6.4.

The threshold of SiO_2 and PMMA scintillation detectors represents the lowest detectable dose that can be measured precisely in most dosimetry systems. This dose is determined by fluctuations of the background readings. For radiotherapy dosimetry in which relatively high doses are administered, the detection limit is usually not a major effect [16]. Also, SiO_2 and PMMA scintillation detectors are expected to have a wide measurement range and they can accurately detect high and low dose radiation due to the relationship between magnitude of dose and response.

Experimentally the lower limit of detection of the SiO_2 and PMMA scintillation detectors was investigated by adding lead attenuation material of different thicknesses in the field of a 6 MV x-ray beam. The dimensions of the lead slabs are 10x10 cm^2 and the third dimension represents the thickness of the lead slabs namely, 1.3cm, 2.6cm, 3.9cm, 5.2cm and 6.5cm. To avoid any scattering contribution, the lead slabs were positioned on the block tray holder at a distance of 60 cm from the detectors. Also, solid water materials were positioned below the detectors to protect them from back scatter contributions. The field size selected for this test was 10x10 cm^2 and the irradiation parameters were 2Gy as

the irradiation dose, SSD = 100 cm, d_{max}= 15mm and 250MU/min as the dose rate.

Figure 6.31 shows the response of the SiO_2 and PMMA scintillation detectors to lead attenuators of different thicknesses. Both SiO_2 and PMMA fibre coupled scintillation detectors show smooth curves consistent with beam attenuation curve is described by the following equation for 6MV photon energy beam.

$$D = D_0 \quad e^{-\mu\rho t} \qquad 6.1$$

where:

μ = total mass attenuation coefficients (cm^2/g).

ρ = the lead density (g/cm^3).

t = the lead slab thickness (cm).

Figure 6.32 plots the response of the SiO_2 and PMMA fibre coupled detectors in logarithmic scale against the thickness of the lead attenuators. The PMMA fibre coupled scintillation detector shows a linear response on the semi-log plot through to a lead thickness of 3.9 cm representing attenuation of the primary beam by a factor of 8. Beyond this point linearity is disturbed smoothly through the tail of the curve. The SiO_2 scintillation detector shows less linearity on the semi-log plot compared with the primary beam and it has a higher threshold than the PMMA scintillation detector as is illustrated in figure 6.32. The PMMA scintillation detector shows a lower threshold response compared with the SiO_2 scintillation detector and the observed PMMA responses are consistent with values calculated using equation 6.1. Thus, PMMA shows a 50% reduction in response when a 1.3 cm lead slab is added in the beam and this is the same result as was obtained during a calibration test for the linear accelerator.

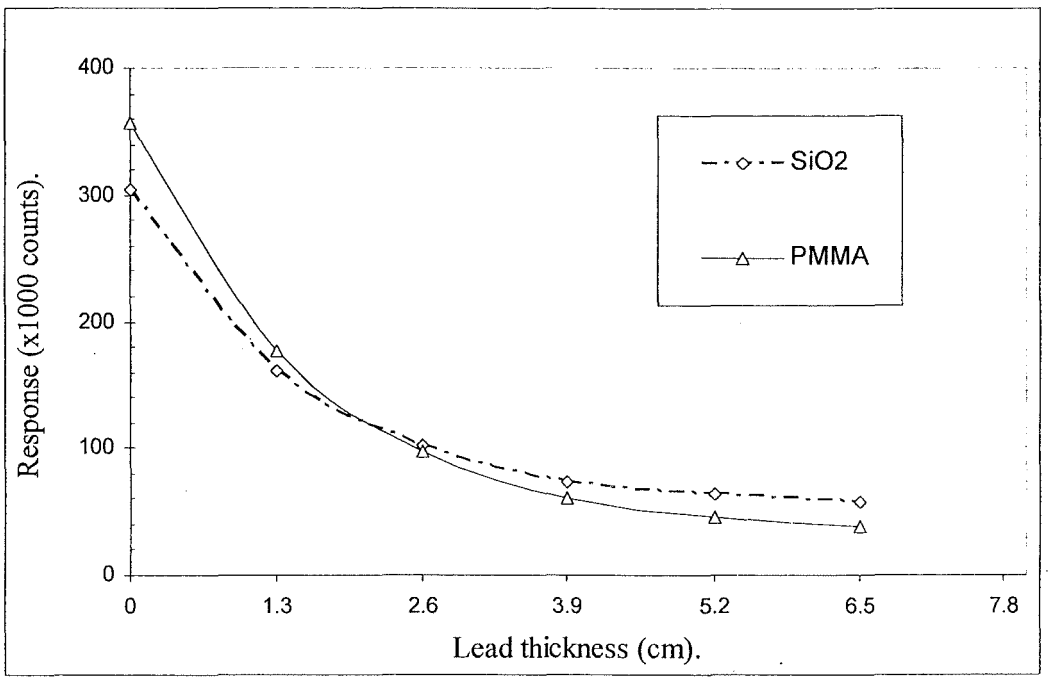

Figure 6.31: Absorption curve (lead absorber) of 6MV x-ray beam. The beam was attenuated by up to a factor of 32 for 10x10 cm^2 field size, dose of 2Gy, SSD=100 cm, d_{max}= 15mm and 250MU/min as dose rate. The lines are drawn to guide the eye.

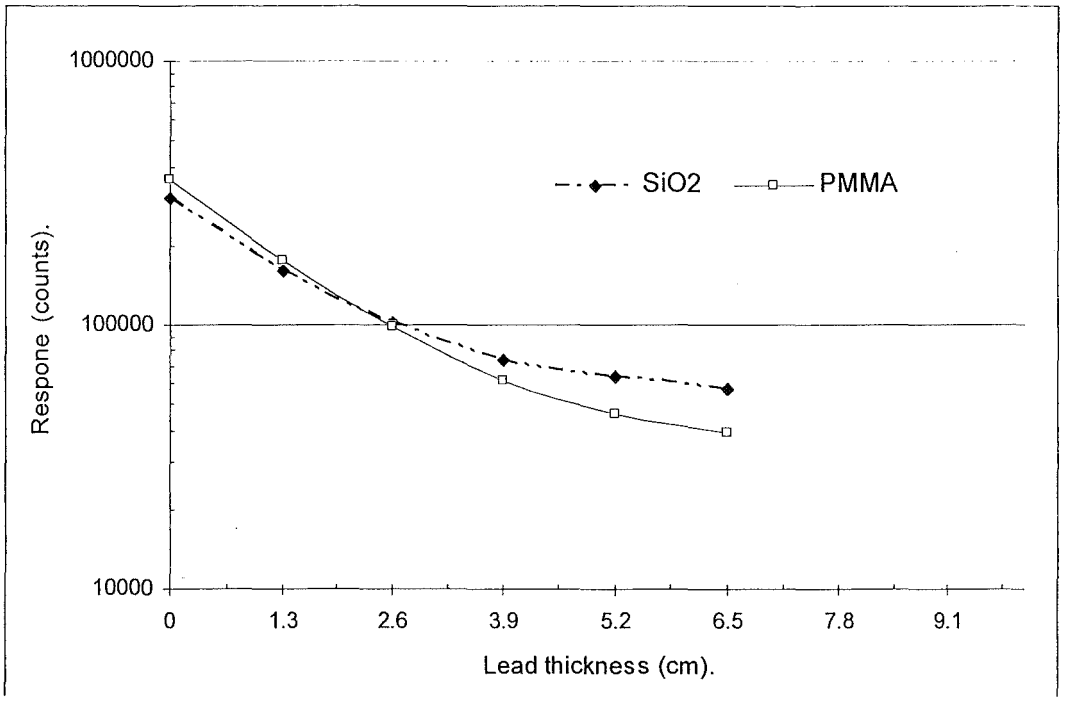

Figure 6.32: Absorption curve (lead absorber) of 6MV x-ray beam as described in figure 6.31 but in semi-log plot to demonstrate the exponential nature of the curves. The lines are drawn to guide the eye.

Conclusions

The objective of this investigation was to construct a minature dosimeter using a small scintillator fixed to the end of an optical fibre. This objective was accomplished using both a SiO_2 fibre and a PMMA fibre, both approximately 1 mm in diameter. The PMMA fibre is more flexible, and therefore has some advantages for medical applications.

The scintillator was coated with a thin covering of reflective paint to reflect the optical light to help with the coupling and to transfer as much light as possible down the fibre. As a result of the better coupling due to the thin reflective layer on the scintillator, more light could be transmitted down the optical fibre, thus giving a better signal to noise ratio. The distal end of the fibre employed a lens system to collect the light from the fibre and focus it on a silicon photodiode. An interference filter was added between the lenses to filter our unwanted background light. The photodiode signal was digitized and synchronised to the accelerator to only measure the light during the accelerator pulses, thus reducing noise.

This combined system was permitted us to create a minature dosimeter with a single fibre. The SiO_2 fibre or the PMMA fibre could be used, although we prefer the PMMA fibre.

Interference radiation, arising from Cerenkov radiation and fluorescence of the fibre is induced in SiO_2 or PMMA optical fibres when exposed to radiotherapy photon beams. The intensity of the fluorescence of interference radiation depends on the length of the fibre under irradiation, while Cerenkov radiation depends strongly on the angle between the long axis of the fibre optics and the incident radiation. When the angle of the incident radiation is perpendicular to the long axis of the fibre, fluorescent radiation might be the predominant interference radiation in the system [43]. Cerenkov radiation is emitted strongly in the UV region of the spectrum, hence use of a light guide fibre

that attenuates the short wavelength UV and transmitts the longer wavelength visible light emitted by a plastic scintillator may act as an inherent filter of Cerenkov radiation. The remaining interference radiation which is generated within an optical light guide is minimized using optical filtration and focusing lenses.

Of the detectors currently used in the dosimetry of radiotherapy photon beams, tissue equivalent plastic scintillator is the best water equivalent material. Also, this plastic scintillator gives better energy independence than the current commercial detectors such as the ionizing chamber, LiF TLD's and silicon diodes [10].

The most valuable feature of plastic scintillation detectors is its potential for *in vivo* measurements including intra-arterial, intra-venous and intra-cavitary measurements. The simplicity and miniaturised size of the detector, which lies within the medical catheterisation range, may also encourage its use in invasive catheterisation techniques. An encouraging result is the ability to remove the background light guide from the plastic scintillation system. The potential of reducing the size of the detector for *in vivo* applications exists

The simplicity of plastic scintillator detection is an important factor toward the use of such detectors in medical applications. For medical applications especially *in vivo*, lack of flexibility of the light guide fibre is an important factor which may limit the use of such system. On account of good flexibility, the PMMA fibre optic is a promising light guide for future applications.

When the dose delivery needs to be very accurate, as in many treatment techniques, then accurate *in vivo* dosimetry is essential. With a simple independent dose calculation program it is not possible to guarantee a dose delivery within 4% without additional patient dose verification [44]. As cited by Essers; Several major accidents have occurred in hospitals, with dramatic consequences for the patients [45]. In principle, *in-vivo* dosimetry can minimize

the chance of incorrectly treating a large number of normal tissue cells. Also, with real time *in vivo* measurements further damage to normal tissue can be avoided. Moreover, such measurements can act as a real time indicator of any movement during irradiation procedures.

Variation in positioning of the organ/patient with respect to the radiation beams causes a temporal dose variation in critical normal tissues adjacent to the treatment target [17]. This temporal variation introduces uncertainties in understanding the normal tissue dose response, thereby limiting reliable treatment evaluation and optimization. Plastic scintillation detectors are promising detectors to make the evaluation and optimization easy.

Hiraoka et al [46] reported data on some radiotherapy accidents from Japan. He states that dosimetry mistakes causing overdoses of 7% can be clinically detected. Overdoses ranged from 10% to 28% for the cases described in Japan. This should encourage real time *in-vivo* dose measurements as routine practice.

It is hoped that the results of the current study will encourage further development toward reducing the size of the detector. Futhermore, it is hoped this present study contributes to increasing the precision of radiation dose delivery and that clinical application studies of plastic scintillation detectors will follow. Another goal for the future is the manufacture of simplified plastic scintillation detectors having a disposable end detector.

Acknowledgements

I acknowledge all the help and support from a number of people who have contributed to this work. I thank Assoc. Prof Lou Reinisch, Director Medical Physics, Department of Physics and Astronomy, University of Canterbury for his encouragement and supervision in the completion of the project. Also, I thank him for many invaluable discussions.

I acknowledge Prof Phil Butler, Head of Department, Department of Physics and Astronomy, University of Canterbury for his co-supervision and his personal and moral support.

I express my gratitude to Prof. Samir Abdul-Majid Alzaidi, the originator of the project and for contributing many ideas and methods upon which this work was based. Also, I express my appreciation to him for his assistant supervision.

I acknowledge Graham Sorell, Principal Physicist, Department of Radiation Oncology, Christchurch hospital, for his invaluable advice, guidance and encouragement throughout the whole practical course of this task. Additional thanks to the medical physicist, the health physicist and the radiotherapy technologist in Christchurch hospital.

I convey my thanks to the members of the department of Physics and Astronomy, in particular Graeme Kershaw, Head of Mechanical Workshop and Ross Ritchie, Head of Electronic Workshop.

I acknowledge the support and guidance of Dr. Jazi Moathe Al-Mokhlef, Department Chairman, Biomedical Physics Department, King Faisal Specialist Hospital and Research Centre, Riyadh, Saudi Arabia for his advice and support during experimental work in his department. Also, I acknowledge Mohammad Al-Asmari, Principal Physicist, King Abdulaziz Oncology Centre, Jeddah, Saudi Arabia for his full co-operation and advice.

The research has been funded under governmental scholarship from Saudi Arabia, Ministry of Health and I am grateful for this generous support from my country. Also, I am grateful for the support from the Saudi Cultural Office in Pakistan and Australia which ensures a very good educational environment during the period of study.

Finally, I acknowledge my host city of Christchurch which provided me and my family with a good educational and social environment.

REFERENCES

1. Van Herk M., Bruce A., Kroes A. P., Shouman T., Touw A. and Lebesque J. V. "Quantification of organ motion during conformal radiotherapy of the prostate by three dimensional image registration" Int J Radiat Oncol Biol Phys; 1995, 33:1311-1320.

2. Herman Cember, " Introduction to health physics", third edition, the McGraw-Hill companies, Inc. 1996.

3. M. A. Clift et al, "A temporal method of avoiding the Cerenkov radiation generated in organic scintillator dosimeters by pulsed mega-voltage electron and photon beams", Phys. Med. Biol., 47(2002) 1421-1433.

4. H.E. Johns and J.R Cunningham, "THE PHYSICS OF RADIOLOGY", Charles C. Thomas Publisher, Springfield, Illinois, USA, 1983.

5. J. Fred Doornbos, "SELECTION AND ADMINISTRATION OF RADIATION THERAPY" Lung tumors multidisciplinary database, University of Iowa, 2002.

6. Eric J. Hall, "RADIOBIOLOGY FOR THE RADIOLOGIST', Lippincott Williams&Wilkins, USA, 2000.

7. J. Walter, H. Miller and C. K. Bomford, "A SHORT TEXTBOOK OF RADIOTHERAPY", Churchill Livingstone, UK, 1989.

8. S. Heukelom et al, " COMPARISON OF ENTRANCE AND EXIT DOSE MEASUREMENTS USING IONIZATION CHAMBERS AND SILICON DIODES" Phys. Med. Biol., 1991; vol. 36 No:1, 47-59.

9. ICRU report 23, "MEASUREMENT OF ABSORBED DOSE IN A PHANTOM IRRADIATED BY A SINGLE BEAM OF X OR GAMMA RAYS" Report 23, 1973 (Washington, DC: ICRU).

10. Peter Metcalfe, Tomas Kron and Peter Hoban," THE PHYSICS OF RADIOTHERAPY X-RAYS FROM LINEAR ACCELERATORS", Medical Physics Publication, Madison, USA, 2002.

11. S. F. de Boer, A. S. Beddar, and J. A. Rawlinson, "Optical filtering and spectral measurements of radiation-induced light in plastic scintillation dosimetry", Phys. Med. Biol. 38 (1993), 945-958.

12. Jaffray D.A., Yan D., Wong J.W. " Managing geometric uncertainty in conformal intensity-modulated radiation therapy.", Semin Radiat Oncol. 1999 Jan;9(1):4-19.

13. J. R. Williams and D. I. Thwaites," Radiotherapy physics in practice", second edition, Oxford university press, 2000.

14. Mavroidis P.; Axelsson S.; Hyödynmaa S.; Rajala J.; Pitkänen M.A.; Lind B.K.; Brahme A. " Effects of Positioning Uncertainty and Breathing on Dose Delivery and Radiation Pneumonitis Prediction in Breast Cancer", Acta Oncologica, 1 September 2002, vol. 41, no. 5, pp. 471-485(15).

15. Rosenthal S.A., Roach M. 3rd, Goldsmith B.J., Doggett E.C., Pickett B., Yuo H.S., Soffen E.M., Stern R.L., Ryu J.K. " Immobilization improves the reproducibility of patient positioning during six-field conformal radiation therapy for prostate carcinoma" Int J Radiat Oncol Biol Phys. 1993 Nov 15;27(4):921-926.

16. Jeremy T. Booth, "Modelling the impact of treatment uncertainties in radiotherapy". PhD thesis, University of Adelaide, March 2002.

17. D. Yan and D. Lockman, "Organ/patient geometric variation in external beam radiotherapy and its effects". Med. Phys. Vol.28 (4), April 2001.

18. Ten Haken R.K., Forman J.D., Heimburge D.K., Gerhardsson A., McShan D.L., Perez-Tamayo C., Scheppel S.L., Lichter A.S. 1991 "Treatment planning issues related to prostate movement in response to differential filling of the rectum and the bladder". Int. J. Radiation Oncology. Biol. Phys., 20(1): 1991; 1317-1324.

19. Glenn F. Knoll, " RADIATION DETECTION AND MEASUREMENT", John Wiley and sons, New York, USA, 1979.

20. A. S. Beddar et al, " WATER EQUIVALENT PLASTIC SCINTILLATION DETECTORS FOR HIGH ENERGY BEAM DOSIMETRY: I. PHYSICAL CHARACTERISTICS AND THEORETICAL CONSIDERATIONS" Phys. Med. Biol., 1992, vol:37, No:10, 1883-1900.

21. Smith D.L et al, " MEASUREMENT OF RESPONSE OF SEVERAL ORGANIC SCINTILLATORS TO ELECTRONS, PROTONS AND DEUTERONS", Nucl. Instr. And meth., 1968 vol:64 : 157-166.

22. ELJEN Technology "ELJEN PLASTIC AND LIQUID SCINTILLAOTRS", PO.Box.870, 300 Crane Street, Sweetwater, Texas 79556 U.S.A.

23. Bicron corporation "INJECTION MOLDED PLASTIC SCINTILLATORS", 12345 Kinsman Road, Newbury, Ohio 44065, USA.

24. Norland Products Inc.,"NORLAND OPTICAL ADHESIVE 63", 2540 Route 130, Suite 100, P.O.Box:637, Cranbury, NJ08512, USA.

25. Bahaa E. Saleh and Malvin Carl Teich, " FUNDAMENTALS OF PHOTONICS", John Wiley and Sons, INC, New York, USA, 1996.

26. Edmund Optics Singapore Pte. ltd, 1093 Lower Delta Road #02-09, Tiong Bahru Industrial Estate, Singapore 169204.

27. Mark R. Arnfield, Hani E. Gaballa, Robert D. Zwicker, Quazi Islam, and Rupert Schmidt-Ullrich "Radiation-induced light in optical fibers and plastic scintillators: Application to brachytherapy", IEEE Transactions on Nuclear Science, Vol. 43, No. 3, June 1996.

28. E. J. Friebele, " Optical fiber waveguides in radiation environments", Optical Engineering Vol. 18 No. 6, Nov-Dec 1979.

29. D. Letourneau, J. Pouliot, and R. Roy " Miniature scintillating detector for small field radiation therapy", Med. Phys. 26 (12), December 1999.

30. Abdou-Samad Beddar and Patrick D. Higgins, " Ionizing radiation response effects on optical fibers in radiation therapy dosimetry applications", SPIE vol. 992 fiber optics reliability: Benign and adverse environments II (1988).

31. Spectra-Physics laser and photonics,1335 Terra Bella Avenue, Post Office Box 7013, Mountain View, USA .

32. J. V. Jelley, " Cherenkov radiation and its applications", Pergamon press, INC., 1958.

33. Frank H. Attix, "Introduction to radiological physics and radiation dosimetry", John Wiley & Sons, Inc., 1986.

34. A. Sam Beddar et al, "Plastic scintillation dosimetry: optimization of light collection efficiency", Phys. Med. Biol. 48 (2003) 1141-1152.

35. RS Components Pty Ltd, ABN 73 009 403 356, 25 Pavesi St, Smithfield. NSW. 2164 (PO Box 6864, Wetherill Park. NSW. 1851).

36. Tektronix, Inc., P.O.Box 500, Beaverton, OR 97077, USA.

37. Varian medical systems, Headquarters, California, 3100 Hansen Way, Palo Alto, CA 94304-1129, USA.

38. PTW-New York Corporation, 201 Park Avenue, Hicksville. New York 11801, USA.

39. A. Sam Beddar, Natalka Suchowerska, and Susan H. Law, "Plastic scintillation dosimetry for radiation therapy: minimizing capture of Cerenkov radiation noise", Phys. Med. Biol., 49(2004) 783-790.

40. Robert Stanton and Donna Stinson" Applied physics for radiation oncology", Medical physics publishing, 4513 Vernon Blvd., Madison, WI 53705, USA.

41. M. A. Clift, R. A. Sutton, and D. V. Webb, "Dealing with Cerenkov radiation generated in organic scintillator dosimeters by bremsstrahlung beams", Phys. Med. Biol., 45(2000) 1165-1182.

42. A. S. Beddar, T. R. Mackie, and F. H. Attix, " Water equivalent plastic scintillation detectors for high energy beam dosimetry: I. Properties and measurements" Phys. Med. Biol., 1992, vol:37, No:10, 1901-1913.

43. B. Porter, P. Auchincloss, P. de Barbaro, A. Bodek, and H. Budd," A STUDY OF AN ACRYLIC CERENKOV RADIATION DETECTOR", Am. J. Phys. 67 (11), November 1999.

44. R. C. Webb, "Response of fiber optic waveguides to ionizing radiation" Optical Engineering, 1979, vol:18, No:6, 568-572.

45. Marion Essers, and Ben J. Mijnheer, "In vivo dosimetery during external photon beam radiotherapy", Int J Radiat Oncol Biol Phys; 1999, Vol 43, No. 2, PP. 245-259.

46. Hiraoka et al, ICRP Annual Meeting (Committee 3). Argentina, November 2003.

47. Faiz M. Khan, "The physics of radiation therapy", third edition, Lippincott Williams &Wilkins, Philadelphia, PA 19106 USA.

48. Radiation protection series, NO.1, " Limiting exposure to ionizing radiation".

APPENDIX A

Background information

X-ray interaction with matter

X-ray refers to radiation originating in transitions of atomic electrons. An x-ray photon can interact with the whole atom, an orbital electron or directly with the nucleus. This will depend on the energy of the incident photon. Low energy photons are likely to interact with the whole atom and intermediate energy photons generally interact with orbital electrons while very high energy photons are capable of interacting with the nucleus. In the therapeutic x-ray range, the interactions commonly take place when the incoming photon passes near the nucleus of the atom and subjected to the strong field of the nucleus The x-ray quanta may disappear as a photon and become a positron and electron pair. An x-ray photon may interact with the absorber to produce high speed electrons by three important mechanisms known as the photoelectric effect, Compton incoherent scattering, and pair production. A less important process termed coherent scattering also takes place. Generally, all four processes take place simultaneously [1].

Photoelectric effect

In the photoelectric effect the incident x-ray photon interacts with an entire atom, the x-ray photon disappears, and one of the electrons around the atom is ejected. The atom recoils in this process, but carries with it little kinetic energy. The kinetic energy of the ejected electron (photoelectron) is equal, therefore, to the energy of the incident photon less the binding energy of the electron, that is, the ionization energy for the ejected electron [47]. If the x-ray photon succeeds in ejecting an inner atomic electron, the vacancy in the electronic structure is later

filled by a transition of one of the outer shell electrons. This transition is accompanied by the emission of characteristic x-rays.

The photoelectric effect is the predominant attenuation process for low energy photons (low long wavelength radiation), in attenuating materials of high atomic numbers. It is thus the main effect in the interaction of diagnostic quality x-rays with bone or metals [4].

The Compton Effect.

The Compton Effect, or Compton scattering, as it is sometimes called, is simply the elastic scattering of a photon by an electron, in which both energy and momentum are conserved. A free electron is one whose binding energy to an atom is very much less than the energy of the photon. On collision of a photon and a free electron not all the energy of the photon can be transferred, hence the photon must be scattered, and the scattered photon must have less energy than the incident photon. This scattered electron is of great importance in radiation dosimetry, because it is the vehicle of energy transfer from the scattered photon to an absorbing medium.

The Compton process is important for high energy photons (short wavelength radiation) passing through low atomic number materials. It is therefore the predominant process for the attenuation of deep therapy beams in soft tissue [4].

Pair production

In this process, the incident photon disappears and an electron/positron pair is created. Since the total rest-mass energy of the electron and positron is 1.02

MeV, this effect does not occur unless the incident photon has at least this much energy.

The total kinetic energy of the electron-positron pair is equal to the energy of the incident photon less 1.02 MeV once formed. These particles move about and lose energy as a result of collisions with atoms in the surrounding medium. After the positron has slowed to very low energies, it combines with an electron, the two particles disappear in an annihilation reaction, and two photons are produced each having 0.511 MeV energy and travelling in opposite directions to each other.

The pair production process occurs for radiation of photon with energies greater than 1.02 MeV. In practice, this process is of little importance in the low atomic number elements of soft tissues except above about 20 MeV radiations [4].

Radiation protection in medical exposure

All medical irradiations should be subject to the principles of justification and optimization. Dose limits restricting occupational and public exposure to radiation are not appropriate for patients undergoing diagnosis or therapy [4]. The oncologist responsible for a patient determines the appropriate medical care. However, recommended levels for medical exposure for particular procedures may assist in optimising patient doses.

For a patient undergoing medical diagnosis or therapy, there are two levels of dose justification. First, the medical practice involving exposure to radiation should be justified in principle [48]. Second, each procedure should be subject to a further justification by the clinician who is responsible for the management of the patient and who determines that the exposure is necessary for therapeutic purposes [48]. Protection should be optimized during medical irradiation. There is often scope for dose reduction; through planning and careful choice of irradiating

techniques, *in-vivo* dosimetery, continuous evaluation of the irradiated part, and by assessing the effectiveness of the planned irradiation.

Radiation dose to the patients

Radiation therapy is the careful use of high energy x-rays, gamma rays, or electrons to treat cancer. Radiation is effective in treating cancer because it damages cancer cells more than it does normal cells. However, normal tissues may also be damaged, which is one reason why side effects can occur. The goal of radiotherapy is to destroy the cancer with as little injury as possible to the surrounding normal tissues. In practice, it is technically difficult to deliver tumour doses without significant risks of damaging normal critical structures.

In an effort to reduce the amount of radiation delivered to normal structures while trying to make certain that the tumour receives the full dose, beams are customarily shaped so that they treat tissues 1.5-2.0 cm beyond the margins of the tumour [2]. In an effort to spare normal tissues from as much irradiation as is possible, high energy beams are used to treat tumours deep in thick body parts. Low energy photon beams and high energy beams are used to treat tumours lying close to the skin and tumours lying over radiation sensitive structures such as the spinal cord.

Slight daily variations in patient position during treatment are expected. For selective tumour irradiation it is necessary that the patient adopts exactly the same position each day. This is achieved using laser light, bite blocks and restraining devices while he or she lies in a comfortable position [2]. The irradiation coming through the patient from each treatment port can be used to expose an x-ray film and thereby produce a port film which is taken weekly and compared to earlier simulator and port films to make certain that the treatment ports do not move from week to week [2].

Since it is a patient that we treat, not just a tumour, the effects of the x-rays on other tissues are clearly of importance. Though we should confine the rays as nearly as possible to the lesion, normal tissues must always be more or less involved [4]. There are definite limits to the amount of radiation that can be tolerated, and doses in excess of these will have serious, even fatal, results.

For radiation therapy treatment, focused high energy photons or electrons are used to treat cancer. In some radiotherapy centres, neutrons and protons are also used in place of photons or electrons. These beams hit and transfer varying amounts of energy to carbon, nitrogen, and hydrogen atoms in or near the DNA chains in the nucleus of cells thereby producing breaks, deletions, or cross linkages in the DNA chains, some of which are dangerous to the cell. A few cells may die within minutes of being hit, but after sustaining dangerous damage most cells survive until they attempt to go through mitosis and cell division. Cells are most sensitive to radiation therapy when they are in mitosis or shortly after cell division [4]. Tissues in which a high proportion of cells are actively multiplying tend to be more sensitive to high energy photons than are tissues where most cells divide relatively infrequently. By giving daily doses of radiation therapy large enough to kill a high proportion of the rapidly dividing cancer cells while killing only a small proportion of the more slowly dividing normal tissue cells in the area, a malignant tumour can be destroyed. The factors that determine whether or not a cancer can be destroyed by radiation therapy include the sensitivity of the tumour to radiation therapy, the volume of tumour cells to be destroyed and the tolerance of the most radiation sensitive vital tissues in the area. This latter factor is influenced by how effectively these structures can be shielded from the irradiation received by the tumour and whether the vital tissues can be sacrificed without death. Thus, radiation therapy is most effective when the volume of tumour cells to be treated is small, i.e. microscopic deposits of tumour cells left behind after the visible part of a tumour has been surgically excised, or when the tumour can be given a high dose of high energy photons or electrons without destroying the function of the vital structures in the area (the spinal cord, a segment of small intestine, both kidneys, all of the liver or heart, the entire brain,

etc.). When the normal tissues in an area can tolerate only moderate doses of high energy photons, cancers in the area can be only temporarily reduced in size to open air passages (bronchi), pain can be relieved when bones are weakened by cancer, and bleeding can be controlled thereby reducing the patient's concern.

Selection and Administration of Radiation Therapy

Before patients receive radiation therapy, any factors which might adversely affect their ability to tolerate radiation therapy must be detected. Therefore, a detailed history of all prior medical diagnoses and treatments is obtained. The radiation oncologist is particularly interested in obtaining a history of prior radiation therapy treatments or surgery in the area to be treated which might interfere with the ability of those tissues to tolerate radiation therapy. Also we need to determine whether there are simultaneous diseases. Recent weight loss and the overall functional status of the patient are also factors which must be considered when deciding whether, what type, when, and how to irradiate the patient.

A limited physical examination is performed to determine whether the patient is sufficiently healthy to tolerate irradiation and to try to discover surgical wounds and other diseases which indicate that the patient has had an operation or an illness that he or she failed to tell his physician about and which could affect his or her ability to tolerate a full course of radiation therapy.

The radiation oncologist must then examine the patient's x-rays and operative reports, pathology reports, and lab reports. Not infrequently additional tests are required to make certain that all metastases to the brain, lungs, or other organs will be detected and that the entire tumour is included in the volume of tissue that is to be irradiated. At times, a CT scan of the region of interest helps the radiation oncologist determine how to direct the treatment beams in order to deliver a maximum dose to the tumour, while sparing as much of the normal radiation sensitive tissues as is possible.

The patient's treatments are planned while he or she lies on the treatment couch of a simulator. A simulator is an x-ray machine that usually will fluoroscope and radiograph each area to be treated. It is called a simulator because it allows the radiation oncologist to see what will be in the path of each beam delivered by the treatment machine. Accurate simulation often requires long times compared with treatment time. Simulated x-rays determine the shape of blocks needed to direct the beam delivering the radiation therapy to the tumour so that as much normal tissue as possible is spared. In situations where the organ or tissues containing a cancer are not visible in plain x-rays, a CT scanner attached to a special dosimetry computer "CT Simulator" can be used to determine how and where each beam needs to be directed and shaped. The CT simulator projects the outline of each treatment port onto the skin of the patient where it is then traced by a technologist. After the treatment ports are planned on the CT-simulator, the patient is placed back in the treatment position on the radiographic simulator and near-diagnostic quality x-rays are taken to confirm what will lie in the path of each treatment port.

After the simulation, the patient is placed on the couch of the linear accelerator in the same position as on the simulator couch. Then each treatment port to be used is projected into the outline of the simulator ports which had been traced on the patient by the technologist. In most cases, the patient receives treatment through each treatment port each day, thereby making certain that all tissues receive the same daily dose. Wide fluctuations in the day to day dose delivered to normal tissues tend to increase the severity of late damage to normal structures.

The quantity of irradiation delivered 1 cm from the edge of a treatment beam is only 85% of the quantity of irradiation delivered to tissues in the centre of the treatment port. At the edge of each port the tissues receive only 50% of the dose delivered to tissues in the centre of the port.

In an attempt to spare normal tissues from as much irradiation as is possible, high energy electromagnetic (photon) beams are used to treat tumours deep in

thick body parts. Low energy photon beams and high energy electron beams are used to treat tumours lying close to the skin and tumours lying over radiation-sensitive structures such as the spinal cord.

Following completion of a course of radiation therapy, most patients are seen six weeks later and then every three months thereafter. This allows the radiation oncologist to detect treatment related complications as early as possible.

Accuracy of Radiation Therapy

An important question with respect to radiation therapy is what degree of accuracy can be achieved for dose delivery in clinical practice. In clinical practice, a desired level of accuracy cannot always be achieved. An overall check of the whole dosimetry procedure is therefore useful and can be carried out by performing dose measurements in real time during treatment. Such *in-vivo* dose measurements can be performed as entrance dose, exit dose or intracavity dose using miniature plastic scintillator dosimeters.

Entrance dose measurements can lead to modification of treatment techniques. Together, entrance dose and exit dose measurements can be used to calculate possible deviations between planned and actual doses. This leads to recommendations for improved dose calculations. Clinical study is expected to show the usefulness of *in vivo* dose measurements for the determination of accurate dose values in patients.

APPENDIX B

Electronic circuits

Diagram 1: Timing diagram of Dual Integrator System.

Diagram 2: Dosimeter integrator Circuit.

Diagram 3: BPW21 Photodiode amplifier circuit.

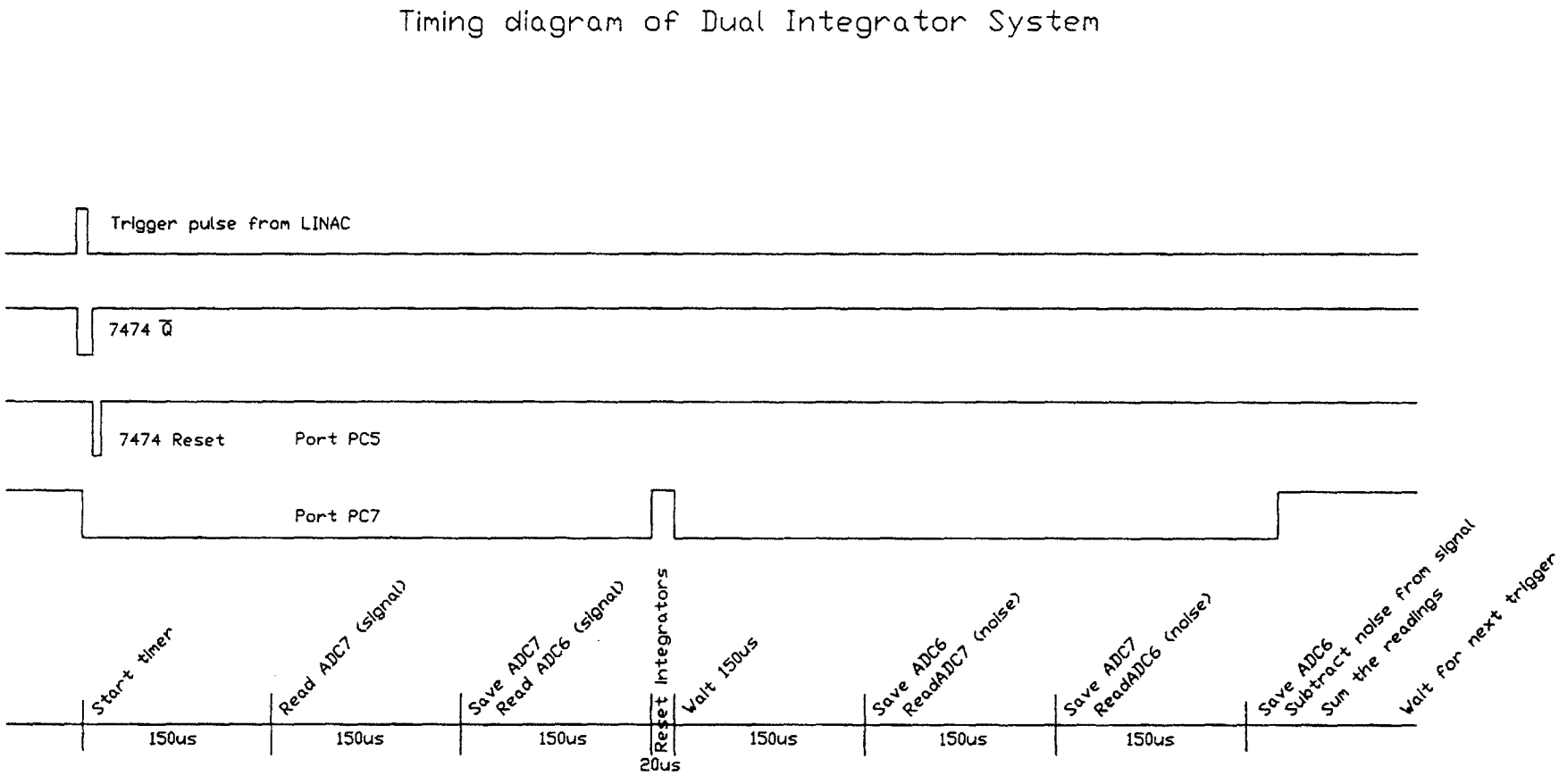

Diagram 1: Timing diagram of Dual Integrator System.

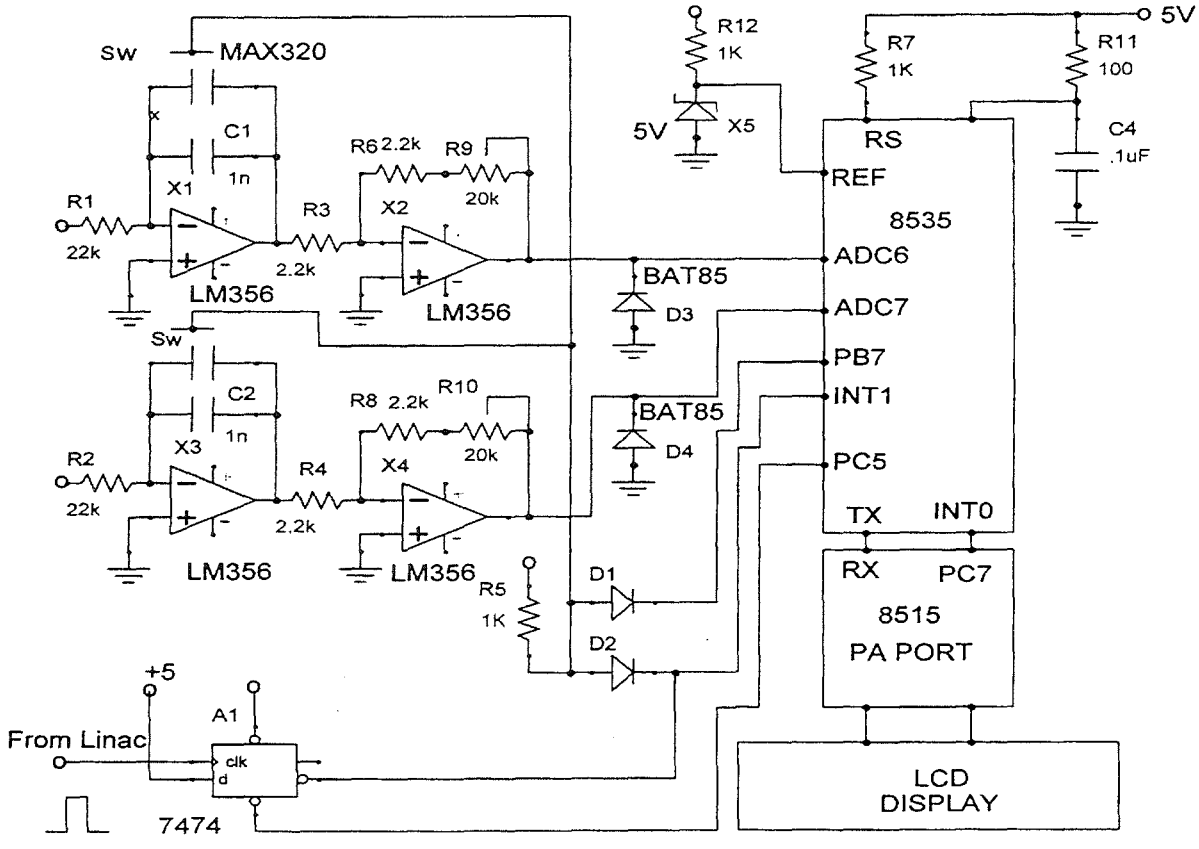

Diagram 2: Dosimeter integrator Circuit.

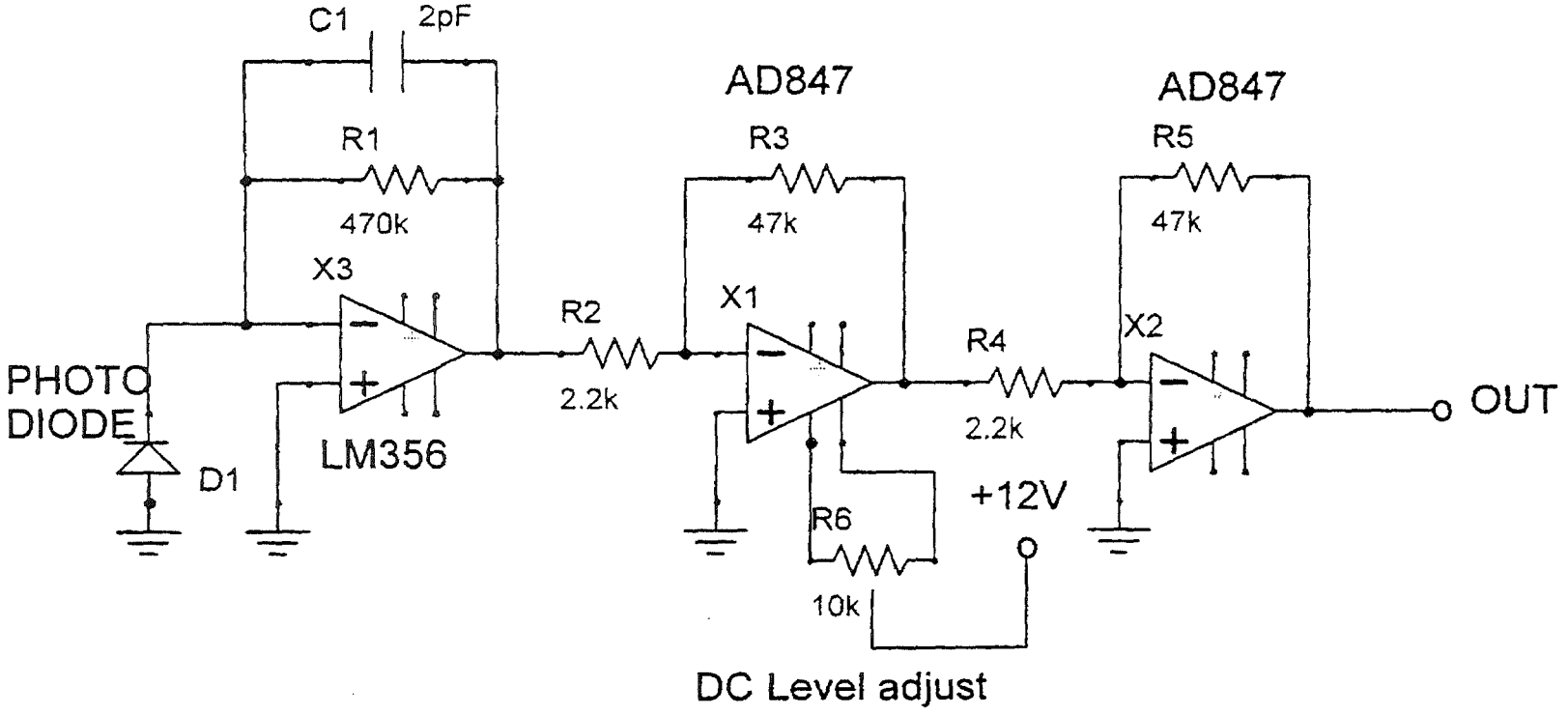

Diagram 3: BPW21 Photodiode amplifier circuit.